UNIVERSITY OF BELGRADE

SCHOOL OF ELECTRICAL ENGINEERING

Abdulgader G. R. Zlitni

MODULATION RESPONSE AND BANDWIDTH OF INJECTION-LOCKED FABRY-PEROT LASER DIODE

Doctoral Dissertation

Belgrade, 2013

UNIVERZITET U BEOGRADU

ELEKTROTEHNIČKI FAKULTET

Abdulgader G. R. Zlitni

MODULACIONI ODZIV I PROPUSNI OPSEG INJEKCIONO SINHRONIZOVANIH FABRI-PERO LASERSKIH DIODA

doktorska disertacija

Beograd, 2013

Mentor and the chair of the committee:

Professor Dejan Gvozdić,
full-time professor at the School of Electrical Engineering - University in Belgrade

Members of the committee:

Professor Jovan Radunović,
full-time professor at the School of Electrical Engineering - University in Belgrade

Professor Vitomir Milanović,
professor in retirement at the School of Electrical Engineering - University in Belgrade

Date of the thesis public defence:

ACKNOWLEDGMENT

I would like to thank my mentor **Prof. Dr. Dejan Gvozdić**, and **Marko Krstić**, for the support they provided and huge amount of patience without which I wouldn't have been able to complete my thesis.

I would also like to thank my **parents** and my **family** for being the constant source of the encouragement and support while completing this work.

MODULATION RESPONSE AND BANDWIDTH OF INJECTION-LOCKED FABRY-PEROT LASER DIODE

Abstract

Synchronization by injection-locking is an advanced technique for controlling mechanical, electrical and microwave devices, with emerging applications in the field of optical communications and optical signal processing in the past decades. Some of the latest applications of injection-locking are related to the new generation of passive optical wavelength multiplexing networks (WDM-PON), in which injection-locked transmitters, instead of much more expensive tunable lasers, achieve upstream signal transmission, from the subscriber to the central office. Injection-locking from the central office and into a side-mode of the multimode laser in the subscriber node, in which stable upstream transmission is achieved, could provide possibility to develop "colorless" transmitters and much simpler architecture of WDM passive optical networks. Theoretical and experimental research have shown that modulation response of a single-mode laser can be significantly improved by applying injection-locking in comparison with free-running regime in which injection-locking is not applied. On the other hand, this technique can provide a single-mode output of a multimode laser, reduce linewidth i.e. frequency chirp, eliminate phase jitter as a result of mode hopping and optical fiber dispersion, etc.

The topic of this dissertation is modulation response and modulation bandwidth of a Fabry-Perot slave laser whose side-modes are injection-locked by some other, master laser. Investigation of the modulation response and bandwidth relies on the "small-signal" analysis. For the sake of this analysis, system of the laser rate equations, which comprises equation regarding carriers dynamics, and equations regarding photon and phase dynamics for every supported longitudinal mode including injection-locked mode, is linearized around steady-state. Once the influence of the injection-locking on the unlocked modes phases is neglected, the "small-signal" analysis reduces to the system of equations equal to the number of supported modes with addition of two equations: carriers dynamics equation and injection-locked phase equation. By solving this equation system with frequency

detuning and injection power as input parameters, one can obtain photon distribution throughout supported longitudinal modes, and total modulation response.

The main focus of this dissertation is the investigation of the injection power and frequency detuning between the master and the slave lasers influence on the modulation response of the slave laser and its bandwidth. Since injection-locking is applied into side-modes of the slave laser, analysis must take into account not only the injection-locked mode, but all the other modes supported by slave laser cavity, especially the ones which are dominant in the free-running regime, when no injection-locking is applied. In this case, the dimension of the rate equation system can be in the order of few hundreds. Special attention is given to the stability of the slave laser, so the analysis is conducted for those parameters of the laser which guarantee stable output.

Starting from the potential application of injection-locked lasers in WDM-PON, and conducted analysis, dissertation shows that it is possible to optimize the parameters of injection, in order to maximize the modulation bandwidth, which becomes significantly larger in comparison with the free-running regime, with stable slave laser operation, on the optical frequency significantly different from the frequency of the dominant mode. In addition to this, the analysis shows that only a small number of modes dominantly determine the modulation response. Indeed, apart from injection-locked mode, it is sufficient to take into account only the free-running dominant mode, while further increase of modes taken into account does not lead to significant change in the modulation response and bandwidth.

Introduction chapter gives an overview of existing technologies which are employed in access passive optical FTTx networks, such are BPON, EPON, GPON and WDMPON. The next chapter gives an overview of WDM-PON architecture, as well as its subsystems and devices employed in them, especially in optical network units. The third chapter deals with applications of injection-locking synchronization techniques in WDM-PON subsystems, and with advantages of injection-locking over the other techniques applied in these networks. In the fourth chapter, basic photon density and phase difference between master

and slave laser rate equations are derived. This derivation starts from the wave equation in adiabatic and paraxial approximation. Apart from this, conditions for stable injection-locking are investigated and defined. In the fifth chapter, the complete multimode rate equation system in the case of intermodal injection locking is defined. This chapter especially deals with steady-state free-running analysis and its verification through transient analysis. Similar analysis is conducted for injection-locked regime as well. Starting from the complete multimode rate equation system in the case of intermodal injection locking, a multimode "small-signal" model, with a small perturbation around steady-state value is derived. Sixth chapter defines and investigates modulation response for both free-running and injection-locking regime. Furthermore, this chapter gives an analysis of the modulation response and bandwidth for symmetrical and asymmetrical optical gain profile. Both cases show very similar behavior of injection-locked laser, and it is established that modulation bandwidth increases for negative and small positive frequency detuning, while for positive frequency detuning, modulation bandwidth decreases with an increase in the injection power. It is shown that modulation bandwidth has maximal value for moderate injection powers, while extremely large injection powers lead to the decrease of the bandwidth. Finally, the last chapter gives conclusion of the thesis, which again goes through basic thesis foundations, and summarizes fundamental scientific contributions.

Keywords: injection-locking, Fabry-Perot laser diode, multimode rate equations, small-signal analysis, modulation response

Research area: Physical electronics

Area of expertise: Optoelectronics and Optoelectronic communications

UDK number: 621.3

MODULACIONI ODZIV I PROPUSNI OPSEG INJEKCIONO SINHRONIZOVANIH FABRI-PERO LASERSKIH DIODA

Rezime

Injekciona sinhronizacija spada u napredne tehnike kontrole rada mehaničkih, elektronskih i mikrotalasnih uređaja, a poslednjih decenija našla je primenu i u oblasti optičkih komunikacija i optičke obrade signala. Neke od najnovijih primena injekcione sinhronizacije odnose se na novu generaciju pasivnih optičkih mreža sa multipleksiranjem po talasnim dužinama (WDM-PON), kod kojih se transmisija signala od korisnika ka centrali uspostavlja primenom injekciono sinhronizovanih predajnika, umesto primenom skupih podešavajućih lasera. U slučaju da se injekcijom signala iz centrale u bočni mod multimodnog lasera, koji priprada optičkoj mrežnoj jedinici, može obezbediti stabilna emisija signala od korisnika ka centrali, ovakvi sistemi omogućili bi realizaciju takozvanih „bezbojnih predajnika“ i uprošćenu arhitekturu WDM pasivnih optičkih mreža. Teorijska i eksperimentalna istraživanja pokazala su da se modulacioni odziv monomodnih lasera može u značajnoj meri popraviti primenom injekcione sinhronizacije u odnosu na režim rada bez primene ove tehnike. Sa druge strane, tehnika injekcione sinhronizacije može da obezbedi monomodni režim rada multimodnog predajnika, smanji Henrijev faktor, odnosno čirp predajnika, eliminiše fazni džiter koji nastaje kao rezultat poskakivanja modova i disperzije optičkog vlakna i druge štetne efekte.

Tema ove disertacije su modulacioni odziv i propusni opseg Fabri-Pero poluprovodničkog lasera koji je putem svojih bočnih modova injekciono sinhronizovan sa drugim master laserom. Ispitivanje modulacionog odziva i propusnog opsega bazira se na analizi „malih signala“. Zbog toga je za ovo razmatranje izvršena linearizacija brzinskih jednačina u okolini mirne radne tačke lasera za injektovan i neinjektovane modove, pri čemu je, osim jednačine po koncentraciji nosilaca i fotona za svaki od modova, u obzir uzeta i jednačina po fazi. Ako se uticaj neinjektovanih modova na fazu zanemari, analiza malih signala dovodi do sistema jednačina koji je jednak broju modova uzetih u obzir uvećanom za dva, zbog potrebe da se u obzir uzmu i jednačina po nosiocima i po fazi za

injektovani mod. Rešavanje ovog sistema u kome učestanost modulacije, injekciona snaga i frekvencijska razdešenost ulaze u proračun kao parametri, obezbeđuje raspodelu fotona po modovima lasera i mogućnost određivanja ukupnog modulacionog odziva.

U fokusu istraživanja disertacije je uticaj snage injekcione sinhronizacije i frekvencijske razdešenosti između pratećeg i vodećeg lasera na modulacioni odziv pratećeg lasera i njemu pridružen propusni opseg. S obzirom da se injektovanje signala vodećeg lasera vrši u bočne modove FP lasera, neophodno je da analiza obuhvati, ne samo mod u koji vodeći laser injektuje signal, već i preostale prisutne modove, posebno one koji u slobodnom režimu rada dominiraju nad injektovanim modom. Zbog toga analiza obuhvata i slučaj kada su u obzir uzeti svi longitudinalni modovi FP lasera, tako da dimenzija analiziranog dinamičkog sistema jednačina može iznositi nekoliko stotina. Posebna pažnja je posvećena stabilnosti rada pratećeg lasera, tako da je ispitivanje sprovedeno za one parametre rada u kojima je prateći laser u stabilnom režimu rada.

Polazeći od potencijalne primene ovih lasera u WDM pristupnim mrežama i sprovedene analize, kroz disertaciju je pokazano da je moguće optimizovati parametre injekcije, tako da propusni opseg ima maksimalnu vrednost, koja je značajno veća u odnosu na slobodan režim rada i pri kojoj prateći multimodni laser može da radi u stabilnom monomodnom režimu i to na talasnoj dužini koja se značajno razlikuje od talasne dužine dominantnog moda. Takođe, analiza je pokazala da je broj modova koji dominantno određuje modulacioni odziv lasera izuzetno mali. Tačnije, osim injektovanog bočnog moda, potrebno je u obzir uzeti dominantni mod iz slobodnog režima rada, pri čemu dalje povećanje modova ne dovodi do značajnije promene modulacionog odziva i propusnog opsega.

U okviru uvodnog poglavlja dat je prikaz postojećih tehnologija koje su našle primenu u relizaciji pristupnih pasivnih optičkih FTTx mreža, kao što su BPON, EPON, GPON i WDMPON. Naredno poglavlje daje osvrt na arhitekturu i tehnologiju WDM-PONa, kao i karakteristike naprava i realizacije podsistema, posebno optičkih mrežnih jedinica. Sledeće poglavlje bavi se primenom injekcione sinhronizacije u realizaciji WDM-

PON podsistema, njenim prednostima u odnosu na druge metode realizacije WDM-PONa. U okviru četvrtog poglavlja izvedene su osnovne brzinske jednačine po koncentraciji fotona injekciono sinhronizovanog lasera i faznoj razlici vodećeg i sinhronizovanog lasera. U ovom izvođenju pošlo se od talasne jednačine u adijabatskoj i paraksijalnoj aproksimaciji. Pored toga, razmotreni su i definisani osnovni uslovi za ostvarenje uspešne i stabilne sinhronizacije lasera. U petom poglavlju definiše se kompletan sistem brzinskih jednačina za slučaj injekcionog sprezanja sa bočnim modovima. U ovom poglavlju posebno se razmatra slobodan režim kroz stacionarnu analizu raspodele modova i njenu potvrdu preko tranzijentne analize. Takođe, slično razmatranje se sprovodi za slučaj injekcione sinhronizacije. Polazeći od kompletnog sistema multimodnih jednačina sa injekcionom sinhronizacijom, izveden je multimodni model za male signale koji se bazira na linearizaciji brzinskih jednačina u okolini mirne radne tačke. U šestom poglavlju, definisan je modulacioni odziv i sprovedena je analiza modulacionog odziva za slučaj slobodnog režima rada multimodnog lasera, a zatim za slučaj injekciono-sinhronizovanog multimodnog lasera. U nastavku je analiziran modulacioni odziv i propusni opseg za slučaj simetričnog i asimetričnog spektra optičkog pojačanja. U oba slučaja potvrđeno je slično ponašanje injekciono-sinhronizovanih lasera i ustanovljeno je da negativne i slabo pozitivne frekvencijske razdešenosti obezbeđuju porast propusnog opsega, dok za pozitivne frekvencijske razdešenosti, propusni opseg opada sa injekcionom snagom master lasera. Pokazuje se da maksimum propusnog opsega nastupa za umerene injekcione snage, dok prevelike snage dovode do smanjenja propusnog opsega. Konačno, poslednje poglavlje predstavlja zaključak rada u kome su ponovo razmotrene osnovne hipoteze disertacije i sumirani fundamentalni naučni doprinosi teze.

Ključne reči: injekciono sprezanje, Fabri-Pero laserske diode, multimodalne brzinske jednačine, analiza malih signala, modulacioni odziv

Naučna oblast: Fizička elektronika

Uža naučna oblast: Optoelektronika i Optoelektronske komunikacije

UDK broj: 621.3

TABLE OF CONTENTS

CHAPTER 1

CHAPTER 2

CHAPTER 3

Chapter 1 - Introduction

1.1 Importance of optical communications in telecommunications

Optical communication is one of the newest and most advanced forms of communication by electromagnetic waves. In one sense, it differs from radio and microwave communication only in that the wavelengths employed are shorter (or equivalently, the frequencies employed are higher). However, in another very real sense it differs markedly from these older technologies because, for the first time, the wavelengths involved are much shorter than the dimensions of the devices which are used to transmit, receive, and otherwise handle the signals.

The advantages of optical communication are threefold. First, the high frequency of the optical carrier (typically of the order of 300,000 GHz) permits much more information to be transmitted over a single channel than is possible with a conventional radio or microwave system. Second, the very short wavelength of the optical carrier (typically of the order of 1 micrometer) permits the realization of very small, compact components. Third, the highest transparency for electromagnetic radiation yet achieved in any solid material is that of silica glass in the wavelength region 1–1.5μm [1, 2]. This transparency is orders of magnitude higher than that of any other solid material in any other part of the spectrum.

Optical communication in the modern sense of the term dates from about 1960, when the advent of lasers and light-emitting diodes (LEDs) made practical the exploitation of the wide-bandwidth capabilities of the light wave. With the development of extremely low-loss optical fibers during the 1970s, optical fiber communication became a very important form of telecommunication almost instantaneously [1-3].

The motivation for developing optical fiber communication systems started with the invention of the laser. However, it also was noted that the properties of optical fiber gave them a number of inherent cost and operational advantages over copper wires and made

them highly attractive for simple on/off keyed links. Included in these advantages are the following:

- **Long transmission distance**. Optical fibers have lower transmission losses compared to copper wires. This means that data can be sent over longer distances, thereby reducing the number of intermediate repeaters needed for these spans. This reduction in equipment and components decreases system cost and complexity.
- **Large information capacity**. Optical fibers have wider bandwidths than copper wires, which mean that more information can be sent over a single physical line. This property results in a decrease in the number of physical lines needed for sending a certain amount of information.
- **Small size and low weight**. The low weight and the small dimensions of fibers offer a distinct advantage over heavy, bulky wire cables in crowded underground city ducts or in ceiling-mounted cable trays. This also is of importance in aircraft, satellites, and ships where small, lightweight cables are advantageous, and in tactical military applications where large amounts of cable must be unreeled and retrieved rapidly.
- **Immunity to electrical interference**. An especially important feature of optical fibers relates to the fact that they consist of dielectric materials, which means they do not conduct electricity. This makes optical fibers immune to the electromagnetic interference effects seen in copper wires, such as inductive pickup from other adjacent signal-carrying wires or coupling of electrical noise into the line from any type of nearby equipment.
- **Enhanced safety**. Optical fibers do not have the problems of ground loops, sparks, and potentially high voltages inherent in copper lines. However, precautions with respect to laser light emissions need to be observed to prevent possible eye damage.
- **Increased signal security**. An optical fiber offers a high degree of data security, since the optical signal is well confined within the fiber and any signal emissions are absorbed by an opaque coating around the fiber. This is in contrast to copper wires where electric signals often can be tapped off easily. This makes fibers attractive in applications where information security is important, such as in financial, legal, government, and military systems [4].

1.2 Application of optical communications in nowadays access networks-FTTx

Optical communication plays a vital role in the development of high quality and high-speed telecommunication systems. Today, optical fibers are not only used in telecommunication links but also used in the Internet and local area networks (LAN) to achieve high signaling rates. The emergence and rapid development of new broadband telecommunications services have led to improvement of the access part of the network appears as an absolute necessity. In order to improve this part of the network, developed in recent years, many technological solutions, among which are the most important digital subscriber loop (xDSL), hybrid fiber coax (HFC) and more recently FTTx technology, which is primarily based on optical fibers, are divorcing to the end user (Fiber to the x = H (Home), B (building), C (Curb)) [5]. The implementation of FTTx technologies worldwide is establishing substantially increased broadband capabilities in many countries and is bringing these capabilities into the homes of millions. The worldwide FTTx number of users is increasing exponentially and new deployments across the globe are continually being initiated. European, North American, and Asian markets all are expected to be high growth areas and many service providers are investing heavily in the deployment of optical access network technologies. Today, numerous research laboratories and equipment providers are actively engaged in major research projects oriented to solutions for enhanced broadband connectivity through the use of optics and photonics [6].

Fiber to the Home or FTTH - enables service providers to offer a variety of communications and entertainment services, including carrier-class telephony, high-speed Internet access, broadcast cable television, direct broadcast satellite (DBS) television, and interactive, two-way video-based services. All of these services are provided over a passive optical distribution network via a single optical fiber to the home. In addition, an FTTH solution based on wavelength division multiplexing (WDM), or a FTTH-based architecture, allows for additional flexibility and adaptability to support future services. The full-service access network (FSAN) initiative, whose objective is to obtain cost-effective solutions to accelerate the introduction of broadband services into the public network, is also testing asynchronous transfer mode (ATM)-passive optical network (PON) technology for FTTH,

which transports network services in ATM cells on a PON. This mode of transport provides key service features, such as multiple quality-of-service (QoS) guarantees, which enables the successful transmission of integrated voice, video, and data services by prioritizing traffic. Fiber to the home (FTTH) is the ideal fiber-optics architecture. In this architecture, fiber deployment is carried all the way to the customer's home (premises). Fiber Optic service to the home is the fastest, most reliable and securest method and far surpasses anything that Broadband or "wireless" could ever even dream of. Many people never know that today's vast cellular and wireless network runs and "communicates" via a fiber optic backbone. This is the only way such vast amounts of data can be transported from caller to caller -quickly and securely [7].

1.3 Overview of FTTx Technology

The general structure of a modern telecommunication network consists of three main portions: backbone (or core) network, metro/regional network, and access network.

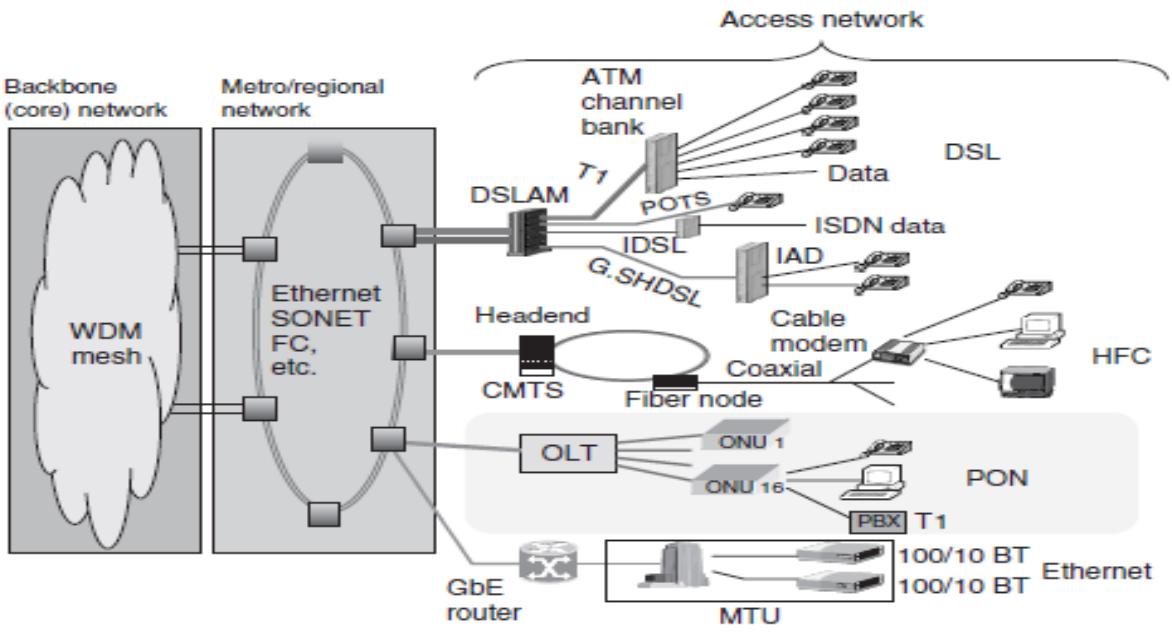

Fig.1. Generic structure of a modern telecommunication network.

On a very high level, core backbone networks are used for long-distance transport and metro/regional networks are responsible for traffic grooming and multiplexing functions. Structures of backbone and metro networks are usually more uniform than access networks and their costs are shared among large numbers of users. These networks are built with state-of-the-art fiber optics and wavelength division multiplexing (WDM) technologies to provide high-capacity connections. Access networks provide end-user connectivity. They are placed in close proximity to end users and deployed in large volumes. As can be seen from Fig.1, access networks exist in many different forms for various practical reasons. In an environment where legacy systems already exist, carriers tend to minimize their capital investment by retrofitting existing infrastructure with incremental changes, whereas in a green-field environment, it often makes more sense to deploy future proof new technologies which might be revolutionary and disruptive.

Compared to traditional copper-based access loops, optical fiber has virtually unlimited bandwidth (in the range of terahertz or THz of usable bandwidth). Deploying fiber all the way to the home therefore serves the purpose of future proofing capital investment. A passive optical network (PON) is a form of fiberoptic access network. Most people nowadays use PON as a synonym of FTTx, despite the fact that the latter carries a much broader sense. In an optical access network, the final drop to customers can be fiber (FTTH), coaxial cable (as in an HFC system), twisted pairs or radio (FTTC). In fact, a PON system can be used for FTTH or FTTC/FTTP depending on whether the optical fiber termination (or the ONU location) is at the user, or in a neighborhood and extended through copper or radio links to the user [8].

1.4 Historical perspective of PONs

The first PON activity was initiated in the mid-1990s when a group of major network operators established the full service access networks (FSAN) consortium. The group's goal was to define a common standard for PON equipment so that vendors and operators could come together in a competitive market for PON equipment. The result of

this first effort was the 155 Mbps PON system specified in the ITU-T G.983 series of standards. This system has become known as the B-PON system and it uses ATM as its bearer protocol (known as the APON protocol). The name B-PON was introduced since the name APON led people to assume that only ATM services could be provided to end users. Changing the name to BPON reflected the fact that BPON systems offer broadband services including Ethernet access, video distribution, and high-speed leased line services. Still, the most common and renowned name for the first generation of FSAN systems is APON.

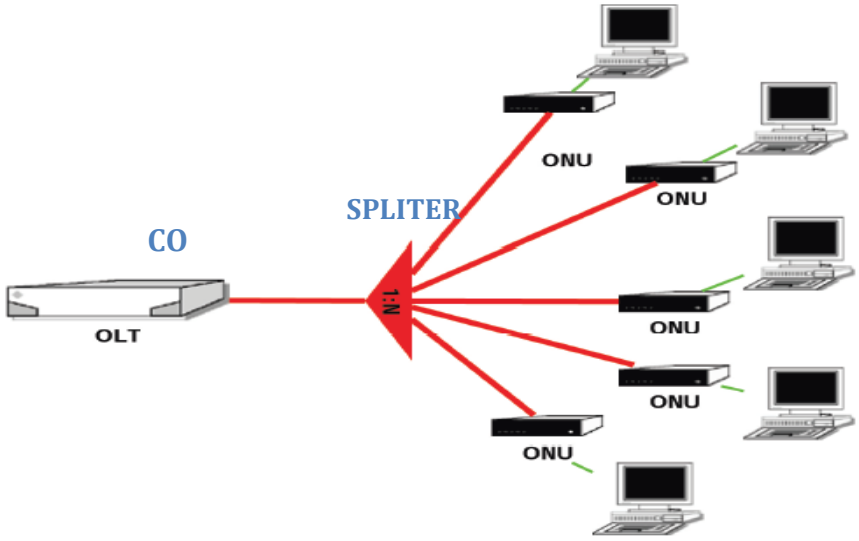

Fig.2. Passive Optical Network

The APON Standards were later enhanced to support 622 Mbps bit rates as well as additional features in the form of protection, Dynamic Bandwidth Allocation (DBA) and others. On a parallel track, in early 2001, the IEEE established the Ethernet in the First Mile (EFM) group, realizing the enormous prospect that lies ahead in the optical access market. The group works under the auspices of the IEEE 802.3 group, which also developed the Ethernet standards, and as such is restricted in architecture and compliance to the existing 802.3 Media Access Control (MAC) layer. The EFM's work is concentrated on standardizing a 1.25 Gaps symmetrical system for Ethernet transport only.

In 2001 the FSAN group initiated a new effort for standardizing PON networks operating at bit rates above 1 Gaps. Apart from the need to support higher bit rates, the overall protocol has been opened for reconsideration and the sought solution should be the most optimal and efficient in terms of support for multiple services, and operation, administration, maintenance and provisioning (OAM&P) functionality and scalability.

As a result of this latest FSAN effort, a new solution has emerged in the optical access market place – Gigabit PON (GPON), offering unprecedented high bit rate support while enabling the transport of multiple services, specifically data and TDM, in native formats and with extremely high efficiency [9].

1.5 Overview of PONs type

1.5.1 BPON: The Broadband passive optical network (BPON) was the first attempt towards a PON standard. It is governed by the ITU-T and is designated as ITU-T G.983. It established the general requirements for PON protocols. BPON use Asynchronous Transfer Mode(ATM) as the underlying transport mechanism to carry used data. BPON did not gain much popularity due to lack of bandwidth and widespread use of Ethernet protocol.

1.5.2 EPON: The Ethernet Passive Optical Network (EPON/GE-PON) is governed by IEEE and is designated as IEEE 802.3ah. EPON is based on Ethernet, unlike other PON technologies which are based on ATM. It provides simple, easy-to-manage connectivity to Ethernet-based IP equipment both at the customer premises and at the central office. It is well suited to carry packetized traffic as well as time-sensitive voice and video traffic. It offers 1.25Gbps data rate for both upstream and downstream. EPON supports 1:16 split ratio i.e. 16 ONUs at a range of 20 km can be connected with a single port of OLT.

1.5.3 GPON: The most recent PON standard is the ITU-T G.984 GPON(Gigabit PON) standard, which offers 2.488 Gbps bandwidth and direct support of both TDM(POTs & E1) and Ethernet traffic at the edge of the network with possible triple play voice, data and video services on the same PON. GPON can support ONUs that is located as far as 30 Km

from the OLT. GPON offer higher split ratio of 1: 32/64/128 which results in an OLT reduction by more than a factor of 2 over EPON.

1.5.4 WDM PON: Wavelength Division Multiplexing Passive Optical Network is the next generation in development of access networks. Ultimately, they can offer the largest bandwidth at the lowest cost. In principle, the architecture of WDM PON is similar to the architecture of the PON. The main difference is that multiple wavelengths operate on single fiber and ONUs operates on different wavelengths. Multiple wavelengths on single fiber enable either more bandwidth per each ONU or more ONUs per each distribution fiber [10].

Chapter 2 – Wavelength division multiplexing passive optical networks – WDM-PON

2.1 General description of WDM-PONs and its types

Wavelength division multiplexers (WDM) are passive devices that combine light signals with different wavelengths, coming from different fibers, into a single fiber. They include dense wavelength division multiplexers (DWDM), devices that use optical (analog) multiplexing techniques to increase the carrying capacity of fiber networks beyond levels that can be accomplished via time division multiplexing (TDM). Figure 2.1 shows the major parts of a generic WDM link. The start of a link (shown on the left) has a series of fixed or tunable laser sources and a multiplexing device for combining the independent light signals from the sources onto a single fiber. Within the link there may be optical amplifiers, add/drop multiplexers for inserting or subtracting individual wavelengths along the path, in the other words optical Add/Drop Multiplexers (OADMs) are used in wavelength-division multiplexing systems for multiplexing and routing fiber optic signals, and other devices to enhance the link performance. At the end of the link there is a demultiplexing device for separating the wavelengths into independent signal streams and an array of tunable optical receivers [11].

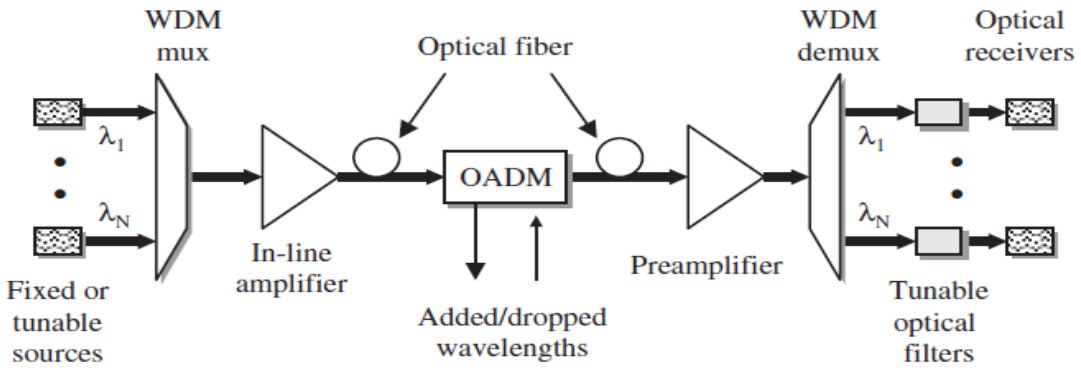

Fig.2.1. The major parts of a generic WDM link.

The two major types of WDM-PONs are coarse wavelength division multiplexing (CWDM)-PON and dense wavelength division multiplexing (DWDM)-PON.

2.1.1 CWDM-PON

Wavelength spacing of more than 20 nm is generally called coarse WDM (CWDM). Coarse wavelength division multiplexing (CWDM) is a method of combining multiple signals on laser beams at various wavelengths for transmission along fiber optic cables, such that the number of channels is from 4 to 8 wavelengths per fiber, sometimes more. The number of channels is fewer than in dense wavelength division multiplexes (DWDM) but more than in standard wavelength division multiplexing (WDM). Optical interfaces, which have been standardized for CWDM, can be found in ITU G.695, while the spectral grid for CWDM is defined in ITU G.694.2. If the complete wavelength range of 1271 nm to 1611 nm, as defined in ITU G.694.2, is used with 20 nm spacing, then a total 18 CWDM channels are available, as can be seen in figure 2.2. A low-water-peak fiber defined in ITU G.652 C & D, which eliminates power attenuation in the 1370–1410 nm range seen in a normal single-mode fiber, can be used for this wide spectrum of transmission.

The dispersion parameter in Fig.2.2 indicates signal broadening, and this factor may limit the transmission distance as the data rate becomes higher. Since strict tuning of wavelengths is not needed for the CWDM-PON, a thermal control part, called a thermo-electric cooler (TEC), is not required, making it cheaper than the DWDM-PON. Furthermore, the wavelength multiplexer with low channel crosstalk can be implemented easily for CWDM. It has been argued that the total system cost is 40% cheaper for the CWDM-PON.

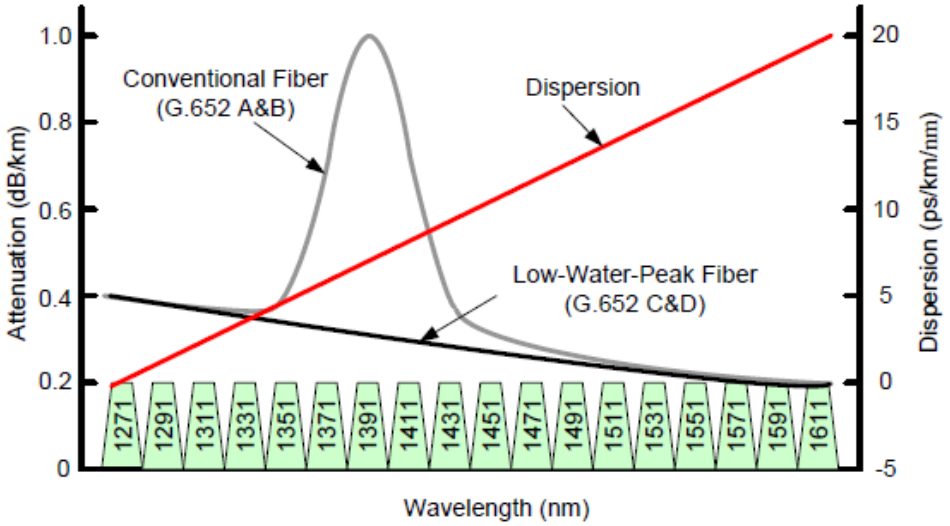

Fig.2.2 Wavelength assignment for CWDM.

The primary disadvantage of CWDM is that the number of channels is limited; therefore, the CWDM-PON lacks in scalability, especially when a normal single-mode fiber with water-peak attenuation range is used. Another disadvantage is that the shorter wavelength channels experience higher loss (see Fig.2.2), thereby limiting the transmission distance or splitting ratio. A brief example of the CWDM-PON can be found in the so-called "triple-play" PON service, where the 1550 nm wavelength channel is used for optional video CATV, the 1490 nm wavelength channel is used for downstream voice and data, while the 1331 nm wavelength channel is used for upstream transmission. An expanded application adopts 1360–1480 nm CWDM channels for premium business services, while usual triple-play services are provided to normal subscribers.

2.1.2 DWDM (wavelength division multiplexing)

Dense WDM (DWDM) has wavelength spacing that is far smaller than that of CWDM, typically less than 3.2 nm, because DWDM has been developed to transmit many wavelengths in a limited spectrum region where an erbium-doped fiber amplifier (EDFA) can be used. DWDM system supports up to hundred wavelengths.

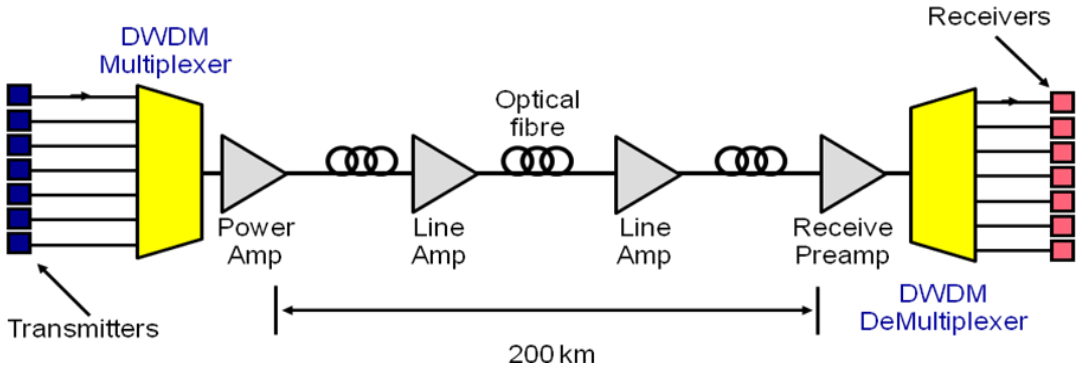

Fig.2.3 DWDM System

A DWDM-PON is expected to be very useful for providing enough bandwidth to many subscribers, and it is regarded as the ultimate PON system. ITU G.692 defines a laser grid for point-to-point WDM systems based on 100 GHz wavelength spacing with a center wavelength of 193.1 THz(1553.52 nm) over the frequency region of 196.1 THz(1528.77 nm) to 191.7 THz(1563.86 nm). This 100 GHz spacing has been applied to many DWDM systems. But 50 GHz spaced laser diodes (LDs) and filters are commercially available today, and they can be used to increase the number of channels. Also, wavelengths reaching up to 1600 nm have been used to exploit the cyclic property of the AWG, by having just one AWG at a remote node for demultiplexing and multiplexing in downstream and upstream directions, respectively. In a DWDM-PON, the wavelength of each optical source and the center wavelength of the WDM filter should be monitored and controlled carefully to avoid crosstalk between adjacent channels. Therefore, the DWDMPON costs more than the CWDM-PON in field deployment since it needs wavelength-tuned devices and temperature control [12]. CWDM has large wavelength spacing compared to the DWDM which has tight wavelength spacing where it fits more channels onto a single fiber, but cost more to implement and operate. DWDM came well before CWDM and CWDM appeared after a market need of technology with affordable prices. CWDM enables carriers to respond flexibly to customer needs in metropolitan regions, in other words the point and purpose of CWDM is short-range communications. Table 2.1 shows the comparison between CWDM and DWDM [13].

Table 2.1 Comparison between CWDM and DWDM [13]

CWDM	DWDM
Short-range communications	Long-haul transmissions
Uses wide-range frequencies	Narrow frequencies
Wavelengths spread far apart	Tightly packed wavelengths
Breaks the spectrum into big chunks	Dices the spectrum into small pieces
Light signal is not amplified	Signal amplification is used
Low cost compared to DWDM	High cost
Simple implementation	Complex implementation

2.2 WDM-PON Architecture

Although PON provides higher bandwidth than traditional copper-based access networks, and with the rapid development of the global communications market, especially with the rise of series of new services such as the internet , high quality video conferencing systems, and multimedia systems, etc, the demand for large capacity and high performance network transmission increases explosively. However traditional Synchronous Digital Hierarchy (SDH) and plesiochronous Digital Hierarchy (PDH) fiber optic transmission systems employ the one fiber one wave mode so that both the transmission capacity and capacity expansion mode cannot meet the requirements due to restrictions of the intrinsic characteristics of devices. Meanwhile, the huge broadband resources of optical fibers have not been completely utilized. So a new transmission technology WDM (wavelength division multiplexing) technology emerges as the most effective and economic way for capacity expansion of optical fibers, with its unique technological superiority, the WDM

technology becomes an approach to rapidly, simply, economically and effectively expands the capacity of the fiber.

WDM is a fiber optic communication technology, which enables multiple optical carrier waves bearing electrical information (analogue or digital) to be transmitted over a single optical fiber, so as to realize system capacity expansion. It combines (multiplex) several optical signals with different wavelength together for transmission and then after transmission separates (demultiplexers) the combined optical signals and sends them to different communication terminals [14]. The key system features of WDM are the following:

- ***Capacity upgrade:*** The classical application of WDM has been to upgrade the capacity of existing point-to-point fiber optic transmission links. If each wavelength supports an independent network channel of a few gigabits per second, then WDM can increase the capacity of a fiber system dramatically with each additional wavelength channel.
- ***Transparency:*** An important aspect of WDM is that each optical channel can carry any transmission format. Thus, by using different wavelengths, fast or slow asynchronous and synchronous digital data and analog information can be sent simultaneously, and independently, over the same fiber without the need for a common signal structure.
- ***Wavelength routing:*** Instead of using electronic means to switch optical signals at a node, a wavelength-routing network can provide a pure optical end-to-end connection between users. This is done by means of lightpaths that are routed and switched at intermediate nodes in the network. In some cases, lightpaths may be converted from one wavelength to another wavelength along their route [11].

WDM-PONs are becoming more affordable, making them an appealing way to provide more efficient, higher-bandwidth networks. Networking-service providers worldwide are facing important challenges. Labor and energy costs are rising. Competition among telecommunications companies-along with financial problems caused by the current economic climate-is cutting into subscriber revenues. Consequently, providers are looking

to save money by creating more efficient systems that increase data rates while reducing the amount of equipment and the number of network facilities required for operations and management. A promising solution to this challenge could be the relatively new wavelength-division-multiplexing passive optical networks (WDM-PONs). However the economic pressures are driving the growing demand for services like those that WDM-PONs provides. Competition for subscribers is driving down carriers' rates, reducing their customer bases, and decreasing the amount of revenue they earn per bit of data they transmit. Providers thus want to reduce costs while still offering enough bandwidth for desirable services such as high definition TV and very-high-speed DSL for Internet access. With optical technology becoming less expensive and easier to work with, carriers are starting to deploy PONs on a large scale. And the cost of the equipment necessary to add WDM to the technology has been dropping. This is also pushing providers to consider WDM-PON technology. The benefits using WDM-PONs promise to offer more network capacity and longer transmission ranges than their TDM-based counterparts. Another benefit is security because WDM-PONs route an entire wavelength to each recipient and thus data for one node doesn't pass through others. WDM-PONs is scalable. Users can change the multiplexers, they can utilize it to increase the number of wavelengths the network offers. They can change their central-office equipment or customers can change the equipment in their nodes to provide more bandwidth. The two major types of WDM-PONs are Coarse (CWDM)-PON and Dense WDM (DWDM)-PON [15].

The straightforward approach to build a WDM-PON is to employ a separate wavelength channel from the OLT to each ONU, for each of the upstream and downstream directions, as shown in Fig. 2.4. This approach creates a point-to-point link between the CO and each ONU. In the WDM-PON of Fig. 2.4, each ONU can operate at a rate up to the full bit rate of a wavelength channel. Moreover, different wavelengths may be operated at different bit rates, if necessary; hence, different varieties of services may be supported over the same network. In other words, different sets of wavelengths may be used to support different independent PON sub-networks, all operating over the same fiber infrastructure.

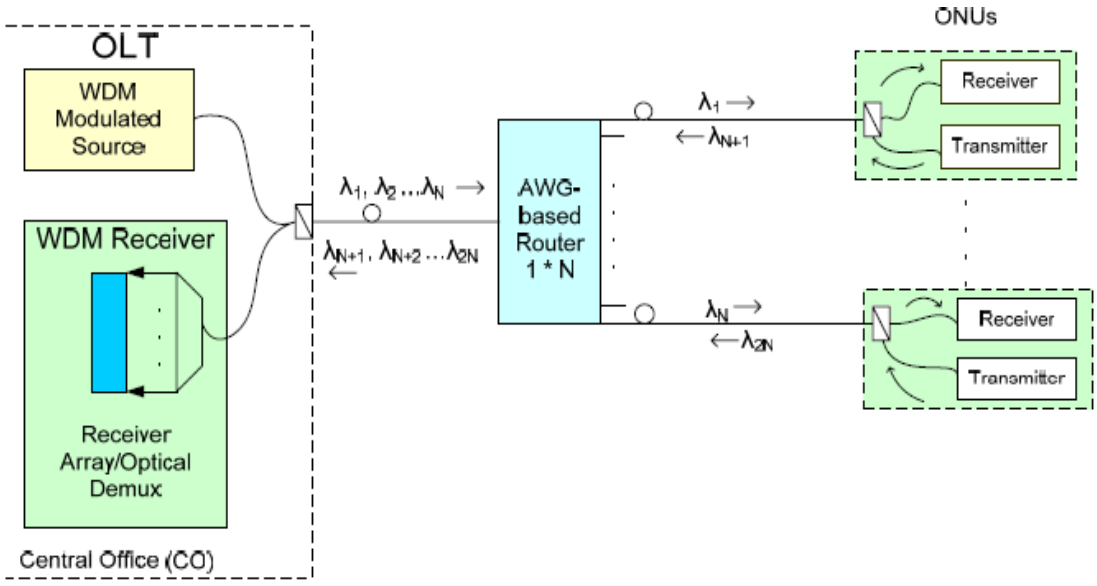

Fig.2.4 WDM-PONs architecture.

In the downstream direction of the WDM-PON (Fig. 2.4), the wavelength channels are routed from the OLT to the ONUs by a passive arrayed waveguide grating (AWG) router, which is deployed at a "remote node" (RN). The AWG is a passive optical device with the special property of periodicity, which is the cyclic nature by which multiple spectral orders are routed to the same output port from an input port. This allows for spatial reuse of the wavelength channels. A multi wavelength source at the OLT is used for transmitting multiple wavelengths to the various ONUs [12].

As mentioned before, In WDM-PON, the optical power splitter is replaced by a wavelength splitting component, e.g. AWG, Instead of optical power splitter is used in TDM PON, which is used to route various wavelength channels to different ONUs. Currently, AWGs are being developed greatly because of their wide application in WDM optical networking system, such as (de)multiplexing, routing, and multicasting [16].

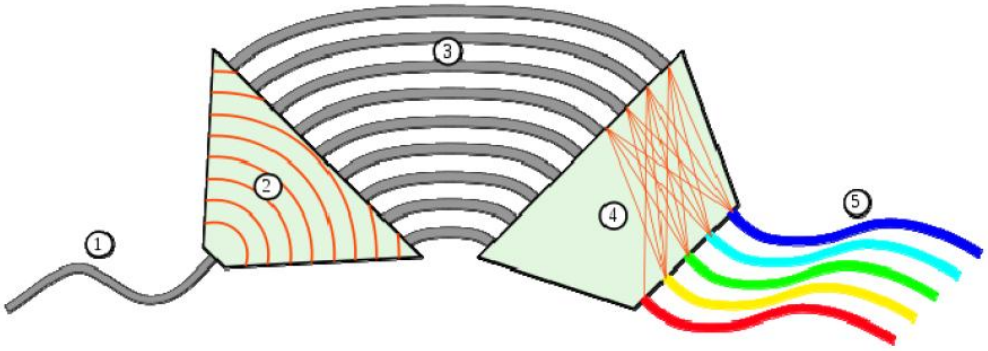

Fig.2.5 The structure of an arrayed waveguide grating (AWG) [17]

For the upstream direction, the OLT employs a WDM demultiplexer along with a receiver array for receiving the upstream signals. Each ONU is equipped with a transmitter and receiver for receiving and transmitting on its respective wavelengths. In this example, the downstream and upstream transmissions occur in different wavelength windows, and these windows are separated using coarse WDM (CWDM). Within each window, the wavelengths are further separated using dense WDM (WDM) [12].

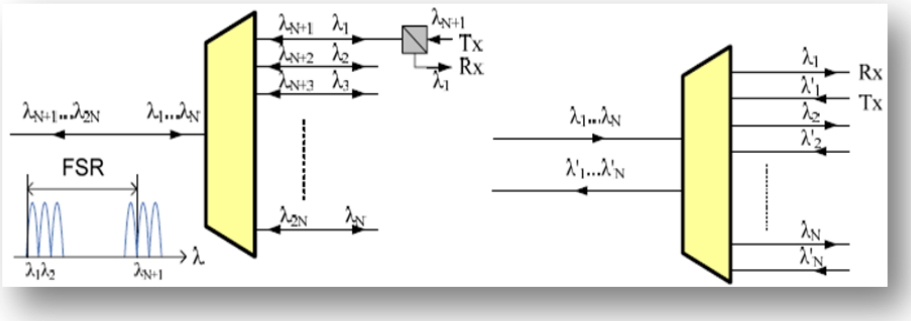

Fig.2.6 RN based on the cyclic wavelength property of the AWG: (a) bidirectional transceiver at the ONU, and (b) unidirectional transceiver at the ONU.

Instead of using a splitter, a WDM-PONs use an optical multiplexer to passively refract light waves and route each wavelength of light in a trunk fiber down a separate smaller fiber to the appropriate recipient node, For traffic that individual customers send out, the multiplexer couples the light from the multiple transmissions into the trunk fiber.

WDM-PONs use either AWGs or thin film filters as multiplexers to redirect and route each wavelength of light to the appropriate recipient node [15].

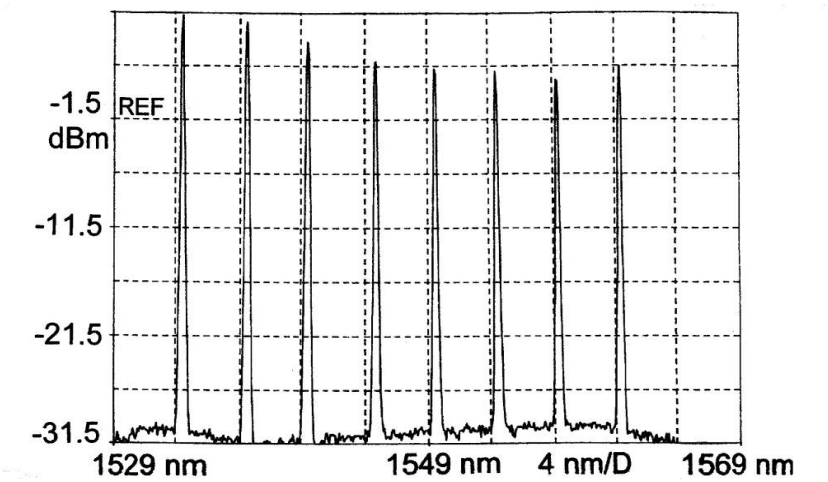

Fig.2.7 Multiplexer Optical Output Spectrum

2.3. WDM-PON Device Characteristics and Options

2.3. A. Wavelength Options

A WDM-PON designer must decide on the appropriate wavelengths and their spacing, based on which the selection of devices may differ significantly. In the previous subsections, 2.1.1 and 2.1.2 the two major CWDM and DWDM are described. In the following subsections, characteristics of the devices used in WDM-PONS are described.

2.3. B. Transmitter Options

Optical sources are classified into four groups depending on the way wavelengths are generated. These are a wavelength-specified source, a multiple wavelength source, a wavelength-selection-free source, and a shared source. The multiple-wavelength source is

applicable only to the OLT, the shared source is applicable to the ONU, and the remaining two are applicable to both OLT and ONUs.

2.3. B. 1. Wavelength-specified source

This optical source emits a fixed wavelength from each component. A wavelength monitoring circuit and a controller for each component are usually needed to tune the source to a required wavelength. A common distributed feedback (DFB) / distributed Bragg reflector (DBR) laser diode, vertical-cavity surface-emitting laser (VCSEL) diodes, and tunable-lasers diode can categorized into this groups.

- **Distributed Feedback (DFB) Laser Diode (LD)**

As a most common scheme for obtaining a single optical longitudinal mode, distributed Bragg gratings are etched inside the cavity of a DFB LD, which allows only the wavelength-matching gratings to be lasing [18]. If the grating is outside the cavity, it is called a distributed Bragg reflector (DBR) LD. Since there may occur a wavelength shift of ~ 0.1 nm/°C, these LDs usually require a thermoelectric cooler (TEC) for stable operation as a WDM source. In addition, a wavelength locker, which helps the LD to lock exactly to its assigned wavelength, is needed. The DFB LD can be modulated directly for a WDM-PON deployment, where the distance is often less than 20 km. And it has good high-speed modulation property because of its narrow linewidth of less than a few MHz. In spite of all these advantages, the DFB-LD is regarded as a costly way to implement a WDM-PON because a number of DFB LDs would usually be required, and each of them should be managed separately.

- **Vertical-Cavity Surface-Emitting Laser (VCSEL) Diodes**

VCSEL has the potential for low-cost mass production since the entire cavity can be grown with one-step epitaxy on a GaAs substrate, which makes manufacturing and testing easy [19]. VCSELs with 850 nm and 1310 nm wavelengths are commercially available and widely used for LAN applications.

However, the VCSEL at 1550 nm wavelength is at its early stage of development because of poor optical and thermal properties of the laser material. Although it cannot be used as a

WDM-PON source today, it can be adopted as an upstream source in a composite PON (CPON). If this source in the 1550 nm DWDM range becomes stable and cheap, it will be a strong candidate for potential integration with other electronics.

- **Tunable Lasers**

To keep in the inventory all different wavelength lasers needed for each channel of a WDM-PON and to install different lasers at each home is costly and not easy to maintain. In this sense, the tunable laser is attractive if it can be used for several WDM channels. The following types of principles are provided.

A mechanical-type laser, also called an external-cavity laser, is implemented by external grating or Fabry–Perot (FP) cavity, which is controlled mechanically. Because of its wide tuning range of up to 500 nm and good wavelength accuracy, it can be used for instrumentation purpose. However, the external-cavity tunable laser requires an external modulator for high-speed modulation because of its long cavity length. Also, the lack of long-term stability hinders the tunable laser's application for telecommunications [12].

A thermally tunable DFB uses the wavelength-shift property of the DFB-LD because of its cavity-index change with temperature. With the aid of optimized thermal design and temperature controllability over a wide range, the wavelength change of the thermally tunable DFB reaches up to 4 nm [20]. This LD's tuning time is long, sometimes up to a few seconds. Thus, this type of LD is not good for an architecture where fast switching is required. However, this LD can be useful for WDM-PON transmitters with fixed wavelength. Based on this scheme, commercial tunable products over multiple (e.g., eight) adjacent ITU DWDM channels have appeared [21, 22]. This eliminates the need to reserve all different wavelengths of DFB LDs for each WDM-PON transmitter.

The tuning time of the DFB/DBR LD is reduced effectively by adjusting the injection current into one or more sections of the LD cavity. Injected carriers change the effective refractive index within the optical cavity, leading to a wavelength change. The tuning time is of the order of nanoseconds, which is the fastest known thus far. Since the maximum index change is about 1%, the maximum tuning range in the wavelength region of our interest is about 10–15 nm [23]. The drawback of this laser is that it is susceptible to

mode hopping and mode competition [24] because of multiple electrodes on a laser cavity required for current injection, which degrades the transmission performance [18, 23].

2.3. B. 2. Multiple-wavelength sources

Individual-wavelength-specified sources are not convenient for use in the OLT of a WDM-PON, because they require many optical sources set to their own wavelengths. If a component generates multiple wavelengths at the same time, it will be very useful for the OLT. Several WDM channels, integrated in a compact device, can be tuned simultaneously. Three types of such multiple sources, which have been proposed in the literature, are shown below.

- **Multi frequency Laser (MFL)**

An AWG and amplifier arrays are integrated in this device for wavelength selection and its amplification, respectively, as shown in Fig.2.8 [24, 25]. Mirrors on cleaved facets define an optical cavity of the laser-diode modules. If the AWG is tuned, it changes whole output wavelengths. A device integrating 18 WDM channels was implemented using this scheme [26]. It can also be used as a tunable LD by turning on each amplifier. Although direct modulation is possible with this device, there is a modulation rate limit because of its long laser cavity.

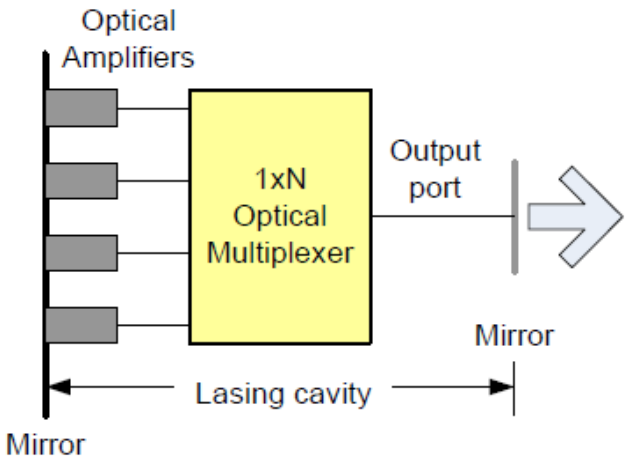

Fig.2.8. Structure of a multi frequency laser [25].

- **Gain-Coupled DFB LD Array**

Another possible way of integrating multiple wavelength sources is to implement DFB LD arrays by combining a gain-coupling mechanism and a tuning capability in one LD module [27]. Thin-film resistors are integrated for tuning wavelengths by controlling the temperature. The advantages are compact size and high speed modulation. But it is difficult to accurately maintain every channel at the correct wavelength, since each lasing wavelength is determined by an independent filter. Considering that different types of gratings are etched inside a chip, this scheme is more realizable for a small number of channels.

- **Chirped-Pulse WDM**

Source a short-pulse generator followed by a roll of fiber can work as a WDM source, as illustrated in Fig.2.9 [28]. A 100 fs Gaussian pulse from a mode locked erbium fiber laser provides 4.4 THz spectral bandwidth, enough for 44 WDM channels at 100 GHz spacing. A fiber roll provides fiber dispersion to this pulse, which broadens it temporally. If this pulse is modulated and then is provided to a following WDM splitter, different channels carrying their own information will come out of different ports. Since each generated pulse is divided into all ONU channels, the number of channels is limited by the ratio of the data-modulation frequency to the repetition rate of the laser. Therefore, this method is better for applications where data rates in each channel are rather low (or modest), but many WDM channels are required. The problems of aligning pulse width, temporal width, and WDM free spectral range (FSR) may be the difficulties that should be solved before the commercial viability of this solution.

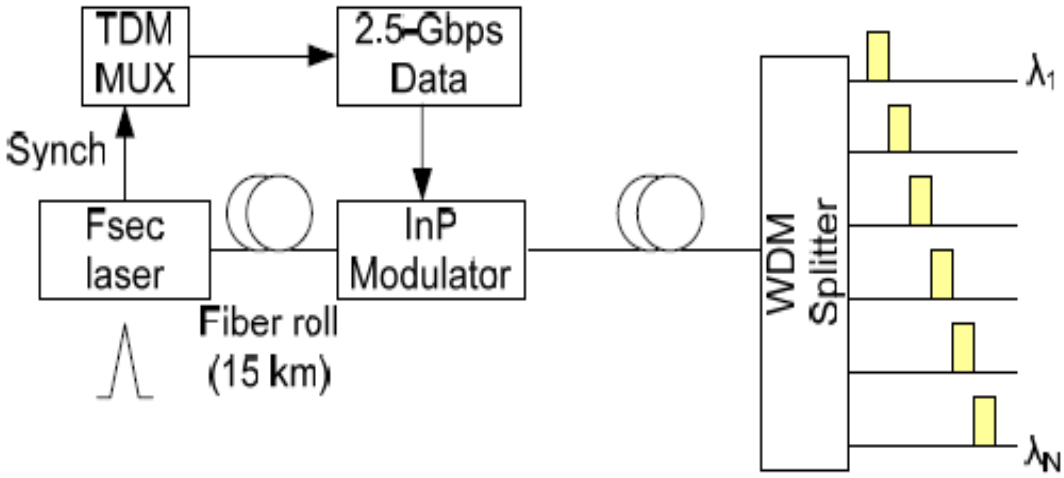

Fig.2.9. Chirped-pulse WDM source for the OLT [28].

2.3. B. 3. Wavelength-selection-free source

In this type of source, the wavelength is decided not by itself, but by external factors such as a filter or injection signal. Sometimes, the wavelength of the source drifts with the ambient temperature, aging effect, or circuit malfunction. The management of each ONU, whose wavelength is unique in a PON group, is not easy because of the difficulty of finding its exact reference wavelength.

A wavelength-selection-free source can help such sources to operate free from the wavelength-tuning problem because the wavelengths are determined less by the environmentally sensitive external factors such as optical filters or injected signals.

- **Spectrum-Sliced Source**

By slicing the spectrum of a broadband optical source with a narrowband optical filter, a unique wavelength for each WDM channel is achieved. Several combinations of broadband optical source and filter have been tried. For example, the super-luminescent light emitting diode (LED) [29], EDFA [30, 31] and FP LD [32] have been used for optical sources, while AWG and FP filters have been used for optical filters. Since only a narrow spectrum part of the original source is used, this source usually lacks power, requiring an optical amplifier. This method also has a limitation on the modulation speed because of

several sources of noise such as mode-partition noise, intensity noise, and optical beat noise, which are inherent properties of multimode or broadband sources.

- **Injection-Locked Laser**

A multimode laser, such as FP LD, has the property that it excites only one mode when a well-adjusted external optical signal is coming in [33]. Careful control of the modulation index, laser bias current, and power of the external optical excitation are required to increase the efficiency of the locking [34]. FP LDs locked to externally injected, spectrum-sliced broadband light sources (BLS) were field tested for commercial use. Antireflection coating on the front facet of the laser is added to increase the injection efficiency. Cavity length is increased to have at least one lasing mode within the bandwidth of the injected amplified spontaneous emission (ASE). This method generates 32 WDM channels at the same time.

A maximum power difference of 7 dB was reported among channels as the injected wavelength deviated from the lasing wavelength or from the envelope peak of the FP LD. It is difficult to increase the data rate but this laser shows better performance than the spectrum-sliced multimode source.

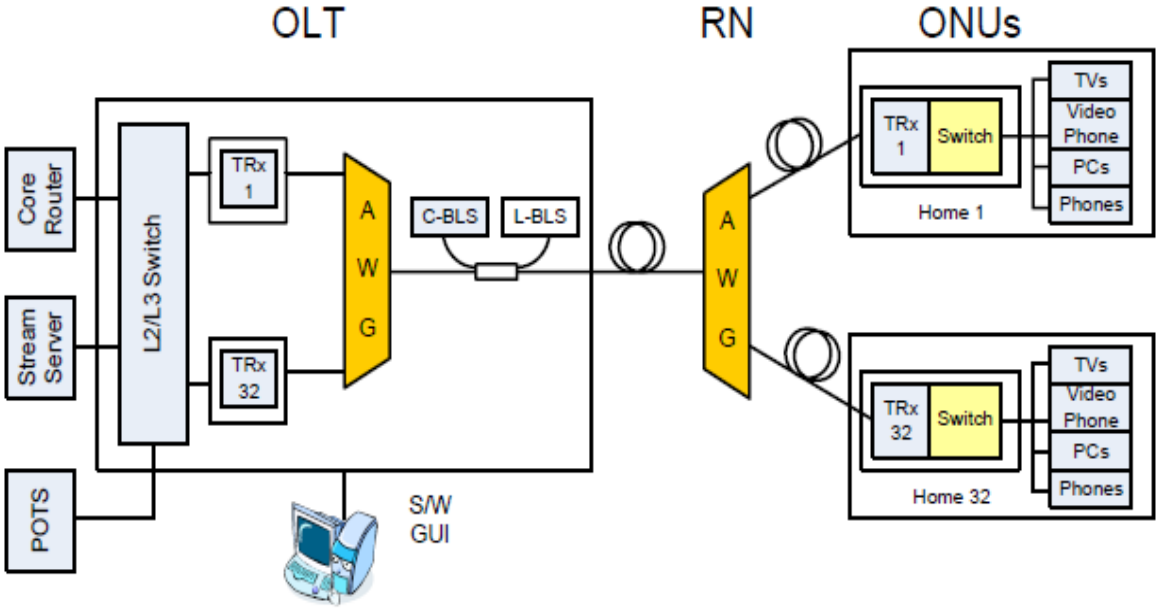

Fig.2.10. Field trial of a WDM-PON based on injection-locked LD scheme [35].

The large scale computer networks needed to support growing web applications require fast and reliable interconnections in order to provide rapid access to information and services to millions of users. As the number of interconnected servers and storage media increases, optical technologies are expected to play a major role due to the high speed, low loss and small foot print of optical fiber communication links. The next generation of optical networks requires efficient, densely packed wavelength division multiple access (WDM) channels to transmit massive amounts of information. An important challenge is the cost and the wavelength versatility of WDM transmitters [36]. An Injection-locked laser has been proposed as a cost-effective solution for WDM transmission.

Most modern WDM-PON systems now rely on a laser-injection locking technique, which allows relatively inexpensive Fabry-Perot-type lasers to operate at virtually any desired wavelength. Every laser has a certain range of wavelengths, or "gain profile", over which it can transmit. If a laser is directly modulated it will transmit data at whatever wavelength within its gain profile has the most feedback. This feedback may be internal, such as that from a grating in a high-performance DFB laser, or it may come from an external reflector. Injection locking is a way to force a laser to operate at a particular wavelength by providing it with a wavelength locking signal, or "seed" wavelength, which is effectively an artificial feedback signal that locks the laser to the desired wavelength. When used in this configuration, these externally seeded lasers are called reflective semiconductor optical amplifiers (R-SOAs) [37].

2.3. B. 4. Shared source (or Loop-Back Source) for ONU

Some researchers have tried to eliminate optical sources at the ONU, because it is risky and costly to let each ONU manage the ONU’s transmission wavelength. If one of them deviates from the assigned wavelength, the deviated channel may degrade not only itself but also its adjacent channels. As a solution, all optical sources are proposed to be provided from the OLT, and the ONU just modulates the provided unmodulated optical source. Sometimes, even one wavelength channel can be used in both directions, leading to

the so-called shared-source solution, by modulating only a partial temporal region for downstream and leaving unmodulated the remaining region for upstream. Two types of modulator-external modulator and semiconductor optical amplifier (SOA)-have been used for this purpose [12].

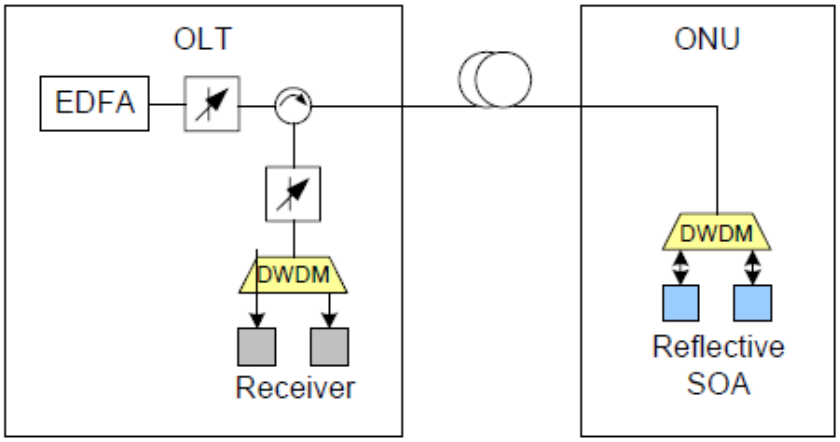

Fig.2.11. Shared source using a reflective SOA [38].

2.3. C. Receiver Options

A receiver module consists of a photo detector (PD) and its accompanying electronics for signal recovery. Common PDs are positive-intrinsic-negative (PIN) and avalanche photodiode (APD), which find different applications according to the required sensitivity.

Electronic parts, usually composed of preamplifier, main amplifier, and clock and data recovery circuits (CDRs), depend on the protocol used on each wavelength. Since each wavelength can work separately in a WDM-PON, each receiver can be configured differently [12].

- **Photodiodes**

The power of the optical signal that reaches a receiver module is determined by its transmission distance and splitting ratio. If the WDM-PON is used in a multistage structure, the received power will become smaller. Therefore, caution should be paid to these

sensitivity options. A PIN-type PD, so called because it is composed of P-doped, intrinsic, and N-doped semiconductors, is very common because of its simple structure, ease of use, and low cost. Its sensitivity, or the required optical power, is not good because it does not have any amplification procedure in itself. As transmission loss becomes larger and the received optical power does not satisfy the receiver sensitivity of the PIN PD, it should be replaced with an APD that has ~10 dB higher sensitivity at the cost of a higher price. The better performance originates from its internal amplification process called the avalanche effect. Various combinations of LDs and PDs may be taken into consideration. If a high power OLT is used, then a cheap PIN PD can potentially be a better candidate at the ONU. But, for the upstream case, having a high-power source at each ONU may be quite costly. Therefore, to have an APD at the OLT with a low-power ONU can be a better solution [12].

- **Recovery Circuits**

A WDM-PON is transparent to the protocols or signals, meaning that it can carry any kind of signal format. Various kinds of transmission protocol, such as EPON, BPON, Ethernet, SONET and others, can use a WDM-PON as their physical layer. But receivers at the OLT and the ONU should satisfy the specification required by the adopted protocol. If multiple ONUs of a WDM-PON share one wavelength using EPON's multipoint control protocol (MPCP), which makes each ONU transmit data in its assigned time slot, the OLT receiver must recover data from signals with different amplitudes and phases (so-called burst-mode signals) coming from several ONUs, as specified in IEEE 802.3ah, while normal constant mode receiver circuits are used in each ONU because the downstream signal is continuous. But, in a WDM-PON, where each unique pair of OLT and ONU is connected by one wavelength, a burst-mode receiver is not needed anymore [12].

2.3. D. RN (Remote Node) Options

The remote node (RN) in a PON can be made of either a power splitter or a passive wavelength router. A power splitter distributes all incoming signals evenly into all output ports, requiring a wavelength filter at each ONU. Insertion loss, uniformity, return loss, and

operating temperature are important features for its selection. Although the splitter is a simple, low-cost, distribution structure, it requires optical filters with different center wavelengths at ONUs. Also, more signal loss occurs with a splitter than with a wavelength router. The AWG has been a successful device in WDM industry. It has been used in many Long-distance WDM systems as a multiplexer/demultiplexer and as an add-drop multiplexer (ADM).

There is another common scheme for multiplexing/demultiplexing wavelengths, called thin-film filters or multilayer interference filters. By positioning cascaded filters in the optical path, wavelengths can be demultiplexed, and vice versa. Each filter is designed to transmit a unique wavelength while reflecting others. This type of filter is better for CWDM while AWG is good for implementing large channel counts. And there is a new type of wavelength router, called a bulk grating, has been suggested for use in a DWDM system [12].

2.4 Overview of WDM-PON technology and solutions

Most of the Fiber-to-the-Home deployments in recent years have been based on industry standard technologies such as Gigabit Ethernet Passive Optical Networks (GEPON) and Gigabit PON (GPON). The success of these deployments has led to significant innovation in both system architecture and the components that are used to build these systems, and the next generation of passive optical networks will inevitably be far more advanced than what is typically deployed today.

At the forefront of PON development there have been two separate approaches that appear to compete for next-generation systems: 10 Gbps PON (be it 10G EPON or 10G GPON), and WDM-PON. Each approach has its own advantages and its own issues, but the progress with both new technologies has accelerated in recent years. Here we will focus on WDM-PON, and examine some of the challenges and new technologies that are making this technology a very viable competitor for next-generation platforms. While WDM-PON has already had early success in Korea, its adoption in other parts of the world has been slowed by relatively high costs compared to GEPON and GPON technologies. That seems

to be changing as WDM-PON competes head-to-head with 10G PON and Point-to-Point systems for next-generation FTTH deployments.

The system architecture in a WDM-PON network is not significantly different from that of a more traditional GEPON or GPON system, although exactly how the network operates is entirely different. And the end result of WDM-PON is a wavelength to each subscriber.

That is contrary to more traditional PON architectures where one optical feed is shared among 32 or more users. In that case each home operates at the same wavelength, and is allotted a $1/32^{nd}$ time slot on the main fiber. In WDM-PON each home is assigned its own wavelength and has continual use of the fiber at that wavelength. A very high-level view of a WDM-PON network is illustrated in Fig. 2.12.

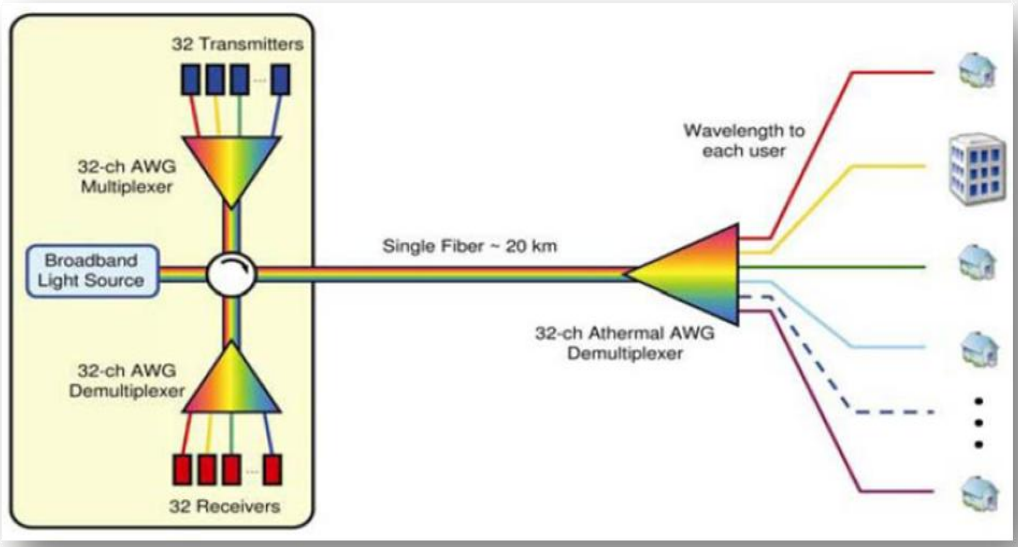

Fig.2.12 Schematic representation of a simplified WDM-PON system

In a standard PON system, a single fiber runs from the central office to a neighborhood, at which point a passive 1x32 splitter splits the optical signal to 32 different homes. Virtually all PON technologies rely on some form of wavelength division multiplexing (WDM) to enable bi-directional communications. For example, in a typical GPON system, the upstream communication runs at 1310 nm wavelength, while the

downstream traffic runs at 1490 nm. A third wavelength at 1550 nm is used for video overlay. So the utilization of WDM in PON systems is already very commonplace. However in a typical GPON or GEPON system all subscribers use those same common wavelengths. This means they have to share the fiber infrastructure, which is done through time division multiplexing (TDM). Each of those 32 homes transmits over the same fiber, but the time in which they are allowed to "occupy" the fiber is allocated by the optical line terminal (OLT) at the central office. While the equipment in each home is capable of transmitting at over 1,250 Mbps, it can only do so during its allotted time on the fiber, and therefore it is not uncommon for each subscriber in a legacy PON system to only achieve sustained data rates of around 30 Mbps. This concept of many users sharing a common fiber helps minimize the fiber infrastructure required in an FTTH deployment. However, this sharing of fiber is one of the main factors limiting higher data rates to subscribers. WDM-PON allows for effectively the same fiber infrastructure to be used, while allowing each subscriber to access the full 1,250 Mbps available to them. There are several changes to the network that are required to enable that change. The first requires that the passive 1x32 power splitters be replaced by passive 1x32 channel demultiplexers, typically a thermal arrayed waveguide gratings (AWGs), as shown in Fig. 2.4. This allows for 32 different wavelengths to be transmitted down the common fiber, and then each home is allocated its own wavelength.

There are several advantages to the WDM-PON architecture over more traditional PON systems. Foremost of course is the bandwidth available to each subscriber. Second, WDM-PON networks can typically provide better security and scalability, since each home only receives its own wavelength. Third, the MAC layer in a WDM-PON is simplified, since WDM-PON provides Point-to-Point (P2P) connections between OLT and ONT, and does not require the Point-to-Multipoint (P2MP) media access controllers found in other PON networks. Finally, each wavelength in a WDM-PON network is effectively a P2P link, allowing each link to run a different speed and protocol for maximum flexibility and pay-as-you-grow upgrades.

The main challenge with WDM-PON is cost. Since each subscriber is assigned his own wavelength this suggests that the OLT must transmit on 32 different wavelengths versus one shared wavelength as found in more traditional PON systems. Likewise, it requires that each of the 32 homes on a link operate at a separate wavelength suggesting that every ONT requires an expensive tunable laser that can be tuned to the correct wavelength for a particular home. This would be very cost prohibitive, particularly in initial set-up costs, and was a major hurdle in early design of WDM-PON systems [37].

Chapter 3 – Injection-locked transmitters in WDM-PON

Wavelength division multiplexed-passive optical network (WDM-PON) is a promising solution for the future high speed access networks such as fiber to the home or fiber to the office by the reasons of large capacity, network security, protocol transparency and upgradability. However, because of the relatively expensive WDM components, the WDM-PON has been considered a next generation solution. WDM-PON typically requires high-cost optical source in the optical network unit (ONU), which become a big bottleneck for a commercial deployment. In order to overcome this problem, it was found that a technique called optical injection locking can drastically improve the performance of a optical transmitter. Optical injection-locking uses a second laser (referred to as the master laser) to inject photons at a similar wavelength into the cavity of the transmitter laser (referred to as the slave laser). The slave laser is thus locked (in wavelength and phase) to the master due to the coherent non-linear interaction inside the laser cavity. The advantage of injection locking is that the slave laser characteristics may change fundamentally, resulting in a far better device performance, achieving large signal modulation at a far higher frequency than achieved today [39].

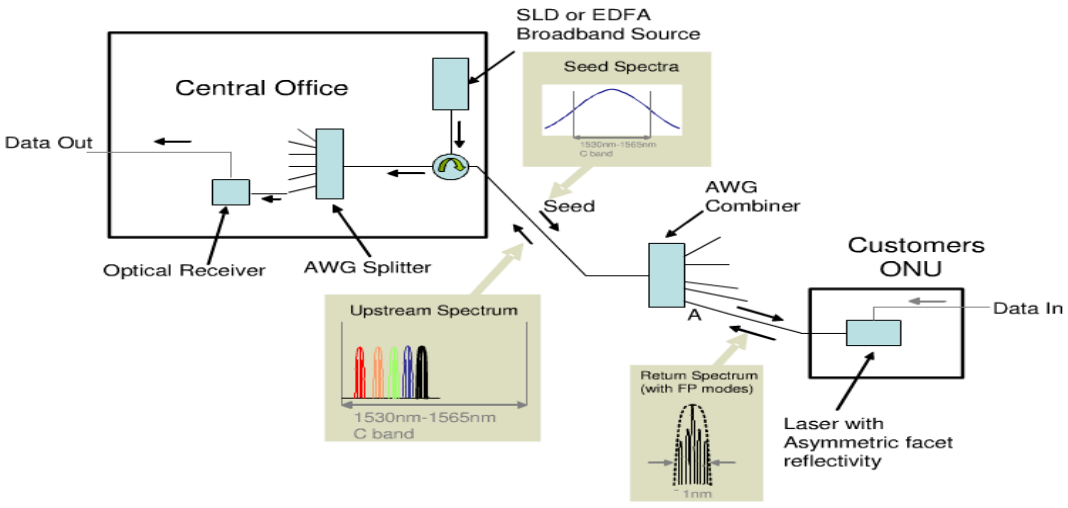

Fig.3.1 WDM-PON with Injection locked FP as ONU transmitter

3.1 Application of injection-locking in optical communications and optical signal processing.

Injection locking is an advanced technique with many applications in the fields of optical communication and optical signal processing. Injection locking of semiconductor lasers can provide an excellent transmitter for high speed optical communication and a candidate for chaotic signals. The effects of injection locking mainly have two aspects: one is to improve the characteristics of the slave and the other is to synchronize the master and the slave. Some recent applications of injection locking are related to the next-generation of wavelength-division-multiplexed passive optical networks, in which upstream transmission from an optical network unit to the central office is achieved by an injection-locked (IL) transmitter [40,41] instead of a more expensive tunable laser. As an example, in our thesis the theoretical and experimental investigations have proved that the modulation response of IL lasers can be significantly improved compared to the free-running lasers [42]. In addition, the technique of injection-locking can ensure single-mode operation, reduce the linewidth of a free-running laser and eliminate mode partition noise, mode hopping and frequency chirp from modulated lasers [42]. These improvements include increasing the modulation bandwidth. One method of reducing the non-linearity of laser diodes is the use of external injection into the directly modulated laser from a second laser source. Under external injection conditions the relaxation frequency of the laser may be increased significantly, and the modulation response at lower frequencies can be made significantly more linear than that without external injection. This helps to greatly reduce IMD problems. The exact alteration in the modulation response of the laser under external injection conditions is dependent on both the injected power and the detuning between the master and slave laser, and by varying these two parameters it is feasible to optimize the lasers modulation response for different applications [43].

Several applications have arisen from the injection- locking technique, including radio-over-fiber (ROF), ROF technique has been considered as a promising way for the applications to combine optical and wireless communications. In ROF transport systems,

light injection technique plays an important role to improve system performance, such as increasing the resonance frequency and side-mode suppression ratio (SMSR) of semiconductor laser diode, as well as reducing the threshold current and chirp of one. Here we find that how external light injection- into a directly modulated laser diode may be used to enhance the performance of a multi-channel radio over fiber system. Broadband wireless networks using a radio over fiber architecture to provide wireless connectivity to their users. In this architecture, data signals are generated at a central station (CS), modulated onto an optical carrier, sent over optical fiber to many base stations (BSs), and then transmitted over the air to users.

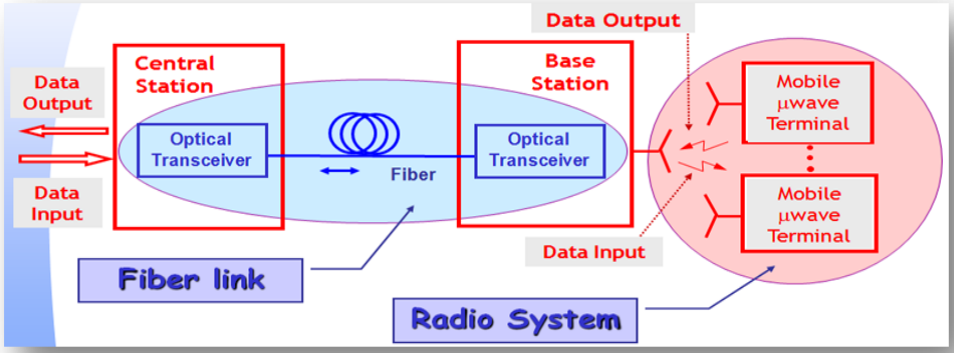

Fig.3.2 RoF–Basic Structure of System

This type of system is extremely cost efficient because it reduces the complexity of the many BSs which must be deployed by having most of the complex processing equipment at the CS. It is expected these broadband hybrid radio over fiber systems will divide the available radio spectrum into a number of channels for broadcast. The major problem that may be encountered in these networks will be nonlinearity problems in the various devices used [43].

The needs of high speed internet service have been increased gradually. Interests of internet service changed to image from voice and text, and there are many high speeds needing internet service like Internet Protocol TV (IPTV). To satisfy the needs of these trends, wavelength division multiplexing-passive optical network (WDM-PON) system is

considered as an attractive next generation optical access network system and there are a lot of researches on WDM-PON system. WDM-PON system can provide large data and high security, and needs simple protocol compared to existing system using an Ethernet or an asynchronous transfer mode (ATM) [44]. Recently, a reflective semiconductor optical amplifier (RSOA) is spotlighted as a device for the upstream re-modulation which makes the system cost-effective because of the absence of additional optical source in optical network unit (ONU). Also, to construct a WDM system with the same device in every ONU, colorless PON systems very important. a RSOA system using wavelength reusing technique comes into spotlight for the WDM-PON system [45, 46]. This system does not need other optical source for transmission of uplink signal because of using re-modulation of downlink signal. However, there are several disadvantages in this system. First of all, frequency response of RSOA is limited. Previously commercialized RSOA has below 2.5 GHz 3 dB frequency response [47].

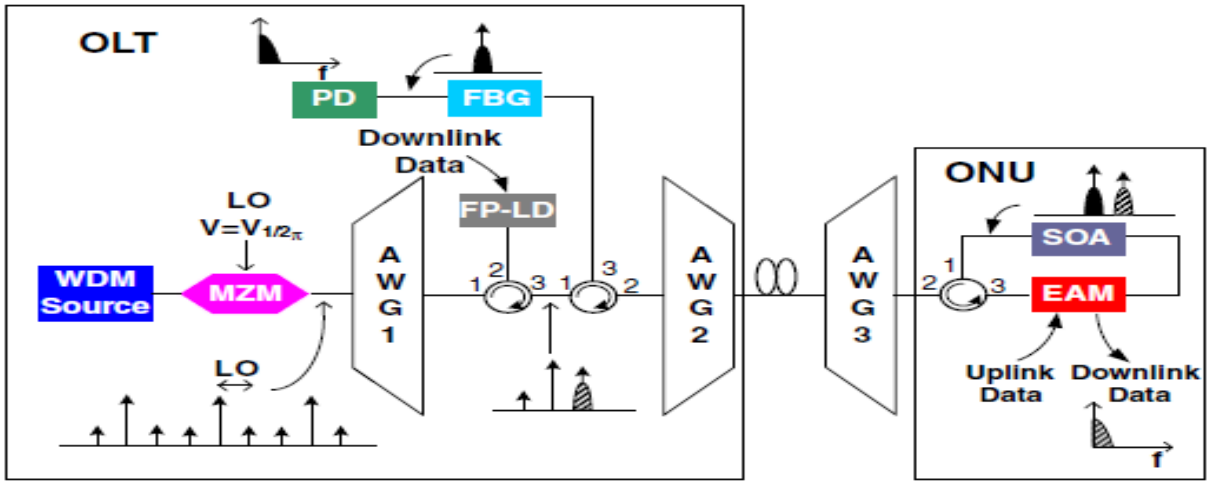

Fig.3.3 Schematic of proposed bidirectional WDM system.

Recently, the RSOA which can modulate 10-Gbps data has been developed and reported [48]. However, compared with external modulators such as the Mach–Zehnder modulator (MZM) and electro-absorption Modulator (EAM), a RSOA has a limited modulation speed extension. When the needs of large data transmission are increased, the system using RSOA cannot guarantee high speed internet service. Moreover, because

RSOA uses re-modulation technique of downlink signal, downlink signal affects uplink signal [49]. In the RSOA, downlink signal is erased by self gain modulation in the gain saturation region.

However, when extinction ratio (ER) of downlink is high, downlink signal cannot be fully erased. So the ER of downlink signal cannot be increased easily.
It has been suggested a novel colorless WDM-PON system using injection locking and electro-absorption transceiver (EAT). By using injection locking, side carrier of the double side band (DSB) is modulated by downlink signal [50]. EAM functions as both detector and modulator, simultaneously [51, 52]. So the uplink data rate could be increased and there are no serious downlink signal effects to uplink signal. And, because polarization sensitivity of EAM is very low, polarization control is not needed. Furthermore, we can construct a single EAT chip as ONU. We experimentally demonstrate bidirectional data transmission over 23 km standard single mode fiber (SSMF) to verify the proposed system.

Light wave transport systems have been developed with high expectations for future communications due to such advantages of optical fiber with low transmission loss and large bandwidth, as well as transparent characteristics for signal transmission [53–55]. However, light wave transport systems for very-short-reach (VSR) end user applications have not been addressed. With the rapid development of information technology, the increasing demands for broadband services raise the needs for high bandwidth, not only for the single-mode fiber (SMF)-based primary networks, but also for the plastic optical fiber (POF)-based in-house ones. SMF, in particular, has already established an undisputable position to distribute high quality signals. As a widespread medium, SMF offers better performances than POF in terms of attenuation and dispersion. However, when the SMF is deployed toward in-house networks, installation cost and convenience are concerned issues needed to be solved. The SMF with relative much smaller core size requires trained persons, high precision devices, and higher cost to install and maintain. POF alternatively has much larger core size, relative smaller bending radius, and easier to be installed characteristics. In result, the in-house connection becomes a critical bottleneck to

successfully deliver high quality signals from the central office (CO) to the client premises. To overcome the challenge, a new kind of in-house network medium is required to replace the existed coaxial cable or twisted pair. Recently, graded-index POF (GI-POF) has been developed with good transmission performance and lower cost [56, 57].

This flash product is a promising candidate to solve the fiber-to-the-home (FTTH) last mile problem. Clear advantages are offered by using the GI-POF for in-house networks: its large core diameter and small bending radius considerably eases coupling and splicing, as well as its ductility and flexibility simplifies installation in customer locations [58–60]. As a result, GI-POF is an ideal medium to integrate fiber backbone networks and in-house ones.

The explosive increase in network traffic has led to a need for high-speed signal processing. Recently, a photonic network based on optical signal processing has attracted much attention. The key components of optical signal processing are optical buffers and compact, high-speed memories with low power consumption. A bistable laser is an attractive candidate for an optical memory because of its compactness, low switching power, and stable switching without holding power. In previous studies, various types of bistable lasers have been demonstrated. A bistable laser using two polarized lights from vertical-cavity surface emitting lasers (VCSEL) was applied to all-optical 4-bit buffer memories with a shift register function [61], [62]. To reduce the number of optical components, planar semiconductor optical devices would be advantageous for large-scale integrated optical memories. Waveguide-based bistable lasers with storable absorbers using a multimode-interferometer (MMI) [63], and a master-slave type coupled micro-cavity laser [64] have been demonstrated. In this application, the optical flip-flop operation of a distributed Bragg reflector (DBR) laser using side mode injection locking [50]. Laser injection locking has been demonstrated in a Fabry–Pérot laser and a distributed feedback (DFB) laser [65], [66]. However, flip-flop operation has not been demonstrated since the lasing spectrum returns to its initial state once the input light is removed. They focused here on the mode suppression induced by spectral hole burning between two longitudinal modes to realize stable bistable operation. Since the optical memory can be controlled by the operating wavelength, access to each memory in a photonic integrated circuit becomes easy

by combining this approach with the wavelength routing techniques developed for wavelength division multiplexing (WDM) systems [67].

All-optical signal processing can alleviate the requirement of electric circuits in high-speed photonic networks. Clock recovery, which is essential to digital communication, can be achieved by injection locking a passively mode-locked laser [68]. All-optical signal regeneration has drawn considerable attention. It has been realized by using an injection-locked DFB laser [69], a side mode injection-locked DFB laser [70], and a two-mode injection-locked FP laser [71]. Figure 3.4, shows the other application schematic of waveform reshaping by optical injection locking. The reshaping process is based on the switching of locking stability as a function of injection ratio. When the frequency detuning is fixed, the locked or unlocked state depends on the injection power. When the optical power higher than locking threshold is injected to a slave laser, the slave laser is locked to the master laser frequency, f_m. On the other hand, when the injection power is small, the slave laser operates at the original frequency, f_g. Due to the threshold behavior of the locking and unlocking processes, distorted signals can be reshaped, resulting in a frequency-modulated signal with a reduced noise. The signal from the slave laser is then filtered by band pass filter, so that the reshaped signal can be obtained. Injection locking for all-optical processing also provides additional all-optical signal processing functions, such as optical inverter [72], all-optical format converter [73], and polarization controller [74].

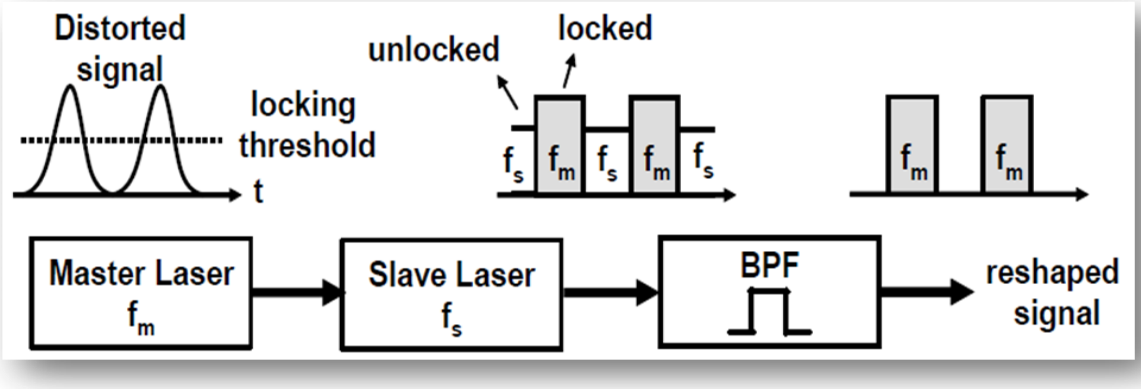

Fig.3.4 Schematic of optical waveform reshaping by injection locking, after [69].

With the recent development of wireless medical applications such as ingestible capsule endoscopy and multichannel neural recording, there is a growing demand for an energy-efficient transmitter with a high data rate. In 1999, the Medical Implant Communication Services (MICS) [75] band of 402–405 MHz with 300-kHz channel spacing has been approved by the Federal Communications Commission (FCC), and it is widely used for implanted medical devices. However, it only allows transmission up to 500 kb/s and cannot support high-resolution (640 480) image transmission with fast frame rate 10 f/s. Although there have been many proposals on high data rate in-body communication targeting for wireless body area networks (WBANs), a standard has yet to be finalized. Various compression or sorting techniques [76], [77] have also been proposed to reduce the size of image data to enable faster frame rate. However, this might deteriorate the image quality and might not be desirable for diagnostic purpose. As a rough estimate, given color depth of 8 bits/pixel, frame size of 640 480 and frame rate of 10 f/s, the required raw data rate is in the proximity of 24.6 Mb/s.

An ingestible medical imaging device such as a pill camera requires at least 8 h of continuous operation once ingested. The device size constraint limits the ultimate capacity of battery. Therefore, it is important for the proposed transmitter to achieve high data rate transmission while consuming very little power. In addition, high chip-level integration is desirable to achieve a small form factor for the prototype. Here, they proposed an alternative architecture for quadrature phase-shift keying (QPSK) or offset-quadrature phase-shift keying (O-QPSK) transmitter centered at a 915-MHz industrial–scientific–medical (ISM) band. The proposed architecture achieves high data-rate transmission with low power consumption through direct phase modulation employing the injection-locking (IL) technique [78].

3.2 General description of WDM-PON injection-locked transmitters

The passive optical network based on wavelength division multiple access (WDM-PON) has been considered as future broadband access network technology because each

subscriber can communicate to the central office (CO) with an assigned wavelength that can carry a different data rate with a different protocol.

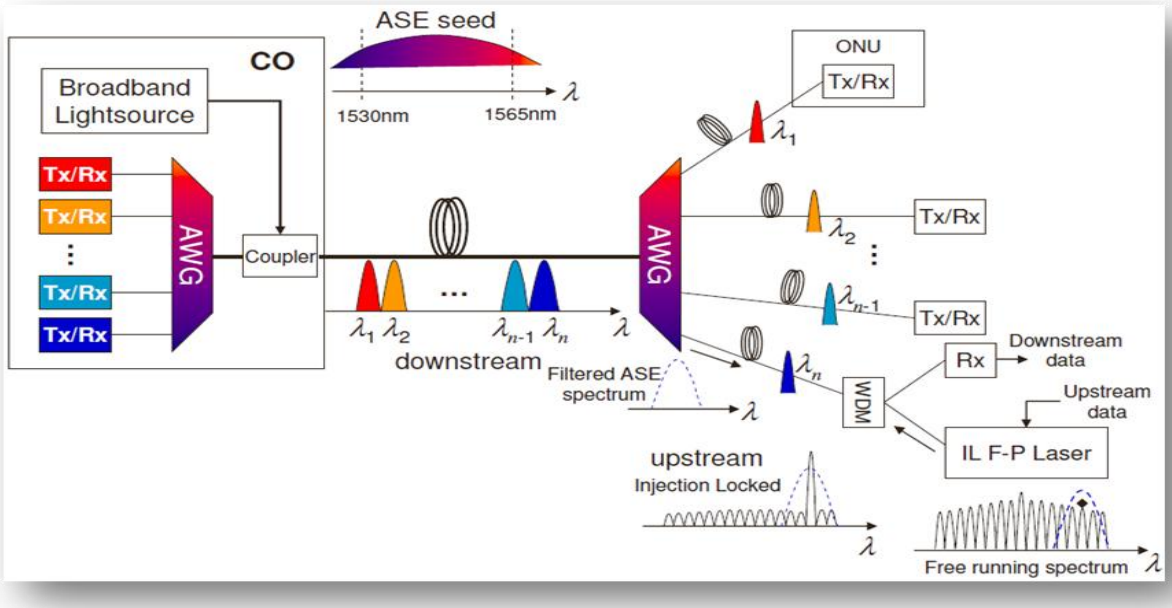

Fig.3.5 WDM-PON Injection Locked FP Laser

However, WDM-PON had a drawback that it has to use expensive wavelength specified sources, e.g. DFB-lasers, in order to maintain assigned wavelength. In addition, it increases management and installation costs considerably [79].

Several approaches have been proposed to solve these problems. The management and installation cost can be reduced by using wavelength independent optical network termination (ONT) that is the optical terminal at the subscriber side. Spectrum-slicing using a broadband incoherent light source such as a Light Emitting Diode (LED) or an Amplified Spontaneous Emission (ASE) from an erbium doped fiber amplifier (EDFA) may be used to realize the wavelength independent ONT [80]-[82]. In this case, the transmission wavelength was determined by spectrum sliced wavelength of the passive optical filter, e.g., an Arrayed Waveguide Grating (AWG), located at the remote node (RN).

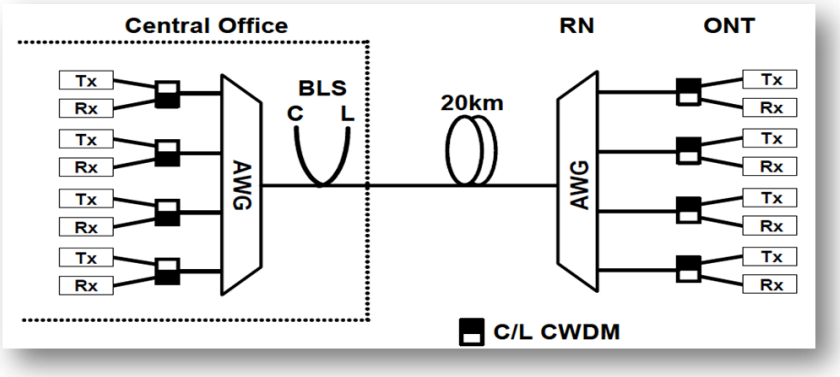

Fig.3.6 WDM-PON system based on wavelength locked FP LD

The LED can be fabricated at a low cost and modulated directly. However, its output power and modulation speed are insufficient for high speed operation. The ASE light from the EDFA can have much higher output power compared with the LED. Unfortunately, it requires an expensive external modulator. The PON employing a spectrally sliced Fabry-Perot Laser Diode (FP LD) was proposed [83]. However, its performance is inherently limited by the mode-partition [84]-[85]. The FP LD can be converted to a single mode laser by injection locking with an extra coherent light source [86]. However it is not cost-effective, since we need a stable coherent light source. In addition, there exists optical power penalty due to back scattering induced relative intensity noise. A Reflective Semiconductor Optical Amplifier (R-SOA) was used to modulate and amplify the spectrum-sliced light [87]-[88]. However, the cost of R-SOA is expensive for access application. Recently, a wavelength-locked FP-LD with external spectrum-spliced ASE injection was proposed for a low cost WDM source for wavelength independent operation of the ONT [89]. By injecting spectrum sliced broadband light source (BLS) into the FP-LD, the laser is forced to operate in a quasi single mode and the mode partition noise of the FP LD is suppressed. Then, we can use the wavelength-locked FP-LD as the WDM light source.

Injection locking techniques have drawn more attention for optical communication applications as a means of achieving chirp free modulation of semiconductor laser diode.

Injection locking techniques have been enriched theoretically and experimentally by different study for locking properties, locking condition and stability properties, locking bandwidth and relaxation oscillation, enhancement of modulation bandwidth, noise and stability due to injection lock of a semiconductor laser. All optical 2R repeater and all optical 3R regeneration techniques have been proposed using injection-locked DFB laser diode. Radio-on-fiber (ROF) technique has been considered as a promising way for the applications to combine optical and wireless communications. In ROF transport systems, light injection technique plays an important role to improve system performance, such as increasing the resonance frequency and side-mode suppression ratio (SMSR) of semiconductor laser diode, as well as reducing the threshold current and chirp of one. Many proposals employing injection locking technique have verified that when injection-locked by a master laser, the slave laser can be enhanced with better performances. Typically, these proposals focus on the main mode of laser diode injection locking only, which means the almost identical central wavelength for both of the injection source and the injection-locked laser.

However, one distributed feedback (DFB) laser diode with main and multiple side modes injection-locked is proposed and demonstrated. DFB laser diode can be successfully injection-locked not only in the main mode but also in different side modes. Besides, the side-mode suppression ratio (SMSR) value of each injection-locked mode is enhanced, in which meaning that a new approach suitable for the use of multiple optical sources. This proposed has the potential to be used as optical sources for radio-on-WDM transport systems to provide multi-service [90].

3.3 Overview of injection locking in WDM-PONs

WDM-PON is a fascinating technology. It does not use any expensive components such as tunable lasers. Instead, it uses simple and inexpensive FP lasers to create all WDM wavelengths.

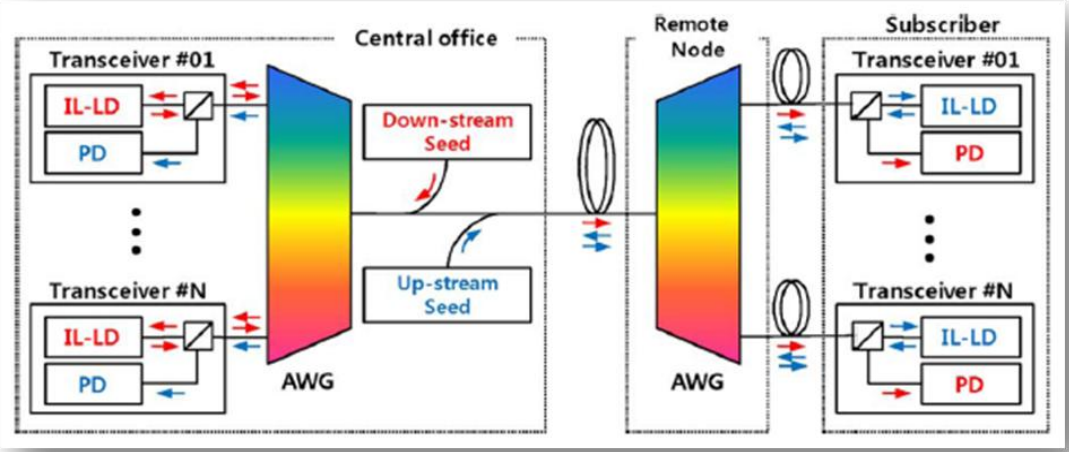

Fig.3.7 Conventional injection-locked WDM PON system

The basic operating principle of WDM-PON is laser injection locking. When an external optical beam of a certain wavelength is injected into a FP semiconductor laser cavity, the FP laser tunes into this wavelength if this wavelength is sufficiently close to the laser native wavelengths and if the external beam is strong enough. And the original multi-wavelength spectrum is replaced by a single wavelength. This phenomenon is called "laser injection locking". The external wavelength is called "locking signal". The locking signal is generated by an AWG. If the FP laser is connected to an output port of a 32 channels AWG demultiplexer and a strong optical beam with a broad wavelength band (say C-band) is connected to the input end of the AWG, the AWG will filter out most wavelengths and allow only one C-band wavelength of the ITU grid to go through on each port, thereby generating the locking signal. So the FP lasers at the customer sites are all the same and it is the AWG that gives them the WDM wavelengths they need. Therefore, you don't need expensive WDM lasers in WDM-PON.

The optical beam emitted from the FP laser (upstream traffic) will go back to the AWG port where the locking signal comes from, and be multiplexed by the AWG. So the same AWG demultiplexer now becomes a multiplexer. At the input end of the AWG

demultiplexer, the multiplexed signal travels to the central office along one long fiber where it will be demultiplexed by another AWG and be detected by 32 detectors.

For downstream traffic, the network structure is the same, except that a different wavelength band (say L-band) is used. And due to an interesting coincidence, a C-band AWG demultiplexer is also a good L-band multiplexer and vice versa. So only two AWGs are used for a 32 channel WDM-PON and each AWG serves three functionalities simultaneously, 1) to generate the locking signal for the upstream traffic, 2) to multiplex upstream traffic, 3) to demultiplex downstream traffic. A 32 channel WDM-PON has at the central office one AWG, 32 detectors, 32 FP lasers, 32 fiber wavelength filters serving the BIDI function, one broadband source. At the customer neighborhood, there is an identical set. WDM-PON is a model of efficiency. This network is capable of providing dedicated and symmetrical transmission bandwidth for each customer. Triple play of phone, Internet and video may be realized using this network [91].

Chapter 4 – Theory of injection-locking

Injection-locking technique provides another degree of freedom other than optimizing the active region design to improve the laser performance. The locking dynamics of the slave laser is, however, rather complicated and a better understanding of the phenomena will prove to be essential to take full advantage of this technique. In order to grasp an insight into the diode laser injection locking phenomena, a simple picture of injection locking between two oscillators will be first presented. Following that, a set of equations describing the interaction between the injected field and the slave laser field is then derived from the wave equation. These equations represent slave laser rate equations in the regime of injection locking. The equations describe dynamics of the injection-locked side-mode, as well as the dynamics of every other unlocked mode. From these equations, the effect of both injection power and wavelength detuning on the laser dynamics can be studied.

Christiaan Huygens was the first one to observe and report the locking phenomenon [92]. He wrote in 1655 that when he was closely observing the clocks hanging on the same wall, the clocks synchronized to each other even though they started with different frequencies and phases. Not until the beginning of nonlinear dynamic study did people start to realize the complexity and beauty between two nonlinearly coupled oscillators. Except for the Huygens clocks, there are abundant examples of locking or synchronization phenomena in our daily life, the synchronization of an atomic watch to the radio signals from a precise atomic clock, of the lighting among fireflies, locking of the human circadian rhythm to the length of the day, or the locking of the Moon's to the Earth's rotation, just to name a few. In 1945 Roy Alder presented the first paper describing the application of the injection locking technique in the electronics and communications [93].

In the early 80’s, when well-engineered semiconductor lasers became available as the transmitters in communication systems, injection-locking technique was proposed and studied extensively. In terms of laser techniques, light form the injection source laser (or master laser) is injected into the cavity of other laser (or slave laser), whereas under certain

conditions, unidirectional coupling can be obtained. If the coupling is mutual, the change in the slave laser due to injection will alter the master laser behaviors. The change of the master will again affect slave laser dynamics and the dynamics can be quite complicated. Here we discuss only unidirectional coupling and effects of this coupling on the slave laser dynamics.

The applications of this technique include receiver end design in optical coherent communication [94], laser spectral narrowing [95], suppression of laser noise [96] and the reduction of frequency chirp under modulation [97]. It was later discovered that injection locking can also improve the laser intrinsic frequency response [98].

4.1. Advantages of Injection Locking

Once the slave laser is locked to the master, there are several interesting observations on the slave laser. First of all, the noise of the slave laser can be reduced. The additional light coming from the master laser competes for the same carriers with all the slave laser modes. For the same current pumping rate, the result is the reduction of carriers and gain available for spontaneous emission and fluctuations. This directly leads to a lower noise floor.

Secondly, the laser linewidth can be reduced. Inside a laser, the strongest mode gets most of the gain and suppresses others. When the laser is locked, its main lasing mode is in coherence with the light from the master laser and becomes stronger than the free running case. Also if the master laser is less noisy (or more stable), there will be less phase fluctuation for the slave laser due to its phase locking to the master source. Combining the domination of the available gain and less phase noise, the new locked mode exhibits a sharper linewidth. If the slave laser is multimode to begin with, the additional injection might promote single mode operation, or at least increase the side mode suppression ratio.
In addition to this, the problem of frequency chirp while the laser is under modulation can also be mitigated. In fact, this might be the most important reason that motivated researchers in the early 80's to explore on this subject. Typically, the lasing wavelength is determined by the round trip phase condition and the gain available for the candidate

modes. Due to the non-perfect clamping of the carriers to its threshold density, the fluctuation of the carriers manifests itself as wavelength variation through Kramer-Kronig relation. When the slave laser is injection-locked, the locking provides an additional mechanism to prevent the laser wavelength drifting away from its CW value. It is an approach independent of the slave laser design to stabilize the laser wavelength.

Another interesting consequence of injection locking is the improvement on the bandwidth of the laser. As discussed above, due to the presence of the external light, the gain available for slave laser modes are suppressed. Effectively, the threshold of the locked mode is reduced compared to its free running case. Since the gain and carrier density relation can be approximated as a logarithmic function, the differential gain is larger if the threshold carrier density is lower. Besides, the higher photon density of the locked mode will enhance the stimulated emission and suppress spontaneous emission. The simultaneous presence of all these factors implies a higher resonance frequency of an injection-locked laser [99].

4.2. Rate Equation Approach

To obtain injection locking rate equations, we start from wave equation:

$$\frac{\partial^2}{\partial z^2}E(z,t)=\frac{1}{c^2}\frac{\partial^2}{\partial t^2}\varepsilon E(z,t) \tag{4.1}$$

Where $E(z,t)$ is the electric field, ε is the dielectric constant of the material and c is the speed of light in vacuum. The electric field can be further decomposed into $E(z,t) = E(t)e^{j(\omega t-kz)}$ where ω is the optical frequency of the field and k is the wave vector along the z direction. Without the optical frequency information, the term $E(t)$ is now just the slowly varying envelope function of the electric field. Substituting this expression in the wave equation and neglecting the d^2/dt^2 term, the equation in a laser structure becomes [100]:

$$\frac{2i\omega}{c^2}\left(\varepsilon_{av}+\frac{\omega}{2}\frac{\partial\varepsilon_{av}}{\partial\omega}\right)\frac{dE}{dt}+\left(\frac{\omega^2}{c^2}\varepsilon_{av}-k^2\right)E=0 \tag{4.2}$$

Here ε_{av} is the average dielectric constant seen by the field in the laser waveguide structure. The equation can be rewritten as:

$$\frac{dE}{dt} = \left[j\omega + \frac{1}{2}\left(G(n) - \frac{1}{\tau_p} \right) \right] E(t) \tag{4.3}$$

In the equation, $G(n)$ is the effective gain inside the cavity at carrier density n and τ_p is the photon lifetime, where $1/\tau_p$ accounts for both the internal and the facet mirror loss.

In the presence of an external coherent light, Eq. (4.3) needs to take into account of this extra driving force and becomes

$$\frac{dE_{sl}(t)}{dt} = \left[j\omega + \frac{1}{2}\left(G(n) - \frac{1}{\tau_p} \right) \right] E_{sl}(t) + k_c E_{ext}(t) \tag{4.4}$$

E_{sl} and E_{ext} denote the slave laser free-running and external injection electric field, respectively. Factor k_c is the injection efficiency of the master field into the slave laser. All the noise terms will be neglected in the derivation for simplicity. Furthermore, the electric field is assumed to be properly normalized such that $|E_{sl}(t)|^2 = S$, where S is the photon density.

The time behavior of the photon density S can be obtained as

$$\frac{dS}{dt} = \frac{d}{dt} \left| E_{sl} E_{sl}^* \right| = 2\,\mathrm{Re}\left\{ E_{sl}^* \frac{dE_{sl}}{dt} \right\} = \left(G(n) - \frac{1}{\tau_p} \right) S + 2k_c \,\mathrm{Re}\left| E_{sl}^* E_{ext} \right| \tag{4.5}$$

Again, the electric fields can be further decomposed into a slow varying amplitude component $\tilde{E}$ and a high frequency oscillating phase factor:

$$E_{sl} = \tilde{E}_{sl}(t)\, \mathrm{e}^{j\,\omega_{sl} t + \theta_{sl}(t)} = \sqrt{S(t)}\, \mathrm{e}^{j\,\omega_{sl} t + \theta_{sl}(t)} \tag{4.6}$$

$$E_{ext} = \tilde{E}_{inj}(t)\, \mathrm{e}^{j\,\omega_{ml} t + \theta_{ml}(t)} = \sqrt{S_{inj}(t)}\, \mathrm{e}^{j\,\omega_{ml} t + \theta_{ml}(t)} \tag{4.7}$$

where ω_{sl} and ω_{ml} stand for optical frequencies of the electric fields in the slave and master laser, respectively, θ_{sl} and θ_{ml} stand for their phases, while S_{inj} stands for injected photon density. The injection contribution to dS/dt, the $2k_c\mathrm{Re}\{E_{sl}^* E_{ext}\}$ term, now becomes:

$$\begin{aligned} &2k_c \sqrt{S(t) S_{inj}(t)}\, \mathrm{Re}\left| \exp\left[j\left(\omega_{ml} - \omega_{sl} \right) t + j\left(\theta_{ml}(t) - \theta_{sl}(t) \right) \right] \right| = \\ &2k_c \sqrt{S(t) S_{inj}(t)} \cos\left[\left(\omega_{ml} - \omega_{sl} \right) t + \theta_{ml}(t) - \theta_{sl}(t) \right] \end{aligned} \tag{4.8}$$

When the slave laser is stably locked to the master laser their optical frequencies become equal. Let θ represent the phase difference between slave and master laser, i.e. $\theta(t) = \theta_{sl}(t) - \theta_{ml}(t)$. The photon density equation is then:

$$\frac{dS}{dt} = \left[G(n) - \frac{1}{\tau_p} \right] S + 2k_c \sqrt{S(t) S_{inj}(t)} \cos\ \theta(t) \tag{4.9}$$

To obtain the phase equation, we start from the slowly varying term of the slave laser electric field $\tilde{E}_{sl}(t) = S(t)^{1/2} \exp\{\theta_{sl}(t)\}$.

$$\frac{d\tilde{E}_{sl}(t)}{dt} = \left[\frac{1}{2} \frac{1}{\sqrt{S(t)}} \frac{dS}{dt} + j\sqrt{S(t)} \frac{d\theta_{sl}}{dt} \right] \mathrm{e}^{j\theta_{sl}(t)} \tag{4.10}$$

Multiplying both sides by $\tilde{E}_{sl}^{*}(t)$ we have:

$$\tilde{E}_{sl}^{*}(t) \frac{d\tilde{E}_{sl}(t)}{dt} = \frac{1}{2} \frac{dS}{dt} + jS(t) \frac{d\theta_{sl}}{dt} \tag{4.11}$$

$$\frac{d\theta_{sl}}{dt} = \frac{1}{S(t)} \mathrm{Im} \left\{ \tilde{E}_{sl}^{*}(t) \frac{d\tilde{E}_{sl}(t)}{dt} \right\} \tag{4.12}$$

The slowly varying envelope is related to the electric field by $\tilde{E}_{sl}(t) = E_{sl}(t) \exp\{-j\omega_{ml} t\}$, where the optical frequency is again chosen to be that of the master laser in the stably locked case. Taking the derivative of this relation and inserting into the above equation, the phase equation can be expressed as:

$$\frac{d\theta_{sl}}{dt} = \frac{1}{S(t)} \mathrm{Im} \left\{ E_{sl}^{*} \frac{dE_{sl}}{dt} - j\omega_{sl} S \right\} = \omega_{sl} - \omega_{ml} - k_c \sqrt{\frac{S_{inj}(t)}{S(t)}} \sin(\theta(t)) \tag{4.13}$$

When slave laser is under modulation, its frequency ω_{sl} will be a time varying function because the carriers inside the cavity will not be perfectly clamped at its threshold level. The variation of the carrier will result in the change of the refractive index through Kramer-Kronig relationship.

The slave laser frequency $\omega_{sl}(t)$ can be calculated using α the linewidth enhancement factor. Linewidth enhancement factor is defined as the ratio of the change in the real part of the refractive index to the change in the imaginary part when the carrier density inside the cavity is varied.

$$\omega(t) = \omega_{n=n_{th}} + \frac{\alpha}{2}\frac{dG}{dn}\ n - n_{th}\ = \omega_{sl} + \frac{\alpha}{2}\frac{dG}{dn}\ n - n_{th} \tag{4.14}$$

The free running slave laser frequency and the corresponding threshold current density are chosen as the reference point in this expression. Inserting this back to the previous equation, assuming that master laser has constant phase θ_{ml} we obtain:

$$\frac{d\theta_{sl}}{dt} = \frac{d\theta_{sl}}{dt} - \frac{d\theta_{ml}}{dt} = \frac{d\theta}{dt} = \frac{\alpha}{2}\frac{dG}{dn}\ n - n_{th}\ +\ \omega_{sl} - \omega_{ml}\ - k_c\sqrt{\frac{S_{inj}}{S}}\sin\ \theta(t) \tag{4.15}$$

With the addition of the rate equation of the carrier in the cavity reservoir, the complete injection locking rate equations of the slave lasers can be organized as the following:

$$\frac{dn}{dt} = \frac{I}{qV} - \ A_{SRH}n + R_{sp}(n) + C_A n^3\ - v_g g(n)\frac{S}{1+\varepsilon S} \tag{4.16}$$

$$\frac{dS}{dt} = \Gamma v_g g(n)\frac{S}{1+\varepsilon S} - \frac{S}{\tau_P} + \Gamma\beta_{sp}R_{sp}(n) + 2k_c\sqrt{S_{inj}S}\cos(\theta) \tag{4.17}$$

$$\frac{d\theta}{dt} = \frac{\alpha}{2}\left(\Gamma v_g g(n)\frac{1}{1+\varepsilon S} - \frac{1}{\tau_P}\right) - \Delta\omega - k_c\sqrt{\frac{S_{inj}}{S}}\sin(\theta) \tag{4.18}$$

where $\Delta\omega = \omega_{\mathrm{ml}} - \omega_{\mathrm{sl}}$. The effective gain term $G(n)$ is replaced by $\Gamma v_g g(n)/(1+\varepsilon S)$ to incorporate the gain saturation with ε as the gain compression factor.

The most important feature of this set of equations is the coupling between photon and phase. In the free running case (by setting S_{inj} and $\Delta\omega$ to zero), the phase equation can be neglected when studying the photon behavior since only photons and carriers are coupled. As the injection is switched on, the new photons-phase coupling dramatically enriches the system dynamics. The coupling strength is proportional to the square root of the relative injection intensity, and the frequency and phase differences between the master and the slave lasers play important roles as well [99].

4.3. Stability

The first question to be asked of a nonlinear system is whether the system is stable for a given parameter set. In the case of semiconductor laser injection locking, the

parameters of the lasers are given. The two variables that can be changed are the injection intensity and the frequency detuning between the two lasers. The interest here is therefore to find out all the possible combinations of these two parameters, or the locking range, that the slave laser will stably locked to the master.

Generally speaking, the locking range when the slave laser is constantly biased is not the same as the one when it is under modulation. The parameter set for which the steady-state slave laser locks to the master will not guarantee its stability when the slave laser is perturbed. In the case of small-signal modulation, stability of the locking needs to be investigated through the analysis of the position of the eigenvalues of the system in the complex plain [101].

From the equations derived above, the conditions that a CW slave laser stably locked to the master can be easily obtained. By setting time derivates to zero in the Eqs. (4.17) and (4.18), and by neglecting spontaneous emission contribution ($\Gamma\beta_{sp}R_{sp} \approx 0$) we get [101]:

$$0 = \left(\Gamma v_g g(n) \frac{1}{1+\varepsilon S} - \frac{1}{\tau_P} \right) S + 2k_c \sqrt{S_{inj} S} \cos(\theta) \tag{4.19}$$

$$0 = \frac{\alpha}{2} \left(\Gamma v_g g(n) \frac{1}{1+\varepsilon S} - \frac{1}{\tau_P} \right) - \Delta\omega - k_c \sqrt{\frac{S_{inj}}{S}} \sin(\theta) \tag{4.20}$$

From these two equations we get:

$$0 = \alpha k_c \sqrt{\frac{S_{inj}}{S}} \cos(\theta) + \Delta\omega + k_c \sqrt{\frac{S_{inj}}{S}} \sin(\theta) \tag{4.21}$$

which gives:

$$\Delta\omega = -k_c \sqrt{1+\alpha^2} \sqrt{\frac{S_{inj}}{S}} \sin(\theta + \arctan(\alpha)) \tag{4.22}$$

From this equation, it is obvious that the phase difference between the locked slave laser and the master laser is determined by the intensity ratio of the two lasers and their

frequency detuning [101]. The phase of the slave laser is locked and lagged behind the phase of the master laser by [101]:

$$\theta = \arcsin\left(\frac{-\Delta\omega}{k_c\sqrt{S_{inj}/S}\sqrt{1+\alpha^2}}\right) - \arctan\ \alpha \tag{4.23}$$

Due to the inverse sine term on the right hand side of Eq. (4.23), the magnitude of the detuning can only fall within a certain range for a given injection power. In terms of injection ratio defined as $r = (S_{inj}/S)^{1/2}$ [101], the last condition can rewritten as:

$$r = \frac{\Delta\omega^2}{k_c^2(1+\alpha^2)\sin^2\ \theta + \arctan(\alpha)} \tag{4.24}$$

which for real θ and extreme values for $\sin(\theta + \arctan(\alpha)) = \pm 1$ defines the boundaries between the injection-locked and the four wave mixing (FWM) regions [101].

Besides this constraint obtained mathematically, there is an additional physical restriction on the stable locking range, i.e. locked range is defined with $\cos(\theta) > 0$ [101]. This conclusion can be made from the fact that the gain in the regime of injection-locking is below threshold. This leads to negative sign of the term $\Gamma v_g g(n)/(1+\varepsilon S) - 1/\tau_p$ in the stationary form of Eq. (3.6), which requires cosine term to be positive. Combining this constraint $\cos(\theta) > 0$ with constraint which defines FWM boundaries, we obtain relation:

$$-k_c\sqrt{\frac{S_{inj}}{S}}\sqrt{1+\alpha^2} < \Delta\omega < k_c\sqrt{\frac{S_{inj}}{S}} \tag{4.25}$$

Using this relation, a locking range plot for the injection-locked laser can be plotted, as shown in Figure 4.1. It is also sometimes referred to as the Arnold tongue plot. This plot shows locking range, for intermodal injection locking, in terms of injection ratio r dependence on the frequency detuning $\Delta\omega$.

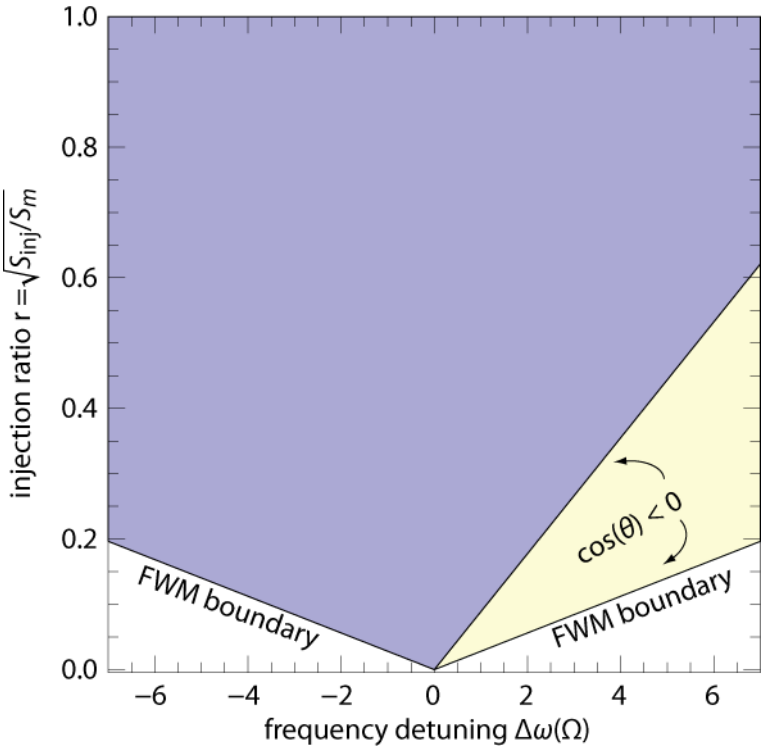

Fig. 4.1 Locking range. Symmetrical boundaries represent FWM boundaries. Yellow region is region in which locking is unstable due to $\cos(\theta) < 0$.

Chapter 5 - Theoretical background of modulation response of injection-locked Fabry-Perot laser diode

Injection-locked transmitter has been proposed as a transmitter solution in the next generation of wavelength division multiplexing passive optical networks (WDM-PON), as a upstream transmission from an optical network unit to the central office [40, 41]. This way, optical network unit transmitter can consist of a cheap Fabry-Perot laser, instead of much more expensive tunable laser. Apart from the economical benefit, injection-locked lasers provide significant improvement of laser dynamics compared to the free-running lasers [50]. The theoretical and experimental investigations have proved that this technique can ensure single-mode operation [40, 41], reduce the linewidth of a semiconductor laser [102], eliminate mode partition noise [40, 41], mode hopping [102], frequency chirp [102], improve modulation bandwidth [42, 103, 104]. In this chapter, we present a model of rate equations for describing the dynamics of the injection-locked lasers, and apply small signal analysis in order to obtain modulation response in both free-running and injection-locked regime. By this we set a theoretical background for investigation of modulation response and modulation bandwidth dependence on injection power and frequency detuning.

5.1 Rate Equations

The model of IL FP semiconductor laser is based on a system of multimode rate equation (MREs) [105, 106], with extra terms describing the locking phenomenon [40, 41, 104, 105, 107]. Apart from injection-locked mode, the model comprises other, unlocked modes. Thus, the full model of multimode rate equations comprises one equation describing the carrier concentration (n) dynamics, l_1+l_2+1 equations describing the photon density (S_j) dynamics for every supported longitudinal mode of the laser including the IL mode ($j = m$) and the central mode ($j = 0$), and one equation describing the time evolution of the phase difference (θ_m) between the free-running and the injection-locked state. l_1 and

l_2 represent number of supported modes on the left (long-wavelength) and right (short-wavelength) side of the central mode, respectively:

$$\frac{dn}{dt} = \frac{I}{qV} - \left[A_{SRH} n + R_{sp}(n) + C_A n^3 \right] - \sum_{j=-l_1}^{l_2} v_g g(n) \frac{S_j}{1+\varepsilon S_j} \tag{5.1}$$

$$\frac{dS_j}{dt} = \Gamma v_g g(n) \frac{S_j}{1+\varepsilon S_j} - \frac{S_j}{\tau_P} + \Gamma \beta_{sp} R_{sp}(n) \tag{5.2}$$

$$\frac{dS_m}{dt} = \Gamma v_g g(n) \frac{S_m}{1+\varepsilon S_m} - \frac{S_m}{\tau_P} + \Gamma \beta_{sp} R_{sp}(n) + 2k_c \sqrt{S_{inj} S_m} \cos(\theta_m) \tag{5.3}$$

$$\frac{d\theta_m}{dt} = \frac{\alpha}{2} \left(\Gamma v_g g(n) \frac{1}{1+\varepsilon S_m} - \frac{1}{\tau_P} \right) - \Delta\omega - k_c \sqrt{\frac{S_{inj}}{S_m}} \sin(\theta_m) \tag{5.4}$$

In the equations above, q stands for electron charge, I stands for the bias current of the slave laser, V is the volume of its active area, corresponding to a laser width w = 4 μm, resonator length L = 250 μm and N_w = 3 equally spaced quantum wells, with well thickness of d = 8.7 nm. $R_{sp}(n) = B_R n^2$ is the total spontaneous optical emission rate, with B_R = 0.8×10^{-10} cm^3/s standing for bimolecular recombination rate [106]. A_{SRH} is Shockley-Reed-Hall recombination rate, which is assumed to be negligible, and C_A = 3.5×10^{-30} cm^{6}s^{-1} [106] is the Auger recombination rate. v_g stands for group velocity with n_g = 4.2, $\tau_p = (\Gamma v_g g_{th})^{-1}$ is the photon lifetime, Γ is the confinement factor calculated as $N_w \times \Gamma_1$, where Γ_1 = 0.0187 is the confinement factor per well. The parameter β_{sp} is the spontaneous emission coupling factor, which takes value of 0.87×10^{-4} [106], k_c = 1.13×10^{11} s^{-1} is the external light coupling factor [40, 41], S_{inj} is the photon density which is proportional to the injection optical power P_{inj} and is given by the relation $S_{inj} = \tau_p \Gamma P_{inj}/(\eta_0 \hbar\omega V)$, where η_0 is the optical efficiency [106] . Parameter α is the linewidth enhancement factor, which is assumed to be equal to 3 [104], and $\Delta\omega$ is the frequency detuning between master and slave lasers. The mode spectrum is assumed to be centered on 0.8 eV which corresponds to the wavelength of 1.55 μm. Gain threshold is calculated with respect to active region losses as $g_{th} = \alpha_{tot}/\Gamma$ [106], where $\alpha_{tot} = \alpha_i + \alpha_m$, represents the sum of the internal losses α_i = 23 cm^{-1}, and mirror losses $\alpha_m = (1/L)\ln(1/R)$ = 45.58 cm^{-1}, with R = 0.32 standing for mirror

reflectivity. Using these values, the threshold gain g_{th} is calculated to be 1222.4 cm^{-1}, with threshold carrier concentration n_{th} = 4.52×10^{18} cm^{-3}. Using this values and relation $I_{th} = qV(R_{sp}(n_{th}) + C_A n_{th}^3)$, threshold current is calculated to be I_{th} = 8.2 mA.

Modal optical gain is modeled as in [106]:

$$g(n,m) = \frac{1}{1+\left(\frac{m}{M}\right)^2} \frac{g_0}{1+\varepsilon S_m} \log\left(\frac{n+n_s}{n_s+n_{tr}}\right) \tag{5.5}$$

where g_0, n_s, and n_{tr} are gain modeling parameters [106], with values given in the Table 5.1. Parameter ε models nonlinear gain suppression, which we assume to be negligible, hence we take ε = 0, since in all simulations photon densities are few orders smaller than those needed to trigger the mechanism of the nonlinear gain suppression. Parameter m is the mode number counted from the central mode, for which m = 0, which is assumed to be aligned with the gain peak. M is the mode number where the gain decays to one half of its peak value.

Table 5.1 Gain parameters

n_{tr}	n_s	g_0	M
2.2×10^{18} cm^{-3}	1.3×10^{18} cm^{-3}	2400 cm^{-1}	30

5.2. Free-running regime analysis

5.2.1. Free-running steady-state regime

Free-running regime is the regime of the slave laser for which there is no injected light i.e. S_{inj} = 0. The steady-state solution of equations (5.1) and (5.2) in the case of free-running regime are found by setting the time derivatives to zero. Solving the equation (5.2) for the steady-state photon density, we get:

$$S_j = \frac{-\Gamma \beta_{sp} R_{sp}(n_{th})}{\Gamma v_g g(n_{th}, j) - 1/\tau_P} \tag{5.6}$$

Steady-state equation for the central mode cannot be solved in this manner since, for the central mode in the case of threshold carrier concentration, denominator of the equation

(5.6) becomes equal to zero. To solve for the central mode steady-state photon density we substitute photon densities of every other side-mode in the stationary form of the equation (5.1) and solve for S_0:

$$0 = \frac{I}{qV} - \left[A_{SRH} n_{th} + R_{sp}(n_{th}) + C_A n_{th}^3 \right] + \sum_{-l_1 < j < -l_2,\, j \neq 0} v_g g(n_{th}, j) \frac{\Gamma \beta_{sp} R_{sp}(n_{th})}{\Gamma v_g g(n_{th}, j) - 1/\tau_P} + v_g g(n_{th}, 0) S_0 \tag{5.7}$$

In Figure 5.1 we show the steady-state mode spectrum in the case of free-running regime with three different values of injection current. Our model of the gain assumes symmetrical gain profile, which leads to symmetrical mode spectrum with respect to the central mode (with photon energy of 0.8 eV corresponding to the wavelength of 1.55 μm). In order to have more realistic and complex numerical model, we take into account somewhat large number of the supported side-modes, with total count of 30 side-modes on the both sides of the central mode. This means that mode number m goes from $l_1 = -30$ (for the long-wavelength side) to $l_2 = 30$ (for the short-wavelength side), resulting in total $l_1+l_2+1 = 61$ modes. In the case of lowest injection current ($I = 1.2I_{th}$), the optical power of the central mode is in the order of the optical power of the first side-mode, resulting in side-mode suppression ratio of just few dB [c.f. Fig. 1(a)]. Side-mode suppression ratio is the figure of merit for successfully achieved monomode output. It is defined as a ratio between a given mode and the strongest side-mode [107]. In this case, it is the ratio between the central mode and the strongest side-mode, i.e. mode $j = \pm 1$, SMSR = $10\log_{10}(S_0/S_{\pm 1})$. On the other hand in the case of high injection currents ($I = 5I_{th}$), SMSR is in the order of 20 dB, which means that the central mode is highly pronounced [c.f. Fig. 1(c)].

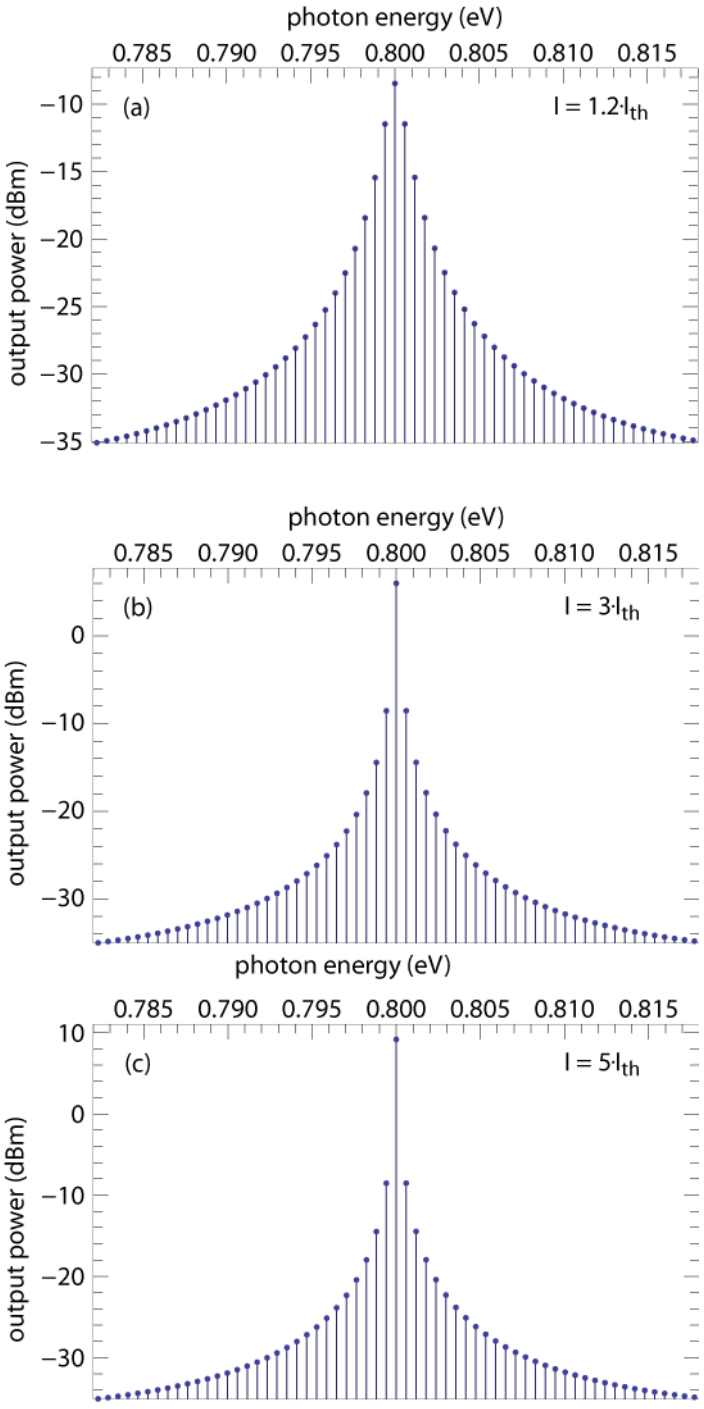

Fig.5.1 Comparison of free running-regime mode spectrum for three different values of injection current: $I = 1.2I_{th}$ (a), $I = 3I_{th}$ (b) and $I = 5I_{th}$ (c).

5.2.2. Free-running transient regime

In Figure 5.2 we present time diagrams of reaching the steady-state, in particular the time dependences of photon densities for the central and two side-modes, with respect to injection current. Figure 5.2 shows that for larger values of injection current, turn on time is smaller, while the decay coefficient and the frequency of the relaxation oscillations are larger. To generate high-speed optical signals by modulating the bias current, the optical pulses have to quickly return to their steady-state values. Therefore, the decay coefficient and the relaxation oscillations frequency have to be large. In addition to this, during the relaxation oscillation, the carrier concentration n deviates from n_{th} value, as shown in the Fig. 5.3. These deviations can be even around 10% of the nominal value of the n_{th}. Due to this modulation in n, the optical gain and the refractive index simultaneously change, which alters the longitudinal modes.

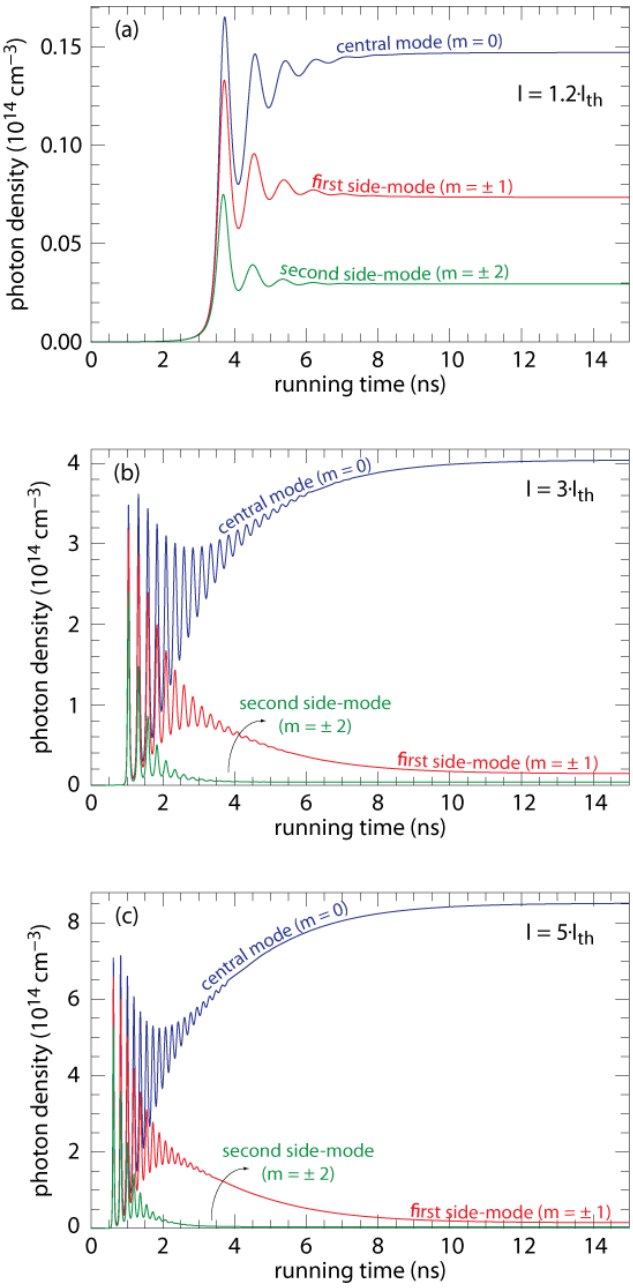

Fig.5.2 Transient analysis of the free running regime, and comparison of photon density time dependence of central mode (blue line), with the first side-mode, $m = \pm 1$ (red line), and the second side-mode $m = \pm 2$ (green line), for three values of injection current $I = 1.2I_{th}$ (a), $3I_{th}$ (b), and $5I_{th}$ (c)

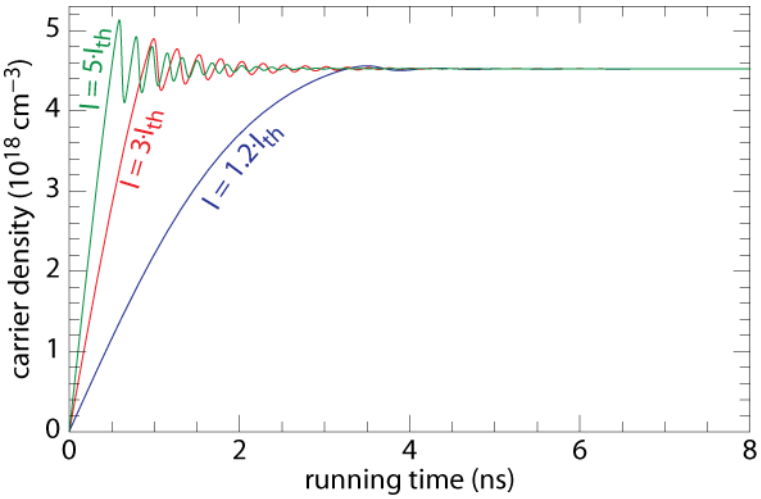

Fig.5.3 Carrier concentration dynamics, for $I = 1.2I_{th}$ (blue line), $I = 3I_{th}$ (red line), $I = 5I_{th}$ (green line)

When carrier concentration n is larger than n_{th}, the optical gain exceeds the threshold value g_{th} and the longitudinal modes with the optical gain $g > g_{th}$ show laser operation. Therefore, in the beginning of the relaxation oscillation, multimode laser oscillations are observed. With a decay in the relaxation oscillation, the number of the lasing longitudinal modes decreases.

On the other hand, the refractive index is also modulated by the free carrier plasma effect. With a deviation in the carrier concentration, the positions of the longitudinal modes shift to a shorter wavelength. Such dynamic changes in the longitudinal modes due to modulation of n are called chirping. Multimode laser operations and chirping are not suitable for large-capacity optical fiber communication systems, because of optical fiber dispersion.

In terms of modulation response of the free-running semiconductor laser, the relaxation oscillations frequency is the resonance frequency, meaning that the modulation response has a maximal value at this exact frequency. Therefore, the relaxation oscillation frequency determines the highest limit in the modulation frequency, i.e. −3 dB modulation

bandwidth. Since this frequency increases with an increase in the bias current, it is expected that the −3 dB modulation bandwidth will also increase.

5.3. Injection locking steady-state regime

As introduced earlier, an injection-locked laser system consists of two semiconductor lasers. The light from a pump laser (master laser) is injected into the cavity of the second laser (slave laser), either in the central mode, when injection locking is referred to as intramodal injection, or in one of the side-modes, when the technique is referred to as intermodal injection.

Either way, the photons injected from the master laser add to existing photons of the slave laser and compete for the same number of the carriers as in the free-running case. This means that, due to optical injection, carrier threshold will be lowered in the case of injection locking, i.e. laser operates below gain threshold, in the regime of spontaneous emission. However, in the case of stable injection-locking, injected photons pronounce injection-locked mode and provide that all of the power of the slave laser is emitted at the optical frequency of the master laser. In this way, slave laser is synchronized with the master laser.

In the analysis of steady-state injection locked regime we follow the approach presented in [107]. This analysis is based on the carrier rate equation (5.1) and investigation of the carrier rate (dn/dt) dependence on the carrier concentration n i.e. the steady-state solutions of this dependence. From the stationary form of the equation (5.2) stationary forms of photon densities for every mode except injection locked mode are found [107]:

$$S_j = \frac{-\Gamma \beta_{sp} R_{sp}(n)}{\Gamma v_g g(n, j) - 1/\tau_P} \tag{5.8}$$

Combining the stationary forms of equations (5.3) and (5.4), by eliminating injection-locked mode phase θ_{m}, a quadratic equation with respect to the steady-state injection-locked photon density S_{m} is derived [107]:

$$\left[A^2 + 4\left(\frac{\alpha A}{2} - \Delta\omega \right)^2 \right] S_m^2 + \left[2AB - 4k_c^2 S_{inj} \right] S_m + B^2 = 0 \tag{5.9}$$

whose solution is given by [107]:

$$S_m^{\pm} = \left\{ -\ 2AB - 4k_c^2 S_{inj} \ \pm \sqrt{2AB - 4k_c^2 S_{inj}\ ^2 - 4B^2 \left[A^2 + 4\ \alpha A/2 - \Delta\omega\ ^2 \right]} \right\} \times 2\left[A^2 + 4\ \alpha A/2 - \Delta\omega\ ^2 \right]^{-1} \tag{5.10}$$

Here, $A = \Gamma v_g g(n, \omega_m + \Delta\omega) - \tau_p^{-1}$ is the effective rate of stimulated photon generation and $B = \Gamma\beta_{sp} R_{sp}(n)$ is the effective spontaneous emission. For all modes in the free-running regime, effective spontaneous emission $B > 0$, while $A < 0$, expect for the central mode for which $A = 0$. In the injection-locking regime, operating point of the carrier concentration is below threshold value nth, so $A < 0$ for all modes, including the central mode $j = 0$. In equation (5.10) S_m^+ is few orders of magnitude higher than S_m^-, moreover photon rate loss for S_m^- (S_m^-/τ_p) is few orders of magnitude smaller than the effective spontaneous emission. Therefore, S_m^- cannot be considered as stimulated emission, and in what follows, we assume $S_m = S_m^+$. We insert (5.8) and (5.10) into the carrier rate equation (5.1) and study its stationary solutions. In Figure 5.4(a) we present dn/dt versus n phase plots for injection into the first side mode from the central mode (ω_0 = 0.8 eV) on the long-wavelength side $m = -1$, for a fixed bias current of $I = 1.2I_{th}$, and fixed frequency detuning of $\Delta\omega = -7\Omega$ ($\Omega = 10^{10}$ rad/s) in cases of five different injection powers. Injection frequency detuning of $\Delta\omega = -7\Omega$ into the side-mode $m = -1$ means that the frequency of the injected light is $\omega_{inj} = \omega_0 + m(\pi c/n_g L) + \Delta\omega$. For small injection powers ($P_{inj} = -18$ dBm) dn/dt versus n plot has only one stationary point which is close to the threshold carrier concentration. Since operating point of the laser is close to the free-running regime and number of injected photons is small, in this case, mode spectrum is similar to the free-running regime, except that injection mode $m = -1$ has slightly increased power, due to injection [c.f. Fig. 5.4(b)]. For some moderate injection power ($P_{inj} = -12$ dBm) dn/dt versus n phase plot has three stationary solutions, which we denote as $n_{sp}^{(1)}$, $n_{sp}^{(2)}$ and $n_{sp}^{(3)}$ in the increasing order of their values. Further increase of the injection decreases the values of the $n_{sp}^{(1)}$, and $n_{sp}^{(3)}$ stationary points, while increasing the value of $n_{sp}^{(2)}$ stationary point. This causes $n_{sp}^{(1)}$ and $n_{sp}^{(2)}$ to move further away from each other, while $n_{sp}^{(2)}$ and $n_{sp}^{(3)}$ shift towards each other. For large injection power ($P_{inj} = -8$ dBm) there is again only one stationary point, but this

point is far away from the threshold carrier concentration. This point is mainly the consequence of injection locking. Due to the lower carrier concentration operating point, laser is in the regime of spontaneous emission, but injected photons pronounce the injection locked mode $m = -1$. Mode spectrum in the case of high injection power is depicted in the Fig. 5.4(c). Limiting cases occur for injection powers $P_{inj} = -15.7$ dBm and $P_{inj} = -9.7$ dBm for which $n_{sp}^{(1)}$ merges with $n_{sp}^{(2)}$ and $n_{sp}^{(2)}$ merges with $n_{sp}^{(3)}$, respectively. The range between critical powers, for which the number of stationary points switches from 3 to 1, determines the region of multiple-stationary points (RMSP). Figs. 5.4(d) and (e) show mode spectra for $n_{sp}^{(1)}$ and $n_{sp}^{(3)}$ state, respectively. In the case of $n_{sp}^{(1)}$ stationary point, injection-locked mode is highly pronounced, while other modes are strongly suppressed, and this is the case of high SMSR value. On the other hand, case of $n_{sp}^{(3)}$ stationary point is close to the free-running regime in which the dominant mode is the central mode. Stability analysis shows that the middle stationary point $n_{sp}^{(2)}$ is not stable, and thus slave laser cannot be stabilized in this point.

Fig. 5.5 shows the manner in which an increase in magnitude of detuning affects the RMSP for a fixed injection power. According to Eq. (5.10), a small negative detuning and $A < 0$ may provide a small denominator, which consequently leads to an increase in S_m and mimics the case of the injection power increase. For a fixed injection power of $P_{inj} = -12$ dBm and small frequency detuning ($\Delta\omega = -4\Omega$), there is only one stationary point with low operating carrier concentration point (c.f. Fig. 5.5). However, a medium negative detuning ($\Delta\omega = -7.7\Omega$) leads to all three stationary points, as in case of medium injection power. The limiting cases are, again, characterized by merging of $n_{sp}^{(1)}$ and $n_{sp}^{(2)}$ for $\Delta\omega = -9.8\Omega$ and merging of $n_{sp}^{(2)}$ and $n_{sp}^{(3)}$ for $\Delta\omega = -5.6\Omega$. Unlike the case of injection power increase, the increase in frequency detuning magnitude shifts both $n_{sp}^{(1)}$ and $n_{sp}^{(2)}$ away from n_{th}^{FR}, while $n_{sp}^{(3)}$ increases and moves slightly toward n_{th}^{FR}. Finally, for some large frequency detuning ($\Delta\omega = -13\Omega$), there is, again, only one stationary point close to the n_{th}^{FR}, similarly to the case of small injection power.

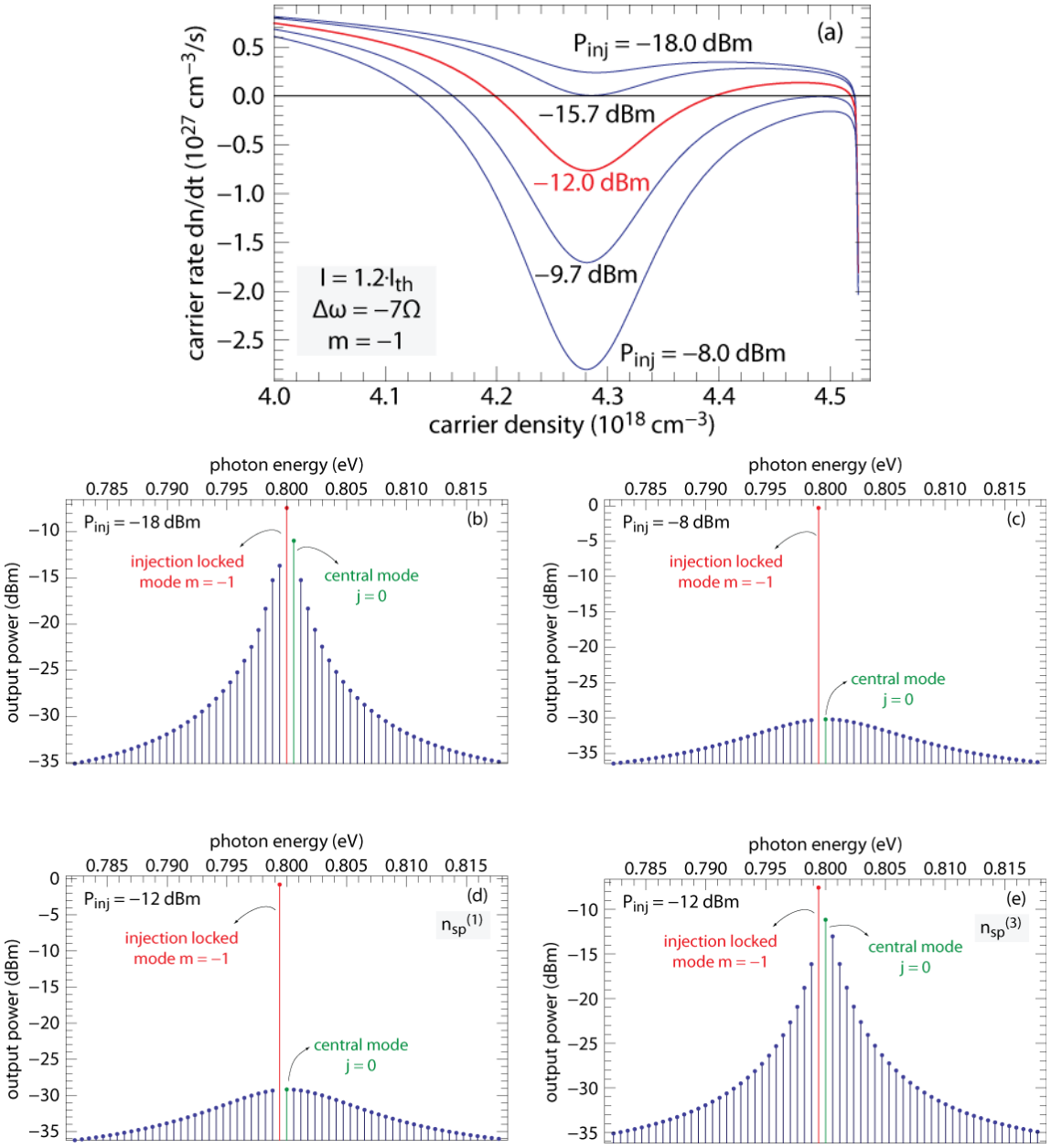

Fig. 5.4 (a) Carrier concentration rate *dn*/*dt* versus *n* phase plot for various injection powers, with fixed value of frequency detuning $\Delta\omega = -7\Omega$. Injection is in the side-mode $m = -1$. (b) Mode spectrum in the case of low injection power $P_{inj} = -18$ dBm. (c) Mode spectrum in the case of high injection power $P_{inj} = -8$ dBm. (d) Mode spectrum for $n_{sp}^{(1)}$ stationary point in the case of moderate injection power $P_{inj} = -12$ dBm. (e) Mode spectrum for $n_{sp}^{(3)}$ stationary point in the case of moderate injection power $P_{inj} = -12$ dBm.

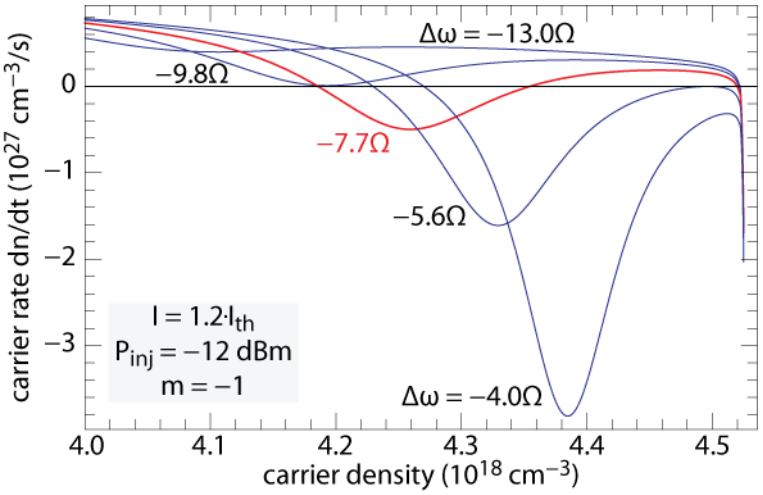

Fig.5.5 Carrier concentration rate *dn*/*dt* versus *n* phase plot for various detuning frequency, with fixed value of injection power P_{inj} = 12 dBm. Injection is in the side-mode $m = -1$.

5.4. Theory of modulation response for injection-locked multimode laser

When the slave laser is injection-locked and under current modulation, the coupled differential equations (5.1)-(5.4) have to be solved for its dynamics. For any arbitrary form of the current modulation, the solution can only be obtained numerically. The computation can be quite time consuming and a physical interpretation of the phenomena may be hard to apprehend given so many parameters involved in the system.

In order to obtain modulation response of the laser, we apply small-signal analysis. In this analysis we assume that the bias current which modulates slave laser is in the form $I(t) = I_0 + i_0\exp(\mathbf{i}2\pi ft)$, where f is the modulation frequency, I_0 is the stationary (dc) bias current, i_0 is the amplitude of the small signal modulation signal which is assumed to be much smaller than the dc value ($i_0 << I_0$), and **i** is the imaginary unit. The current modulation leads to the modulation of n, S_j, S_m and θ_m, which follow the form of the bias current: $S_j(t) = \Phi_j + \sigma_j(f)\exp(i2\pi ft)$, $S_m(t) = \Phi_m + \sigma_m(f)\exp(i2\pi ft)$, $\theta_m = \Theta_m + \psi_m(f)\exp(i2\pi ft)$, $n(t) = N + \rho(f)\exp(i2\pi ft)$, where Φ_j, Φ_m, Θ_m and N stand for the stationary components of the response, while $\sigma_j(f)$, $\sigma_m(f)$, $\psi_m(f)$ and $\rho(f)$ represent their small variations, respectively.

The equations (5.1), (5.2), (5.3), and (5.4) shown above are used as the starting point for all injection-locking simulations and analytic solutions. In this section, a small-signal analysis is performed, to derive small-signal modulation response. By taking the derivative of equations, we have:

$$d\left(\frac{dn}{dt}\right)=\frac{dI}{qV}-\left(A_{SRH}dn+\frac{dR_{sp}(n)}{dn}dn+3C_An^2dn\right)-\sum_{j=-l_1}^{l_2}\left(v_g\frac{dg(n,\omega_j)}{dn}\frac{S_j}{1+\varepsilon S_j}dn+v_g g(n,\omega_j)\frac{dS_j}{1+\varepsilon S_j{}^2}\right) \tag{5.11}$$

$$d\left(\frac{dS_j}{dt}\right)=\Gamma v_g\frac{dg(n,\omega_j)}{dn}\frac{S_j}{1+\varepsilon S_j}dn+\frac{S_j}{\tau_P}+\Gamma v_g g(n,\omega_j)\frac{dS_j}{1+\varepsilon S_j{}^2}-\frac{dS_j}{\tau_P}+\Gamma\beta_{sp}\frac{R_{sp}}{dn}dn \tag{5.12}$$

$$d\left(\frac{dS_m}{dt}\right)=\Gamma v_g\frac{dg(n,\omega_m\pm\Delta\omega)}{dn}\frac{S_m}{1+\varepsilon S_m}dn+\frac{S_j}{\tau_P}+\Gamma v_g g(n,\omega_m\pm\Delta\omega)\frac{dS_m}{1+\varepsilon S_m{}^2}-\frac{dS_m}{\tau_P}+\Gamma\beta_{sp}\frac{R_{sp}}{dn}dn+k_c\sqrt{\frac{S_{inj}}{S_m}}\cos\theta_m dS_m-2k_c\sqrt{S_{inj}S_m}\sin\theta_m d\theta_m \tag{5.13}$$

$$d\left(\frac{d\theta_m}{dt}\right)=\frac{\alpha}{2}\Gamma v_g\frac{dg(n,\omega_m\pm\Delta\omega)}{dn}\frac{1}{1+\varepsilon\cdot S_m}dn-\frac{\alpha}{2}\Gamma v_g g(n,\omega_m\pm\Delta\omega)\frac{dS_m\varepsilon}{(1+\varepsilon S_m)^2}+\frac{k_c}{2}\sqrt{S_{inj}}S_m^{-3/2}\sin(\theta_m)dS_m-k_c\sqrt{\frac{S_{inj}}{S_m}}\cos(\theta_m)d\theta_m \tag{5.14}$$

Rearranging the terms we get:

$$d\left(\frac{dn}{dt}\right)=\frac{dI}{qV}-dn\left(A_{SRH}+\frac{dR_{sp}(n)}{dn}+3C_An^2\right)-$$
$$dn\sum_{j=-l_1}^{l_2}v_g\frac{dg(n,\omega_j)}{dn}\frac{S_j}{1+\varepsilon S_j}-dS_j\sum_{j=-l_1}^{l_2}v_g g(n,\omega_j)\frac{dS_j}{1+\varepsilon S_j{}^2} \tag{5.15}$$

$$d\left(\frac{dS_j}{dt}\right)=dn\left(\Gamma v_g\frac{dg(n,\omega_j)}{dn}\frac{S_j}{1+\varepsilon S_j}+\Gamma\beta_{sp}\frac{dR_{sp}}{dn}\right)+$$
$$dS_j\left(\Gamma v_g g(n,\omega_j)\frac{1}{1+\varepsilon S_j{}^2}-\frac{1}{\tau_P}\right) \tag{5.16}$$

$$d\left(\frac{dS_m}{dt}\right)=dn\left(\Gamma v_g\frac{dg(n,\omega_m\pm\Delta\omega)}{dn}\frac{S_m}{1+\varepsilon S_m}+\Gamma\beta_{sp}\frac{dR_{sp}}{dn}\right)+$$
$$d\theta_m\ -2k_c\sqrt{S_{inj}S_m}\sin\theta_m\ +$$
$$dS_m\left(\Gamma v_g g(n,\omega_m\pm\Delta\omega)\frac{dS_m}{1+\varepsilon S_m{}^2}-\frac{1}{\tau_P}+k_c\sqrt{\frac{S_{inj}}{S_m}}\cos\theta_m\right) \tag{5.17}$$

$$d\left(\frac{d\theta_m}{dt}\right)=dn\left(\frac{\alpha}{2}\Gamma v_g\frac{dg(n,\omega_m\pm\Delta\omega)}{dn}\frac{1}{1+\varepsilon S_m}\right)+$$
$$dS_m\left(\frac{k_c}{2}\sqrt{S_{inj}}S_m^{-3/2}-\frac{\alpha}{2}\Gamma v_g g(n,\omega_m\pm\Delta\omega)\frac{\varepsilon}{(1+\varepsilon S_m)^2}\right)- \tag{5.18}$$
$$d\theta_m\left(k_c\sqrt{\frac{S_{inj}}{S_m}}\cos(\theta_m)\right)$$

These equations can be expressed in the matrix form:

$$\frac{d}{dt}\begin{bmatrix} dS_{-l_1} \\ \vdots \\ dS_m \\ \vdots \\ dS_{l_2} \\ d\theta_m \\ dn \end{bmatrix} = \|A\| \cdot \begin{bmatrix} dS_{-l_1} \\ \vdots \\ dS_m \\ \vdots \\ dS_{l_2} \\ d\theta_m \\ dn \end{bmatrix} + \begin{bmatrix} 0 \\ \vdots \\ 0 \\ \vdots \\ 0 \\ 0 \\ -dI/(qV) \end{bmatrix} \tag{5.19}$$

Chapter 6 - Results and discussion on modulation response

6.1. Modulation response of free running Fabry-Perot laser

In the free-running regime $S_{inj} = 0$, and the phase of the injection-locked mode θ_m has no influence on the modulation response, thus, for the free-running regime, system of equations which underlies the small-signal analysis is:

$$\frac{dn}{dt} = \frac{I}{qV} - \left[A_{SRH} n + R_{sp}(n) + C_A n^3 \right] - \sum_{j=-l_1}^{l_2} v_g g(n) \frac{S_j}{1+\varepsilon S_j} \tag{6.1}$$

$$\frac{dS_j}{dt} = \Gamma v_g g(n) \frac{S_j}{1+\varepsilon S_j} - \frac{S_j}{\tau_P} + \Gamma \beta_{sp} R_{sp}(n) \tag{6.2}$$

Current modulation leads to the modulation of n and S_j, which follow the form of the bias current: $n(t) = N + \rho(f)\exp(i2\pi ft)$, $S_j(t) = \Phi_j + \sigma_j(f)\exp(i2\pi ft)$, where i stands for imaginary unit, N and Φ_j stand for the stationary components of the response, while $\rho(f)$ and $\sigma_j(f)$ represent their small variations, respectively. The small-signal multimode rate equations can be expressed similar to Eq. (5.19):

$$\frac{d}{dt}\begin{bmatrix} dS_{-l_1} \\ \vdots \\ dS_{l_2} \\ dn \end{bmatrix} = \|A\| \cdot \begin{bmatrix} dS_{-l_1} \\ \vdots \\ dS_{l_2} \\ dn \end{bmatrix} + \begin{bmatrix} 0 \\ \vdots \\ 0 \\ -dI/(qV) \end{bmatrix} \tag{6.3}$$

which can be, according to the modulation forms of n and S_j, written as:

$$\left[\|A\| - i2\pi f \|I\| \right] \times \left[\sigma_{-l_1}(f) \quad \ldots \quad \sigma_{l_2}(f) \quad \rho(f) \right]^T = \begin{bmatrix} 0 & \ldots & 0 & -i_0/qV \end{bmatrix}^T \tag{6.4}$$

where $||I||$ is the identity matrix, while

$$\|A\| = \begin{Vmatrix} a_{-l_1,-l_1} & \cdots & a_{-l_1,l_2} & a_{-l_1,n} \\ \vdots & \ddots & & \vdots \\ a_{l_2,-l_1} & & a_{l_2,l_2} & a_{l_2,n} \\ a_{n,-l_1} & \cdots & a_{n,l_2} & a_{n,n} \end{Vmatrix} \tag{6.5}$$

The coefficients of the matrix ||*A*|| different from 0 are:

$$\begin{aligned} a_{jj} &= \Gamma v_g g(N,\omega_j) - 1/\tau_p, \\ a_{jn} &= \Gamma \beta_{sp} \left.\frac{dR_{sp}(n)}{dn}\right|_{n=N} + \Gamma v_g \Phi_j \left.\frac{dg(n,\omega_j)}{dn}\right|_{n=N}, \\ a_{nj} &= -v_g g(N,\omega_j), \\ a_{nn} &= -A_{SRH} - \left.\frac{dR_{sp}(n)}{dn}\right|_{n=N} - 3C_A N^2 - \sum_{j=-l_1}^{l_2} v_g \Phi_j \left.\frac{dg(n,\omega_j)}{dn}\right|_{n=N}. \end{aligned} \tag{6.6}$$

where $-l_1 \le j \le l_2$. The modulation response of the particular mode of interest can be calculated as:

$$M_j(f) = 10\log_{10}\left(\frac{\sigma_j(f)^2}{\sigma_j(0)^2}\right) \tag{6.7}$$

However, due to multimode character of the FP-LD emission, the total modulation response is obtained as [42]:

$$M(f) = 10\log_{10}\left(\frac{\left|\sum_{j=-l_1}^{l_2}\sigma_j(f)\right|^2}{\left|\sum_{j=-l_1}^{l_2}\sigma_j(0)\right|^2}\right) \tag{6.8}$$

In the Fig. 6.1 we present modulation responses both for the central mode according to the equation (6.7) and total modulation response according to the equation (6.8), for three values of the injection current, i.e. $I = 1.2I_{th}$, $I = 3I_{th}$ and $I = 5I_{th}$. As injection current becomes larger, SMSR becomes higher, which means that the influence of the side-modes on the modulation response becomes more negligible, hence modulation response for the central mode becomes more similar to total modulation response [c.f. Fig. 6.1(c)]. In addition to this, higher injection currents lead to more pronounced modulation response resonance peak, thus pronouncing the modulation response nonlinearity.

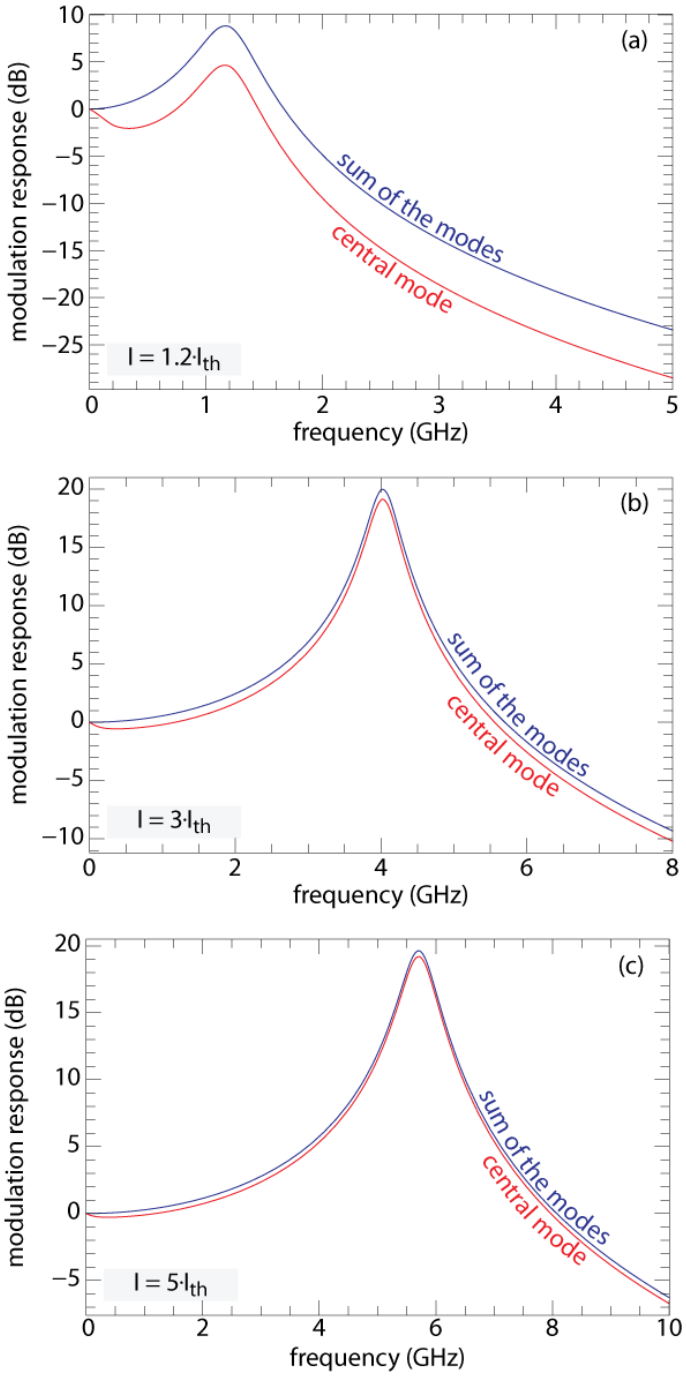

Fig.6.1 Comparison of modulation response for FR regime for sum of the modes (blue line), and central mode (red line), with $I = 1.2I_{th}$ (a), $I = 3I_{th}$ (b) and $I = 5I_{th}$ (c).

As previously said, increase in the injection current can lead to the increase of modulation response bandwidth. In Fig. 6.2 we present −3 dB modulation bandwidth in the case of free-running slave laser with respect to the injection current.

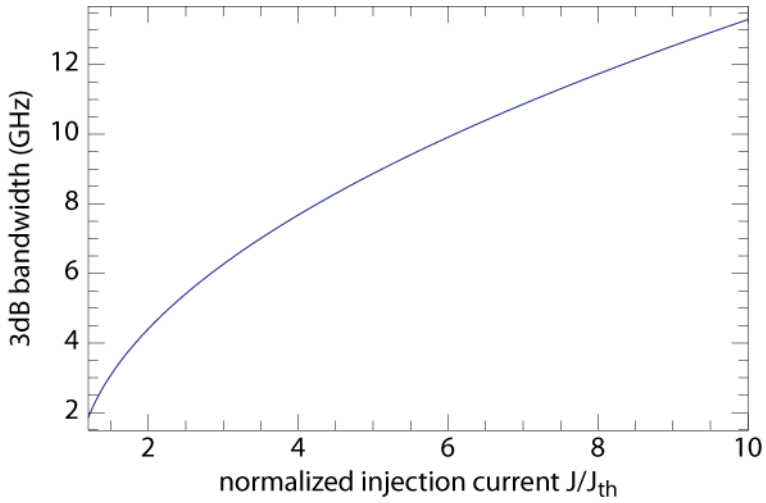

Fig.6.2 −3 dB Bandwidth versus injection current for FR regime

6.2. Modulation response of injection-locked Fabry-Perot laser

The gain model described with equation (5.5) considers parabolic gain profile. The gain maximum is at central optical frequency, corresponding to $\hbar\omega$ = 0.8 eV i.e. to m = 0. In the Fig. 6.3(a) we show the gain profile for various levels of carrier concentration. It can be seen that in this model the side-modes, both on the long- and short-wavelength side, are fully equal in terms of provided gain, which leads to symmetrical mode spectrum. Thus, this model does not recognize the difference between injection-locking into side-modes on different sides of the mode spectrum. On the other hand in the Fig. 6.3(b) we show gain model [107] calculated for a structure in which as an active region we use $In_{0.75}Ga_{0.25}As_{0.87}P_{0.13}$ (well)/$In_{0.46}Ga_{0.39}Al_{0.15}As$ (barrier) 1.55 μm strain-compensated multi quantum well (MQW) material. For the threshold carrier concentration, gain maximum is at $\hbar\omega$ = 0.8 eV, similar to the previous gain model. This exact gain model shows that in reality, gain profile is asymmetrical and that, as opposed to the simple parabolic model,

gain maximum slightly shifts its corresponding photon energy while reaching the threshold. Thus, this exact gain model will provide more precise insight in the laser dynamics, when it comes to intermodal injection-locking in which light is injected in one of the side-modes. However, simple parabolic gain model shows to be a good approximation when it comes to the central mode gain dependence on carrier concentration. In Fig. 6.4 we show gain for $\hbar\omega$ = 0.8 eV versus carrier concentration n in the case of parabolic gain model [Fig. 6.4(a)], and exact gain model [Fig. 6.4(b)]. Due to this good approximation, simple gain model can be effective when it comes to injection-locking into the side-modes close to the central mode.

In further analysis we will show modulation responses obtained for this simple gain model, as well as results obtained with exact gain model, calculated for the structure that is recognized as the one which provides high modulation bandwidths.

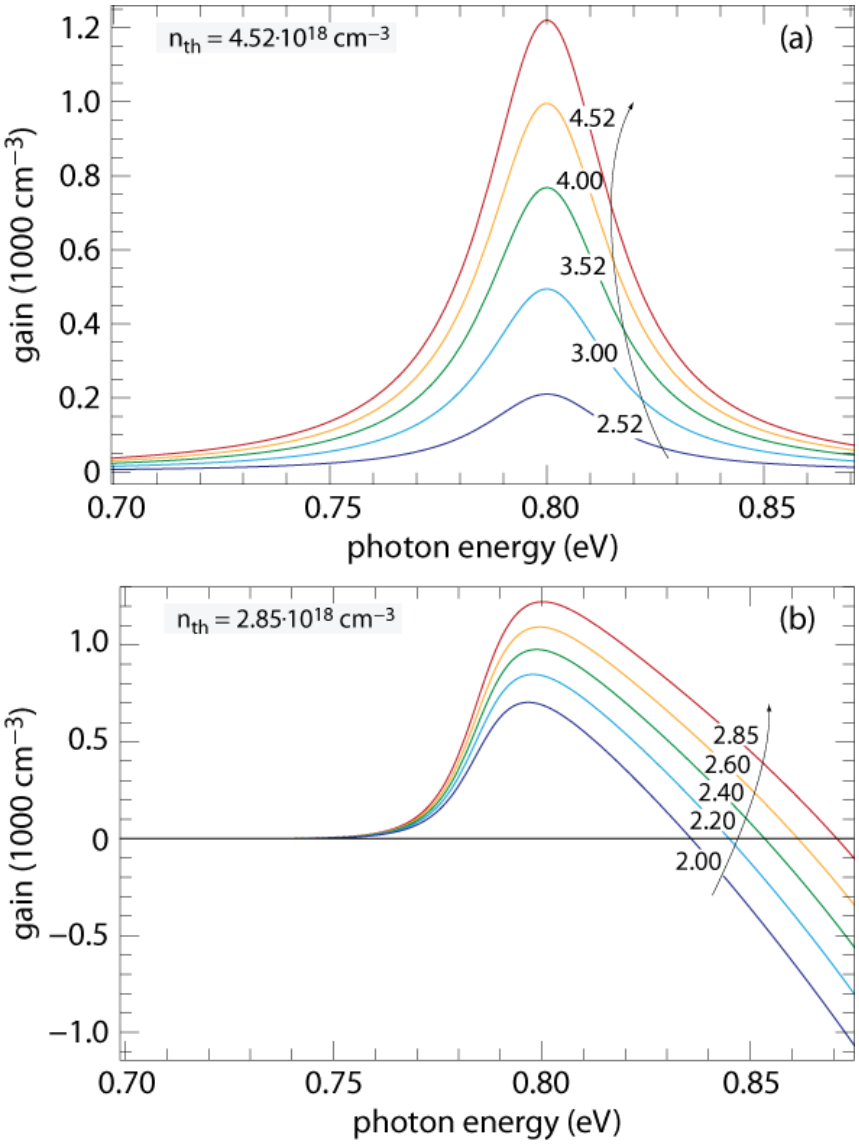

Fig. 6.3 Gain profile in the case of parabolic gain model (a) for carrier concentrations $n = n_{th} = 4.52\times10^{18}$ cm^{-3}, $n = 4\times10^{18}$ cm^{-3}, $n = 3.52\times10^{18}$ cm^{-3}, $n = 3\times10^{18}$ cm^{-3} and $n = 2.52\times10^{18}$ cm^{-3}, and in the case of exact gain model (b) for $n = n_{th} = 2.85\times10^{18}$ cm^{-3}, $n = 2.6\times10^{18}$ cm^{-3}, $n = 2.4\times10^{18}$ cm^{-3}, $n = 2.2\times10^{18}$ cm^{-3} and $n = 2\times10^{18}$ cm^{-3}

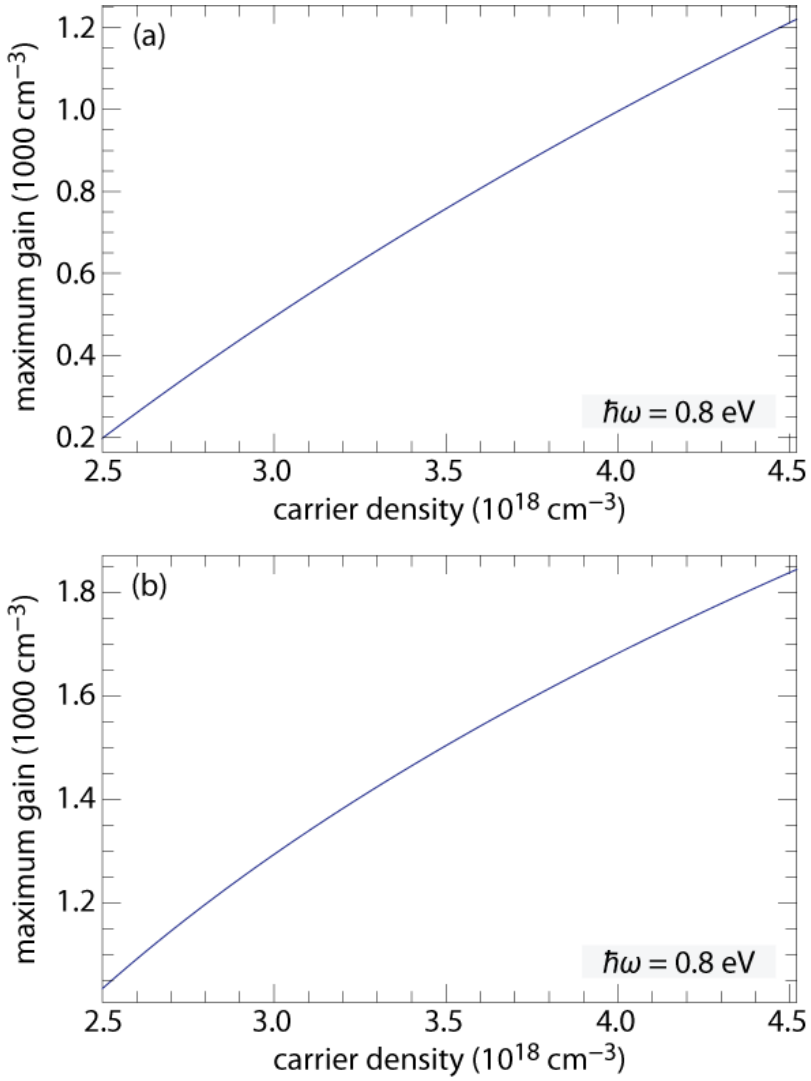

Fig. 6.4 Gain at photon energy of 0.8 eV versus carrier concentration for (a) parabolic gain model (b) exact gain model

The main focus of the dissertation is the dependence of the modulation response and corresponding −3 dB bandwidth of side-mode IL Fabry–Perot laser diodes on injection power of the master laser and frequency detuning between the master and the slave FP-LD laser. Our analysis is based on the small-signal modulation response, derived from the set of linearized multimode rate equations (5.1) – (5.4). As in the case of the modulation response for free-running regime we assume that the bias current of the slave laser is

modulated as $I(t) = I_0 + i_0\exp(\mathrm{i}2\pi ft)$, where f is the modulation frequency, I_0 is the stationary (dc) bias current, i_0 is the amplitude of the small signal modulation signal which is assumed to be much smaller than the dc value ($i_0 << I_0$), and i is the imaginary unit. The current modulation leads to the modulation of n, S_j, S_m and θ_m, which follow the form of the bias current: $S_j(t) = \Phi_j + \sigma_j(f)\exp(\mathrm{i}2\pi ft)$, $S_m(t) = \Phi_m + \sigma_m(f)\exp(\mathrm{i}2\pi ft)$, $\theta_m = \Theta_m + \psi_m(f)\exp(\mathrm{i}2\pi ft)$, $n(t) = N + \rho(f)\exp(\mathrm{i}2\pi ft)$, where Φ_j, Φ_m, Θ_m and N stand for the stationary components of the response, while $\sigma_j(f)$, $\sigma_m(f)$, $\psi_m(f)$ and $\rho(f)$ represent their small variations, respectively. Similar to free-running analysis, the small-signal multimode rate equations can be expressed as follows:

$$\left[\|A\| - \mathrm{i}2\pi f \|I\|\right] \times \left[\sigma_{-l_1}(f) \quad \cdots \quad \sigma_m(f) \quad \cdots \quad \sigma_{l_2}(f) \quad \psi_m(f) \quad \rho(f)\right]^T = \begin{matrix} 0 & \cdots & 0 & \cdots & 0 & 0 & -i_0/qV \end{matrix}^T \tag{6.9}$$

where $\|I\|$ is the identity matrix, while

$$\|A\| = \begin{Vmatrix} a_{-l_1,-l_1} & \cdots & a_{-l_1,m} & \cdots & a_{-l_1,l_2} & a_{-l_1,\theta} & a_{-l_1,n} \\ \vdots & \ddots & & & & & \vdots \\ a_{m,-l_1} & & a_{m,m} & & a_{m,l_2} & a_{m,\theta} & a_{m,n} \\ \vdots & & & \ddots & & & \vdots \\ a_{l_2,-l_1} & & a_{l_2,m} & & a_{l_2,l_2} & a_{l_2,\theta} & a_{l_2,n} \\ a_{\theta,-l_1} & & a_{\theta,m} & & a_{\theta,l_2} & a_{\theta,\theta} & a_{\theta,n} \\ a_{n,-l_1} & \cdots & a_{n,m} & \cdots & a_{n,l_2} & a_{n,\theta} & a_{n,n} \end{Vmatrix} \tag{6.10}$$

The coefficients of the matrix $\|A\|$ different from 0 are:

$$
\begin{aligned}
a_{jj} &= \Gamma v_g g(N,\omega_j) - 1/\tau_p, \\
a_{jn} &= \Gamma \beta_{sp} \left.\frac{dR_{sp}(n)}{dn}\right|_{n=N} + \Gamma v_g \Phi_j \left.\frac{dg(n,\omega_j)}{dn}\right|_{n=N}, \\
a_{m,m} &= \Gamma v_g g(N,\omega_m) - 1/\tau_p + k_c \sqrt{S_{inj}/\Phi_m}\cos\Theta_m, \\
a_{m,\theta} &= -2k_c \sqrt{S_{inj}\Phi_m}\sin\Theta_m, \\
a_{\theta,m} &= \frac{1}{2} k_c \sqrt{S_{inj}/\Phi_m^3}\sin\Theta_m, \\
a_{\theta,\theta} &= -k_c \sqrt{S_{inj}/\Phi_m}\cos\Theta_m, \\
a_{\theta,n} &= \frac{\alpha}{2}\Gamma v_g \left.\frac{dg(n,\omega_m)}{dn}\right|_{n=N}, \\
a_{nj} &= -v_g g(N,\omega_j), \\
a_{nn} &= -A_{SRH} - \left.\frac{dR_{sp}(n)}{dn}\right|_{n=N} - 3C_A N^2 - \sum_{j=-l_1}^{l_2} v_g \Phi_j \left.\frac{dg(n,\omega_j)}{dn}\right|_{n=N}.
\end{aligned}
\tag{6.11}
$$

Again, total modulation response is calculated as:

$$
M_j(f) = 10Log_{10}\left[\left|\sum_{j=-l_1}^{l_2}\sigma_j(f)\right|^2 \Big/ \left|\sum_{j=-l_1}^{l_2}\sigma_j(0)\right|^2\right] \tag{6.12}
$$

In this dissertation it is assumed that the slave laser is set in the stationary state dominantly determined by the injected photons, i.e. the $n_{sp}^{(1)}$ states and states obtained for high injection powers. In this case side-modes are strongly suppressed, and their contribution to the modulation response can be neglected. This allows simplification of the total modulation response, by taking into account only the injected side-mode *m* and the central longitudinal mode $j = 0$. The total modulation response in this case can be written in a somewhat simpler form:

$$
M(f) = 10Log_{10}\left[\left|\frac{\sigma_0(f)+\sigma_m(f)}{\sigma_0(0)+\sigma_m(0)}\right|^2\right] \tag{6.13}
$$

Although this equation requires less calculation, in our analysis we keep all unlocked side-modes, thus in order to obtain total modulation response we use equation

(6.12). At the end of the chapter, comparison between full-scale model and simplified form, represented with equation (6.13), will be given.

It is assumed that the modulation response is calculated for stable locking. This requirement sets an additional limitation for detuning and the injection power given in chapter 4 with equation (4.25):

$$-k_c\sqrt{S_{inj}/\Phi_m}\sqrt{1+\alpha^2} < \Delta\omega < k_c\sqrt{S_{inj}/\Phi_m} \tag{6.14}$$

6.2.1. Modulation response for symmetric gain spectrum

We start our analysis with modulation response for the IL mode $m = -1$ (with corresponding wavelength λ = 1551.14 nm), with a moderate value of negative frequency detuning ($\Delta\omega = -7\Omega$) and fixed injection power (P_{inj} = 0 dBm). In the case of negative detuning and high values of injection power, slave laser is stabilized in the stationary state with low values of carrier concentration, far from threshold value. This is the state which is mainly consequence of the injection locking, and a state in which injection-locked mode is highly pronounced, while other unlocked modes, including the central mode, are strongly suppressed. Figure 6.5 shows obtained total modulation response as a function of the modulation frequency for the injection mode $m = -1$ (blue line), and free-running total modulation response (red line), for three different values of the bias current ($I = 1.2I_{\text{th}}$, $I = 3I_{\text{th}}$ and $I = 5I_{\text{th}}$). Figure 6.5(a) clearly shows that with small amount of bias current $I = 1.2I_{\text{th}}$, the modulation bandwidth is higher for the free-running case (red line) than for IL case (blue line). However, figures 6.5(b) and (c) show that with increase of the bias or injection currents the modulation bandwidth is higher for the IL mode (blue lines) than for the free-running mode (red lines). Apart from this, injection locking decreases the peak value of modulation response, thus providing more linear curve.

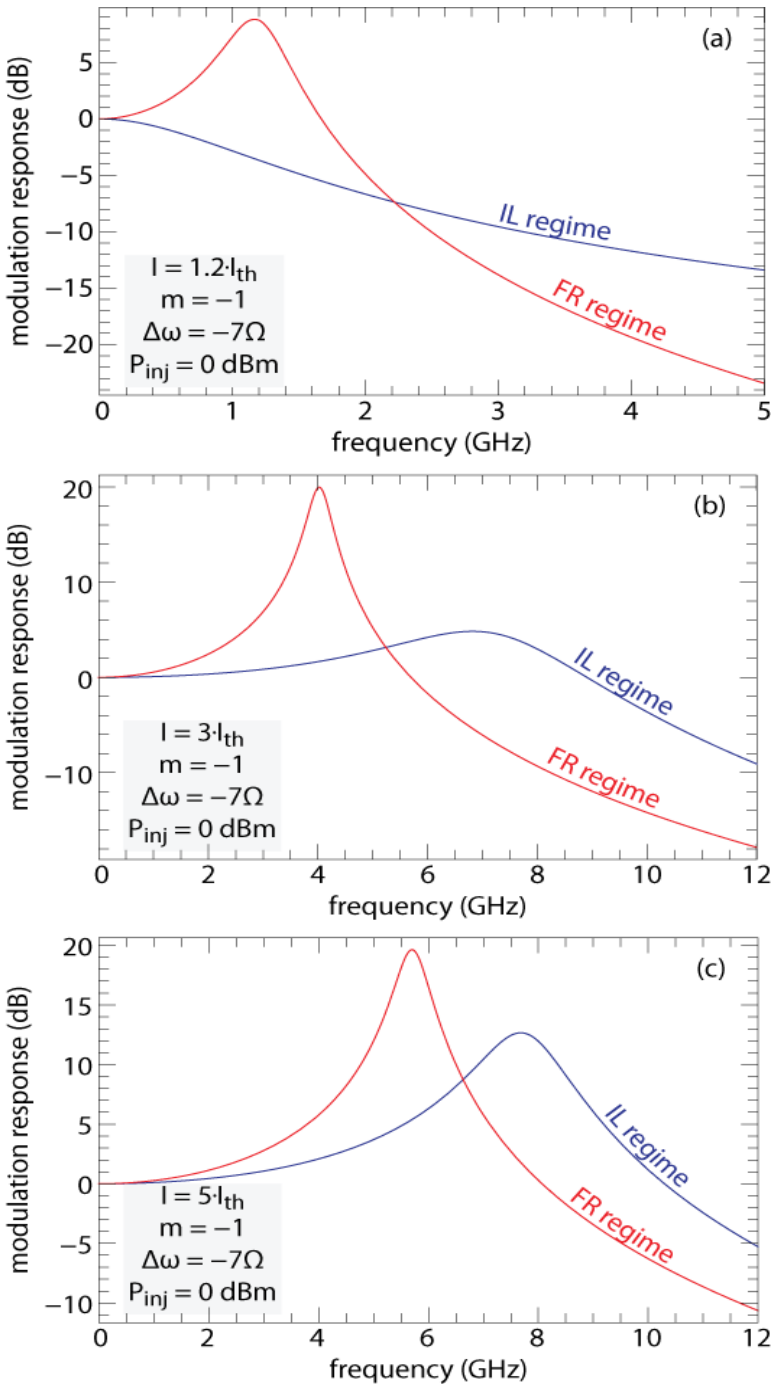

Fig.6.5 Total modulation responses for injection locking regime (blue line) in the case of injection in the side-mode $m = -1$, with $\Delta\omega = -7\Omega$ and $P_{inj} = 0$ dBm and for free-running regime (red line), obtained for three values of injection current $I = 1.2I_{th}$ (a), $3I_{th}$ (b) and $5I_{th}$ (c).

For further analysis we calculate modulation responses for positive value of frequency detuning $\Delta\omega = 4\Omega$, keeping high value of the injection power. For positive frequency detuning numerical analysis of the dn/dt versus n phase plots, shows that there is no RMSP, i.e. regardless of injection power magnitude, slave laser always has just one stationary point. Again, this stationary point is a consequence of the injection locking, and for high injection powers this point is far away from the free-running threshold. In addition to this, numerical investigation shows that in the case of positive frequency detuning this point is closer to the n_{th}, compared to the case of negative frequency detuning. This means, that in this case, suppression of unlocked-side modes is somewhat smaller. However, modulation responses shown in the Fig. 6.6 show same trend as those showed in Fig. 6.5.

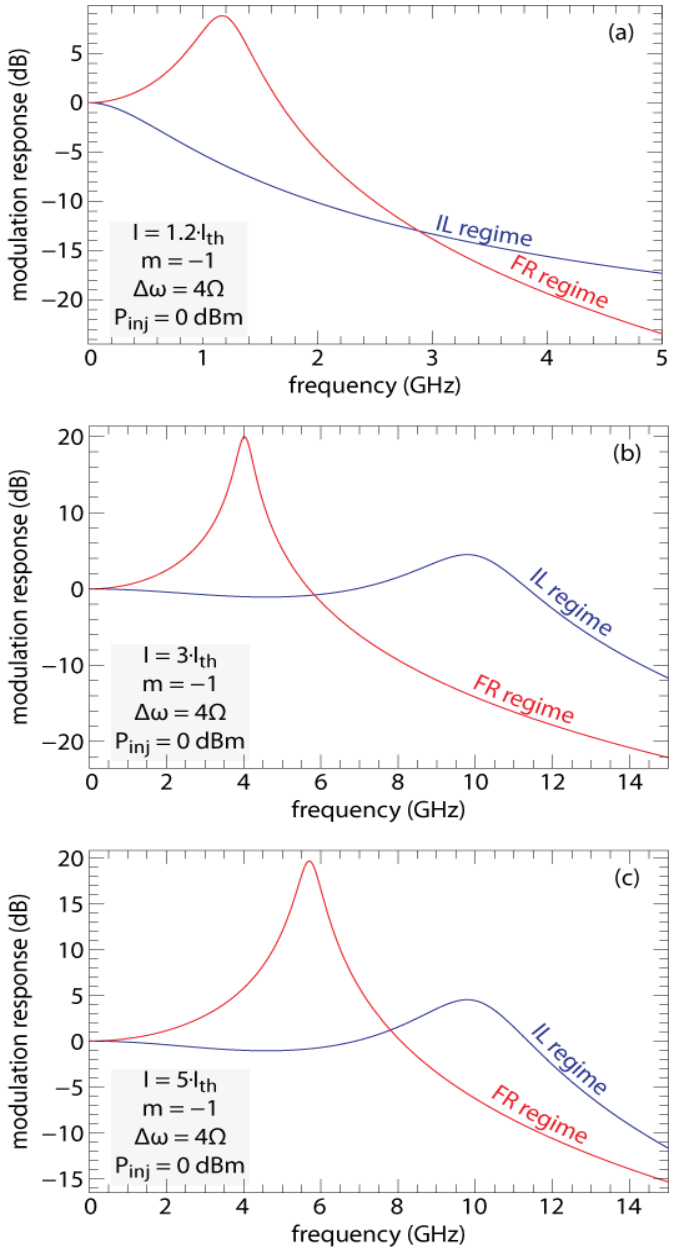

Fig.6.6 Total modulation responses for injection locking regime (blue line) in the case of injection in the side-mode $m = -1$, with $\Delta\omega = 4\Omega$ and $P_{inj} = 0$ dBm and for free-running regime (red line), obtained for three values of injection current $I = 1.2I_{th}$ (a), $3I_{th}$ (b) and $5I_{th}$ (c).

In Fig. 6.7 we present total modulation responses for fixed injection current and frequency detuning, and various injection powers. Injection current is set to moderate value of $3I_{th}$, while frequency detuning is set to high negative value of -7Ω. Although this

frequency detuning can lead to formation of three stationary states, for injection powers employed in this figure, there is only one stationary point, for which slave laser has strongly suppressed side-modes, and highly pronounced injection-locked mode. It can be seen that increase in the injection power leads to the increase of −3 dB modulation bandwidth, and also to the improved linearity of the response. In addition to this extremely high injection power can lead to total suppression of the modulation response resonance peak, since pole of the characteristic shifts to smaller frequencies.

In Fig. 6.8 we analyze the dependence of the total modulation response on frequency detuning. We set injection current to $3I_{th}$ and injection power to 5 dBm. Figure 6.8 shows that positive detuning shifts resonance peak to higher frequencies, thus providing higher −3 dB modulation bandwidth. However, in terms of SMSR ratio, more positive frequency detuning needs higher injection powers in order to achieve high value of SMSR. Interesting thing happens for high positive frequency detuning ($\Delta\omega = 7\Omega$, c.f. Fig. 6.8). For such a positive detuning, the dip in the modulation response lowers the response below, while the resonant peak brings it above –3 dB. As a result, there are two frequency regions for which the modulation response is above –3 dB.

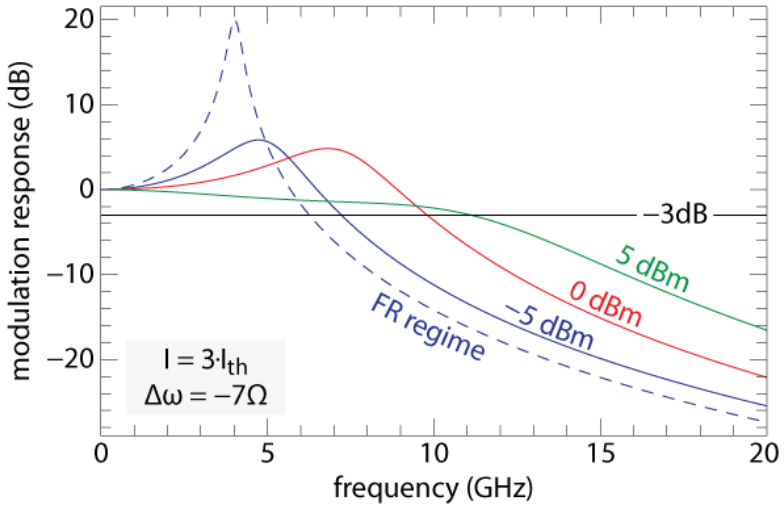

Fig.6.7 Total modulation responses for fixed frequency detuning $\Delta\omega = -7\Omega$, and different values of injection powers $P_{inj} = -5$ dBm (blue line), 0 dBm (red line), 5 dBm (green line) compared to the total modulation response in the free-running case (dashed line). Injection current is set to $3I_{th}$.

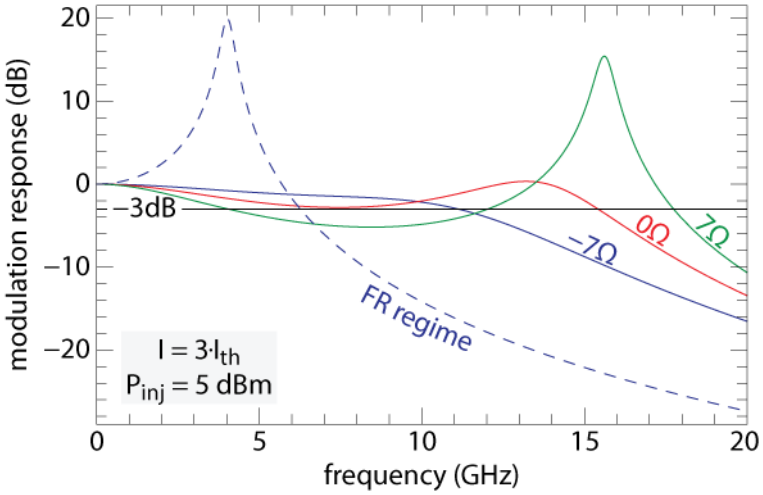

Fig.6.8 Total modulation responses for fixed injection power P_{inj} = 5 dBm and different values of frequency detuning $\Delta\omega$ = −7Ω (blue line), 0Ω (red line), 7Ω (green line), compared to the total modulation response for free-running regime (dashed line). Injection current is set to $3I_{th}$.

In our further analysis of the noticed effect, we calculate the −3 dB modulation bandwidth frequency versus injection power and frequency detuning. In Fig. 6.9 we show that the modulation response has the maximum, after which rapidly decays with increasing injection power, which means that too strong injection can be harmful for bandwidth improvement. In addition to this, for positive detuning, as showed in the Fig. 6.8, modulation response can exhibit a dip below −3 dB, and then for larger frequencies it rises above −3 dB. In such cases there are two frequency regions in which modulation response is above −3 dB. Thus the bandwidth becomes a multiform function on injection power. As an example, for frequency detuning $\Delta\omega$ = - 3Ω, for injection powers in the range from 4.2 dBm to 7.2 dBm, modulation there are two frequency regions in which modulation bandwidth are above −3 dB (c.f Fig 6.9). This analysis shows that the bandwidth of the slave laser can be optimized with respect to the injection power and detuning. The example presented in Fig 6.9 shows that for P_{inj} = 4.2 dBm, and for detuning $\Delta\omega$ = - 3Ω, −3 dB bandwidth exhibits its maximum, which is approximately 16 GHz. This bandwidth is more

than two times larger than the bandwidth in the free-running regime, which is limited to about 6.3 GHz.

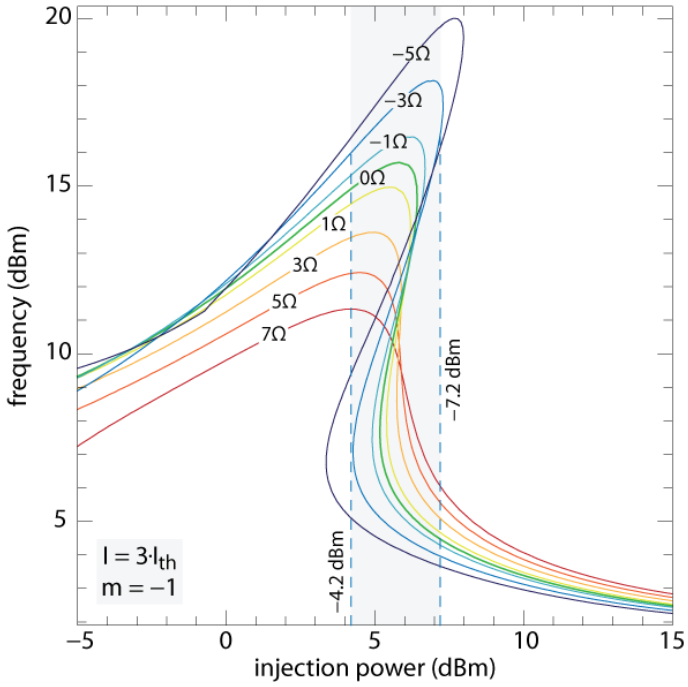

Fig.6.9 −3 dB modulation bandwidth versus injection power, for different values of frequency detuning ,starting from the bottom, −5Ω (dark blue line), −3Ω (blue line), −1Ω (light blue line), 0Ω (green line), 1Ω (yellow line), 3Ω (light red line), 5Ω (red line), 7Ω (dark red line). For positive values of frequency detuning, −3 dB modulation bandwidth becomes a multiform function on injection power.

Finally, we discuss modulation responses with injection in different side-modes. In Fig. 6.10 we present total modulation responses for injection current set to $3I_{th}$, frequency detuning $\Delta\omega = -7\Omega$, $P_{inj} = 0$ dBm [Fig. 6.10(a)] and $P_{inj} = 5$ dBm [Fig. 6.10(b)], for injection in side-modes $m = -1$, $m = -5$ and $m = -10$. It can be seen that all three modulation responses have very similar shape, and that differences in −3 dB modulation bandwidth is in order of few GHz (for modes $m = -1$ and -5 the bandwidth is around 10 GHz, while for mode $m = -10$ is around 9 GHz). This means that even far side-modes like

m = −10 can have the same injection locking characteristic as side-modes close to the central mode, which enables wide wavelength operation range of the IL FP slave laser. This is particularly interesting for application of the injection-locked lasers in the ONUs, where wide wavelength operation range is of high importance, since it can provide large number of different wavelengths i.e. channels for upstream communication with CO.

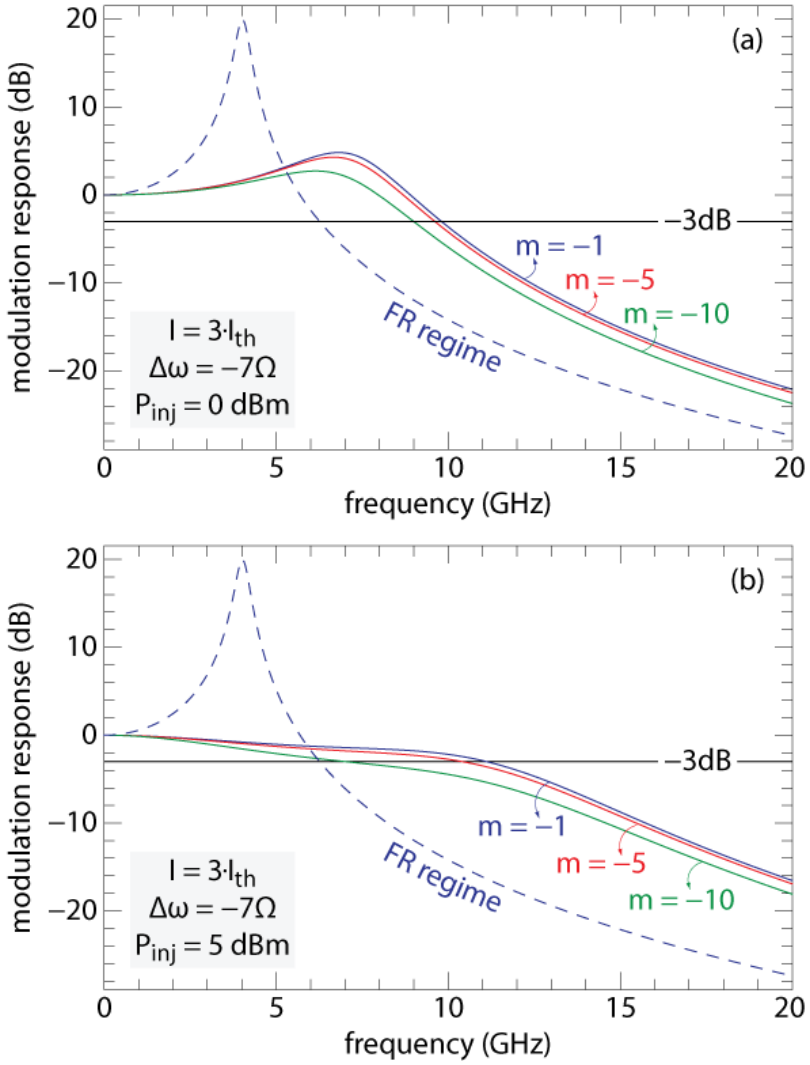

Fig.6.10 Total modulation responses for fixed frequency detuning $\Delta\omega$ = −7Ω, (a) with fixed injection power P_{inj} = 0 dBm, (b) P_{inj} = 5 dBm, and different values of side modes m = −1 (blue line), m = −5 (red line), m = −10 (green line), compared to the free-running total modulation response (dashed line)

As previously said, the parabolic gain model, which gives symmetric mode spectrum, can be a good approximation for side-modes close to the central mode. For this reason, in further analysis we use much more complex and more realistic gain model, taken from [107]. Apart from being realistic, this gain is calculated for the specially optimized structure, in order to optimize modulation bandwidth of the slave laser.

6.2.2. Modulation response for asymmetric gain spectrum

In order to analyze modulation response of injection locked regime for asymmetric gain spectrum it is necessary to use realistic calculation of gain spectrum. Therefore, the analysis is based on already optimized laser structure which might provide for high modulation bandwidth [107]. The active region of the slave laser consists on $In_{0.75}Ga_{0.25}As_{0.87}P_{0.13}$ (well)/$In_{0.46}Ga_{0.39}Al_{0.15}As$ (barrier) 1.55 μm strain-compensated multi quantum well (MQW) material [107]. This material system is recognized as the one that provides high modulation bandwidth of lasers, due to the balanced and, therefore, improved carrier transport through MQW structure.

In [107] authors apply the "model-solid theory" [108] combined with the interpolation schemes and material parameters as given in [109] to calculate the conduction band (CB) and valence band (VB) edges for a given composition of both InGaAsP and InGaAlAs alloys. The simulations assume a constant device temperature of 300 K. By utilizing 1.05% compressive strained well and 0.5% tensile strained barrier, they perform precise band structure adjustment resulting in λ = 1698 nm optimized well (E_g = 0.73 eV) with CB discontinuity ratio $\Delta E_c/(\Delta E_c + \Delta E_{v,HH\text{-}LH})$ = 81.1%. The band-edge diagrams for InGaAsP/InGaAlAs hetero-junction with and without strain taken into account are shown in Figure 6.11(a). The MQW active region consists of 3 equally spaced QWs with well thickness d = 8.7 nm, although the number of wells can be increased and still maintain good carrier transport and population inversion in all the wells simultaneously.

In order to set a detailed model of the rate equations, calculated material gain $g(n,\hbar\omega)$ versus carrier concentration n and photon energy $\hbar\omega$ [c.f Fig 6.11(b)] is taken from [107].

The total spontaneous recombination rate $R_{sp}(n) = \int R_{sp}(n,\hbar\omega)d(n,\hbar\omega)$, is also taken from [107] instead of its modeling by bimolecular recombination coefficient B_R.

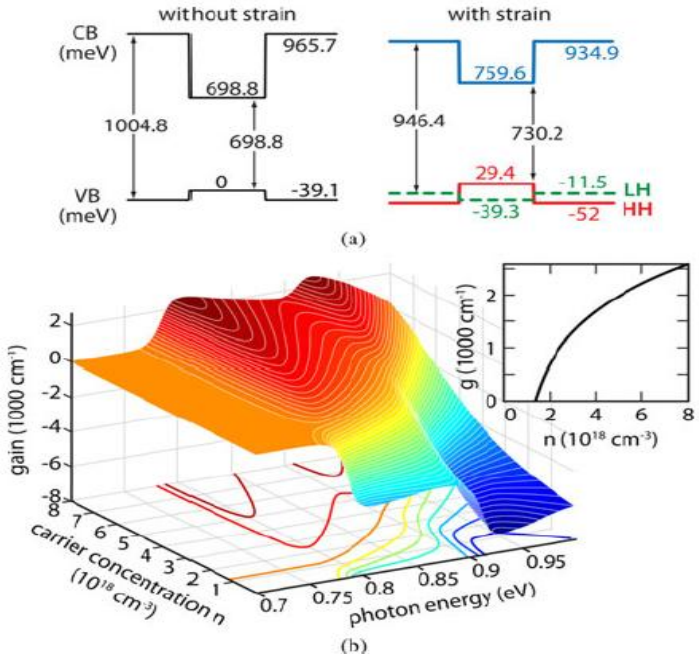

Fig.6.11. (a) Band-edge levels and (b) material gain spectrum for $In_{0.75}Ga_{0.25}As_{0.87}P_{0.13}$ 1.05% compressive well with $In_{0.46}Ga_{0.39}Al_{0.15}As$ 0.5% tensile barrier [107]. Inset: Gain versus carrier concentration at $\hbar\omega$ = 0.8 eV.

The gain calculation is based on the single-QW band structure obtained by the 8□8 **k.p** method [110]. For the calculated threshold gain g_{th} = 1225 cm^{-1}, the threshold concentration in the FR regime, $n_{th} = 2.85\square10^{18}$ cm^{-3}. The corresponding threshold current of the FR FP-LD is I_{th} = 2.45 mA. The laser emission is centered around 0.8 eV, but due to the asymmetry of the gain profile, the number of the supported modes is different for ω < 0.8 eV (l_1 = 170) and ω > 0.8 eV (l_2 = 120). The equation model used in the simulations is (5.1) – (5.4). In those equations τ_p is calculated to be 2.04 ps, confinement factor Γ = 0.056, $A_{SRH} = 1.1\square10^8$ s^{-1}, $C_A = 5.82\square10^{-29}$ cm^6s^{-1} and $\beta_{sp} = 2.15\square10^{-4}$. Other parameters are the same as in previous simulations for parabolic gain profile.

The analysis starts with modulation response for the IL mode $m = -5$, two different values of detuning ($\Delta\omega = \pm5\Omega$) and two different injection powers (P_{inj} = 0 and P_{inj} = 10

dBm) (Fig 6.12). The bias current is set to a moderate value $I = 3I_{th}$ preventing too strong stimulated emission and nonlinear gain suppression. Figure 6.12 shows the modulation response for the mode $m = -5$. $[M_{-5}(f)]$, for the central mode $j = 0$, $[M_0(f)]$, and the total modulation response $M(f) = M_{-5,0}$ calculated according to equation (6.13). However, in figure 6.12, $M_{-5,0}$ and M_{-5} overlap since the influence of IL mode is dominant over the central mode. The same modulation characteristic is obtained by relation (6.12) if we take into account all $l_1+l_2+1 = 291$ modes. Since equation (6.13) has much simpler form, in further calculation we use only injection-locked and central mode.

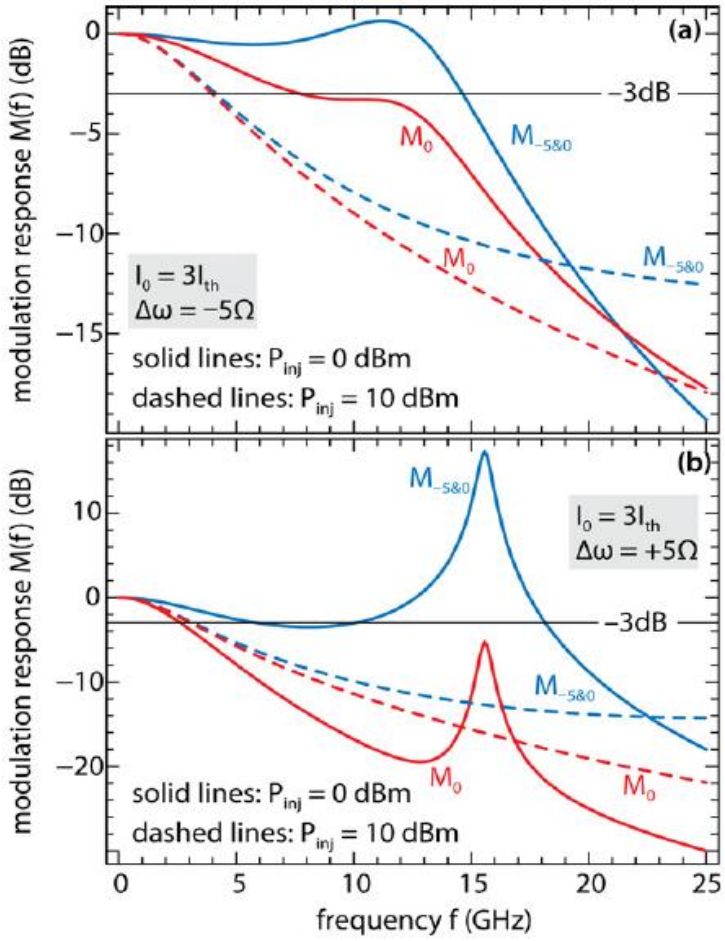

Fig.6.12. Modulation response $M(f)$ of the slave laser for injection into side mode $m = -5$ at the stationary bias current $I_0 = 3I_{th}$, detuning $\Delta\omega = \pm 5\Omega$ and two values of injection power P_{inj}. M_0 is the modulation response of the central mode. $M_{-5,0}$ is the total modulation response, which overlaps the modulation response of the single mode M_{-5}.

Figure 6.12 clearly shows that −3 dB bandwidth is higher for the IL mode than for the central mode. Moreover, it can be seen that a larger injection power deteriorates the modulation response and the bandwidth of the slave laser. Interestingly, the modulation response significantly differs for positive and negative detuning. The reason for that is the stationary phase difference (Θ_m) between the free-running and the IL state, which is, according to equation (5.4), directly affected by the sign of detuning. It can be further seen that coefficients of the matrix and consequently the poles and zeros of the modulation response depend on Θ_m in a nontrivial way, which does not provide much deeper insight into the dependence of modulation response on detuning sign. For $\Delta\omega = -5\Omega$ [Fig. 6.12(a)], the modulation response exhibits a rather small resonant peak and a flat characteristic up to the bandwidth frequency. On the other hand, a positive detuning, $\Delta\omega = 5\Omega$ [Fig 6.12(b)], leads to a pronounced resonant peak and a dip in the modulation response. For such a positive detuning, the dip in the modulation response lowers the response below, while the resonant peak brings it above −3 dB. As a result, there are two frequency regions for which the modulation response is above −3 dB. In our further analysis of the noticed effect, we calculate the modulation response versus injection power and frequency for a fixed detuning $\Delta\omega = 4\Omega$.

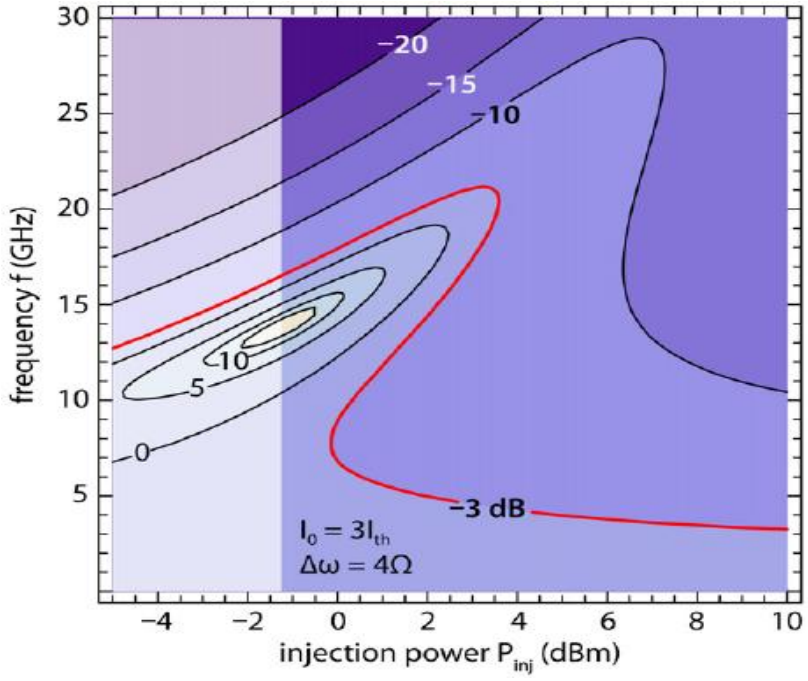

Fig.6.13. Contour plot of modulation response $M_{-5,0}$ versus frequency f and injection power P_{inj}, at bias current $I_0 = 3I_{th}$ and detuning $\Delta\omega = 4\Omega$. The left brighter part of the plot corresponds to unstable locking, while the right larger part is the region of stable locking. The red line denotes −3 dB bandwidth of the slave laser.

The contour plot in Fig. 6.13 shows that the modulation response has the maximum, which occurs as a result of the weakly suppressed resonance. Although the modulation response can be easily evaluated for various injection powers and detuning, the region of small injection power cannot provide stable locking and thus only the right side of the contour plot for $P_{inj} > -1.24$ dBm depicts the stable modulation response. The resonant peak is positioned at the border of the stable and unstable-locking regions. Due to the peak the bandwidth on the stable side of the border vicinity is greater. In fact, the modulation response usually decays with frequency and thus the occurrence of the resonant peak in the border vicinity leads to flattening of the modulation response and an increase of bandwidth. It can be seen the resonance peak occurs for relatively small or even moderate powers,

leading to significant improvement of the bandwidth. This means that too strong injection can become harmful for bandwidth improvement.

In order to investigate the possibility for further improvement of the bandwidth of the slave laser, the bandwidth dependence on detuning is investigated. Fig. 6.14, shows that for a relatively large negative detuning as $\Delta\omega = -9\Omega$ the bandwidth of the slave laser slowly increases with injection power and, on reaching the maximum, steeply decays with increasing injection power. A similar trend can be observed for less negative detuning, i.e. for $\Delta\omega = -5\Omega$, with the exception that the maximum of the bandwidth is more pronounced, while the decay is more rapid than in the case of more negative detuning. For small negative and for positive detuning, the border of stable locking moves toward larger injection powers. Thus the bandwidth is considered only for sufficiently large injection powers, for which the locking is stable. For larger injection power, the modulation response exhibits a dip as shown in Fig. 6.12, which goes below −3 dB and then, for larger *f*, rises above −3 dB, due to the resonant peak. Thus the bandwidth becomes a multiform function on injection power. Since the bandwidth is determined by the lowest frequency *f* for which the response drops below −3 dB, only the lowest branch of the multiform function should be considered. Dashed lines in Fig. 6.14 show two upper branches of this function for $\Delta\omega = -1\Omega$, and $\Delta\omega = 3\Omega$.

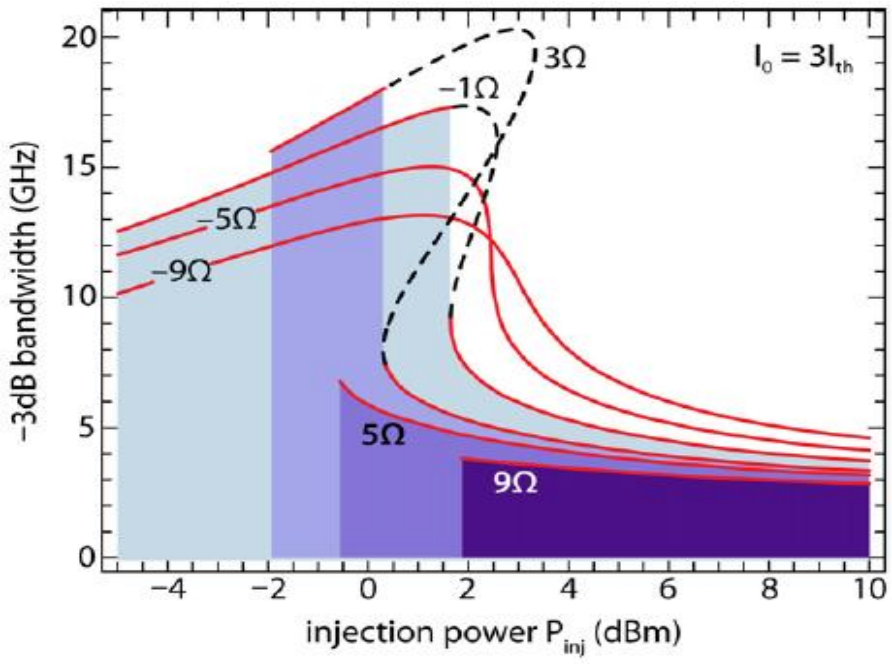

Fig.6.14. The modulation bandwidth versus P_{inj} for various values of $\Delta\omega$. Solid red curves show the actual bandwidth. They start at the borders of stable locking, while discontinuities occur at injection powers for which the modulation response exhibits a dip larger than −3 dB. Dashed lines together with the corresponding shaded area encircle the region where the modulation response rises above −3 dB due to the uncompensated resonant peak.

At the injection power, for which the function character changes from "one-to-one" to multiform, there is a sudden drop in the bandwidth. For a large positive detuning (e.g. $\Delta\omega = 5\Omega$, and $\Delta\omega = 9\Omega$), the region of stable locking occurs for large injection powers, for which the dip in modulation response is a common effect. In this case only the lowest branch of the multiform dependence determines the actual bandwidth. This analysis shows that the bandwidth of the slave laser can be optimized with respect to the injection power and detuning. The example presented in Figure 6.14 shows that for $P_{inj} = 0.27$ dBm and for detuning $\Delta\omega = 3\Omega$, −3 dB bandwidth exhibits its global maximum, which is approximately 18 GHz. This bandwidth improvement is more than twice as large as the bandwidth in the free-running regime, which is limited to about 7 GHz.

The optimized structure provides higher −3 dB modulation bandwidth in comparison with symmetrical gain model. In the Fig. 6.15 we present comparison of modulation bandwidth versus injection power, for different values of frequency detuning and gain model. For negative detuning of $\Delta\omega = -5\Omega$ (solid lines in Fig. 6.15), modulation bandwidth remains "one-to-one" function on injection power, with a global maximum, which is shifted towards smaller injection powers in the case of asymmetrical gain model. This maximum is higher in the case of asymmetrical gain model (blue solid line in Fig. 6.15) and has a value around 15 GHz, while in the case of symmetrical gain model (red solid line in Fig. 6.15) it is around 12 GHz. Thus, optimized structure reduces the injection power needed for optimal modulation bandwidth, while providing higher bandwidth. For positive frequency detuning of $\Delta\omega = 3\Omega$ (dashed lines in Fig. 6.15), modulation bandwidth is a multiform function on injection power in both gain models. However, asymmetrical gain model, again, provides higher value of modulation bandwidth at lower value of injection power. In the case of asymmetrical gain (blue dashed line in Fig. 6.15), this maximum is obtained for P_{inj} around 0.65 dBm and has a value around 18.6 GHz, while for symmetrical gain this maximum is obtained for P_{inj} around 4.5 dBm, but has smaller value, around 16 GHz.

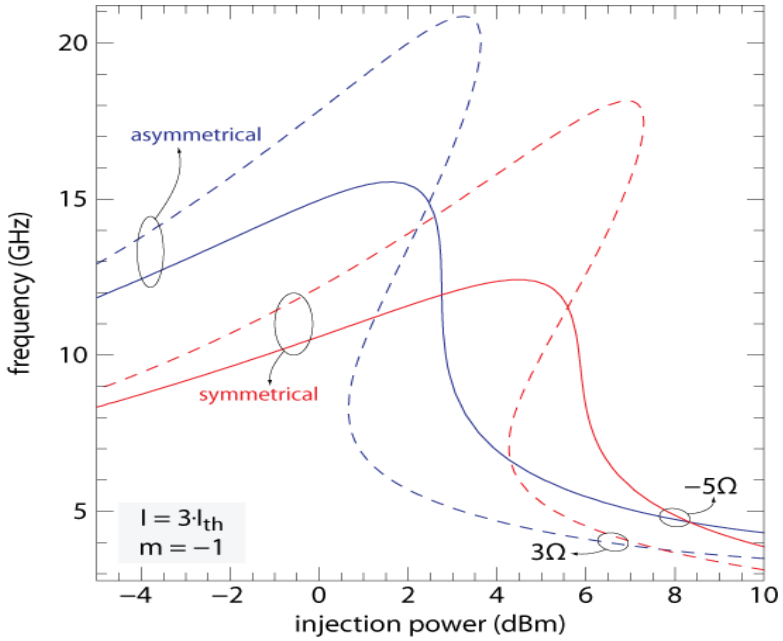

Fig. 6.15. Modulation bandwidth versus P_{inj}, for $I = 3I_{th}$, $\Delta\omega = -5\Omega$ (solid lines) and 3Ω (dashed lines), for asymmetrical gain model (blue lines) and symmetrical gain model (red lines). Injection is in the side-mode $m = -1$.

In Fig. 6.16. we present modulation responses for $I = 3I_{th}$, $\Delta\omega = -5\Omega$, and injection power P_{inj} = 1.5 dBm for which asymmetrical gain model has maximal value of −3 dB modulation bandwidth which is around 15 GHz (blue line in the Fig. 6.16). Injection is in the side mode $m = -1$. On the same figure, we present modulation response obtained for the same injection power, but with symmetrical gain model (red line in Fig. 6.16), which has lower value of modulation bandwidth, even on higher injection powers. Apart from having higher value of modulation bandwidth, optimized structure provides more linear modulation characteristic in the region of −3 dB modulation. In Fig. 6.17. we present modulation responses for $I = 3I_{th}$, $\Delta\omega = 3\Omega$, and injection power P_{inj} = 0.65 dBm, for which optimized structure has maximal value of modulation bandwidth (blue line in Fig. 6.17), while symmetrical gain model provides smaller value of modulation bandwidth (red line in Fig. 6.17).

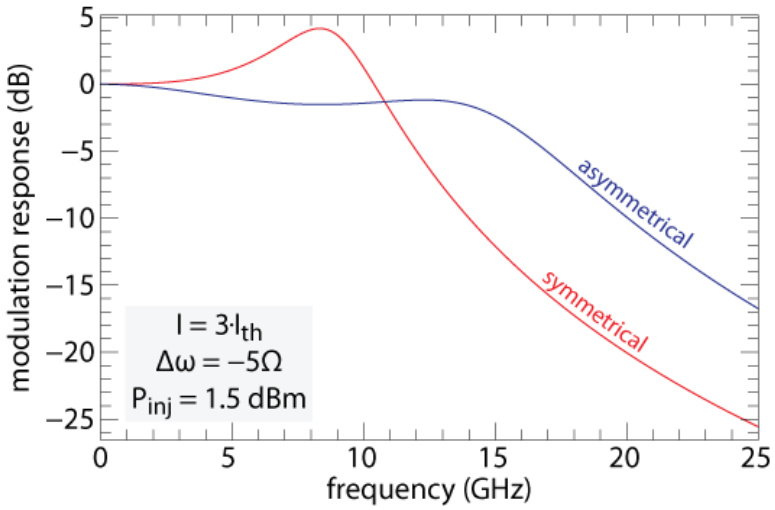

Fig. 6.16. Modulation response for $I = 3I_{th}$, $\Delta\omega = -5\Omega$, and injection power P_{inj} = 1.5 dBm, in the case of asymmetrical gain model (blue line) and symmetrical gain model (red line).

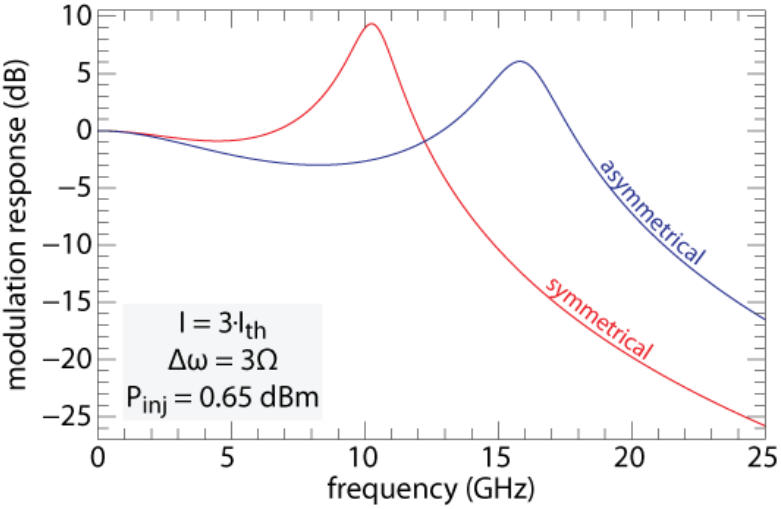

Fig. 6.17. Modulation response for $I = 3I_{th}$, $\Delta\omega = 3\Omega$, and injection power P_{inj} = 0.65 dBm, in the case of asymmetrical gain model (blue line) and symmetrical gain model (red line).

Chapter 7 – Conclusion

The new generation of wavelength-division-multiplexing passive optical access networks (WDM-PONs) introduces a need for cost effective colorless transmitter solutions in optical network units. Recently, injection-locked multimode semiconductor lasers are proposed as highly promising candidate for WDM-PON [40, 41, 107, 111]. Injection-locked lasers can provide cost effective solutions for optical network units, since they can replace much more expensive tunable lasers in upstream transmission form optical network units to the central office. One contribution of this dissertation is a precise theoretical answer to the question of how and on what terms is possible to use such type of lasers for colorless transmitter design. For that reason, the results obtained in this dissertation are very important step forward in further research and improvement of the optical network units design in WDM-PONs. There are three main areas of dissertation contribution:

1. Determination of injection parameters; injection power and frequency detuning in particular, for which directly modulated injection-locked laser has improved modulation bandwidth in comparison with free-running state, as well as injection parameters optimization in order to obtain maximal value of the modulation bandwidth. The increase in the injection power leads to resonant peak suppression, and to the modulation bandwidth improvement up to some moderate injection power. For the examples studied in this dissertation the injection power for which the slave laser exhibits improvement in modulation bandwidth lies in the range 0dBm-2dBm, depending on the frequency detuning.
2. A significant improvement of the bandwidth is possible for negative and small positive frequency detuning, while for moderate and large positive detuning the bandwidth is suppressed below the free-running bandwidth.

3. Results of this dissertation can be used to investigate the influence of the unlocked side-modes on the modulation bandwidth, i.e. to determine the number of the

unlocked side-modes which should be taken into account in order to obtain more realistic model of injection-locked lasers and to calculate modulation bandwidth more precisely. It has been shown that in addition to injection-locked mode, the inclusion of the dominant mode corresponding to free-running regime is relatively good substitution for other unlocked modes. However, in the case of the broad gain spectrum this approach can't provide satisfactory results and number of unlocked modes taken into account must be much larger.

4. In order to investigate modulation characteristics of injection-locked lasers more thoroughly, and to get more precise insight into unlocked modes contribution to the injection-locking dynamics, we employ a more realistic, complex gain model based on 8x8 k.p band structure calculations and compare the results with the simple gain model. This complex gain model is calculated for the optimized quantum well structure, designed for high modulation bandwidths [107, 111]. We find that for the complex gain model, the bandwidth reaches the maximum for smaller injection powers injection power, if the bias currents and the frequency detuning are kept fixed. In other words, the conclusion regarding the bandwidth improvement derived on the basis on the simplified gain model are valid in the case of more realistic gain spectrum profile, suggesting that the maximum can be achieved for even smaller injection powers.

5. Finally, one important contribution is the model itself, since it is developed to take into account an arbitrary number of the unlocked side-modes. To the author's knowledge, such multimode models of the modulation response have not been researched in the literature, so far.

References

[1] P.P. Iannone, K.C. Reichmann, N.J. Frigo, "High-speed point-to-point and multiple broadcast services delivered over a WDM passive optical network", *IEEE Photon. Technol. Lett.* Vol. 10, pp. 1328–1330, (1998).

[2] M. Zirngibl, C.H. Joyner, L.W. Stulz, C. Dragone, H.M. Presby, I.P. Kaminov, "LARnet, a local access router network", *IEEE Photon. Technol. Lett.* Vol. 7, pp. 215–217, (1995).

[3] http://www.answers.com/topic/optical-communication

[4] G. Keiser, "Optical Communications Essentials," *McGraw-Hill*, (2003).

[5] Dejan M. Gvozdić, "Trends in the development of optical communication systems," *Telekomunikacije*, No. 2, pp. 19-28, (2009).

[6] A. Nirmalathas, "Greening the Broadband Wireless Access Networks," *Access Networks and In-house Communications (ANIC)*, Cheyenne Mountain Resort, Colorado Springs, Colorado, (17 June - 21 June 2012).

[7] http://www.americantechsupply.com/fibertothehometodaysneeds.htm

[8] Cedric F. Lam, "Passive Optical Networks Principles and Practice," *Academic Press*, (2007).

[9] M. Oren, S. Eyal, "GPON-The Next Big Thing in Optical Access Networks," *Network Architectures, Management and Applications, Proceedings of the SPIE*, Vol. 5282, pp. 199-209, (2004).

[10] www.slideshare.net/RockyS11/passive-optical-network-4150599

[11] G. Keiser, "Optical Communications Essentials," *McGraw-Hill*, (2004).

[12] A. Banerjee, Y. Park, F. Clarke, H. Song, S. Yang, G. Kramer, K. Kim and B. Mukhrjee, "Wavelength-division-multiplexed passive optical network (WDM-PON) technologies for broadband access," *J. Opt. Net.*, Vol. 4, No. 11, pp. 737-758, (2005).

[13] King Saud University Saudi Arabia, "Wavelength Division Multiplexing (WDM)", *College of Engineering Electrical Department*, course EE-424, (summer semester 2010).

[14] S.S. Agrawal, K.D. Kulat, M.B. Daigavane, "High Performance WDM Using Semiconductor Tunable Laser," *Emerging Trends in Engineering and Technology (ICETET) 2nd International Conference*, pp. 483-487, (2009).

[15] G. Lawton, "WDM-PONs Hold Promise for the Long Haul," *Computer*, Vol. 42, No. 3, pp. 13-16, (2009).

[16] D. Fonseca, R. Luis and A. Cartaxo, "Design and performance of AWG multiplexer/demultiplexer in WDM systems," *Conferencia Nacional de Telecomunicacoes*, pp. 164-168, (2001)

[17] http://www.search.com/reference/Arrayed_waveguide_grating.

[18] G. Agrawal, "Fiber-Optic Communication Systems", *Wiley & Sons*, (2002).

[19] C. Chang-Hasnain, "Progress and prospects of long-wavelength VCSELs," *IEEE Opt. Commun. Mag.*, Vol. 41, No. 2, pp. S30–S34 (2003).

[20] T. Mukaihara , H. Nasu, T. Kimoto, S. Tamura, T. Nomura, T. Shinagawa, A. Kasukawa, M. Oike, H. Matsuura, T. Shiba, T. Ninomiya, "Highly reliable 40-mW 25-GHz×20-ch thermally tunable DFB laser module, integrated with wavelength monitor," *Optical Communication, ECOC 2002,* Vol. 3, (2002).

[21] http://www.aznacorp.com/

[22] http://www.bookham.com/

[23] J. Hong, H. Kim, and T. Makino, "Enhanced wavelength tuning range in two-section complexcoupled DFB lasers by alternating gain and loss coupling," *J. Lightwave Technol.*, Vol. 16, pp. 1323–1328 (1998).

[24] M. Zirngibl, C. H. Joyner, L. W. Stulz, U. Koren, M.-D. Chien, M. G. Young, and B. I. Miller, "Digitally tunable laser based on the integration of a waveguide grating multiplexer and an optical amplifier," *IEEE Photon. Technol. Lett*., Vol. 6, pp. 516–518 (1994).

[25] M. Zirngibl, "Multifrequency lasers and applications inWDMnetworks," *IEEE Commun. Mag.* Vol. 36, No. 12, pp. 39–41 (1998).

[26] M. Zirngibl, C. H. Joyner, C. R. Doerr, L. W. Stulz, and H. M. Presby, "An 18-channel multifrequency laser," *IEEE Photon. Technol. Lett*.Vol. 8, pp. 870–872 (1996).

[27] T. Makino, G. P. Li, A. Sarangan, and W. Huang, "Multiwavelength gain-coupled MQW DFB laser array with fine tunability," *Optical Fiber Communications, OFC '96*, pp. 298-299, (1996).

[28] M. C. Nuss,W. H. Knox, and U. Koren, "Scalable 32 channel chirped-pulse WDM source," *IEEE Electron. Lett*. Vol. 32, pp. 1311–1312 (1996).

[29] K. Liou, U. Koren, E. C. Burrows, J. L. Zyskind, and K. Dreyer, "A WDM access system architecture based on spectral slicing of an amplified LED and delay-line multiplexing and encoding of eight wavelength channels for 64 subscribers," *IEEE Photon. Technol. Lett*. Vol. 9, pp. 517–519 (1997).

[30] W. T. Holloway, A. J. Keating, and D. D. Sampson, "Multiwavelength source for spectrumsliced WDM access networks and LANS," *IEEE Photon. Technol. Lett.*, Vol. 9, pp. 1014–1016 (1997).

[31] D. K. Jung, C. J. Youn, H. G. Woo, and Y. C. Chung, "Spectrum-sliced bidirectional WDM PON," *IEEE Optical Fiber Communication Conference*, Vol. 2, pp. 160-162, (2000).

[32] S. L.Woodward, P. P. Reichmann, and N. C. Frigo, "A spectrally sliced PON employing Fabry-Perot lasers," *IEEE Photon. Technol. Lett*., Vol. 10, pp. 1337–1339 (1998).

[33] H.Sanjoh, H. Yasaka, Y. Sakai, K. Sato, H. Ishii, and Y. Yoshikuni, "Multiwavelength light source with precise frequency spacing using mode-locked semiconductor laser and arrayed waveguide grating filter," *IEEE Photon. Technol. Lett*., Vol. 9, pp. 818–820 (1997).

[34] F. An, K. S. Kim, Y. Huseh, M. Rogge, W. Shaw, and L. Kazovsky, "Evolution, challenges and enabling technologies for future WDM-based optical access networks," *in Proc. of JCIS 2003*, pp. 1449-1453, (2003).

[35] S. J. Park, C. H. Lee, K. T. Jeong, H. J. Park, J. G. Ahn, and K. H. Song, "Fiber-to-the-home services based onWDMpassive optical network," *J. Lightwave Technol*., Vol. 22, pp. 2582–2590 (2004).

[36] Y. B. M'Sallem, Q. T. Le, L. Bramerie, Q. T. Nguyen, E. Borgne, P. Besnard, A. Shen, F. Lelarge, S. LaRochelle, L. A. Rusch, and J. C. Simon, "Quantum-Dash Mode-Locked Laser as a Source for 56-Gb/s DQPSK Modulation in WDM Multicast Applications," *IEEE Photon. Techol. Lett.*, Vol. 23, No. 7, (2011).

[37] M. Pearson, "WDM-PON: A Viable Alternative for Next Generation FTTP," *FTTH Prism Magazine*, (July, 2010).

[38] P. Healey, P. Townsend, C. Ford, L. Johnston, P. Townley, I. Lealman, L. Rivers, S. Perrin, and R. Moore, "Spectral slicing WDM-PON using wavelength-seeded reflective SOAs," *IEEE Electron. Lett.*, Vol. 37, No. 19, pp. 1181-1182, (2001).

[39] L. Chrostowski, "Optical Injection Locking of Vertical Cavity Surface Emitting Lasers", *A dissertation submitted in partial satisfaction of the requires for the degree of Doctor of Philosophy in Engineering – Electrical Engineering and Computer Science*, University of California, Berkeley, (2003).

[40] N. Kashima, "Dynamic properties of FP-LD transmitters using side-mode injection locking for LANs and WDM-PONs", *IEEE J. Lightwave Technol*. Vol. 24, pp. 3045, (2006).

[41] N. Kashima, "Injection-locked Fabry–Perot laser diode transmitters with semiconductor optical amplifier for WDM-PON", *IEEE J. Lightwave Technol*. Vol. 27, pp. 2132, (2009).

[42] X. Jin and S. L. Chuang "Bandwidth enhancement of Fabry–Perot quantum-well lasers by injection locking", *Solid-state Electron.* Vol. 50, pp. 1141, (2006).

[43] F. Smyth, A. Kaszubowska and L.P. Barry, "Overcoming Laser Diode Nonlinearity Issues in Multi-Channel Radio over Fiber Systems", *Optics Communication*, Vol. 231, pp. 217-225, (2004).

[44] C.H. Lee, S.M. Lee, K.M. Choi, J.H. Moon, S.G. Mun, K.T. Jeong, J.H. Kim, B.W. Kim, "WDM-PON experiences in Korea," *J. Opt. Netw.*, Vol. 6, No. 5, pp. 451-464. (2007).

[45] Y.Y. Won, H. C. Kwon, M.K. Hoang, S. K. Han , "Bidirectional colorless gigabit WDM-passive optical networks by use of injection locking and optical carrier suppression," *Opt. Fiber Technol*., Vol. 15, No. 1, pp. 10-14, (2009).

[46] E. Wong, K.L. Lee, T.B. Anderson, "Directly Modulated Self-Seeding Reflective Semiconductor Optical Amplifiers as Colorless Transmitters in Wavelength Division Multiplexed Passive Optical Networks," *J. Lightw. Technol*., Vol. 25, pp. 67, (2007).

[47] D.C. Kim, B.S. Choi, H.S. Kim, K.S. Kim, O.K. Kwon, D.K. Oh, "2.5 Gbps Operation of RSOA for Low Cost WDM-PON Sources," *Optical Communication, ECOC '09*, Vienna, (2009).

[48] S. Bernhard, G. Valicourt, O. Mireia, J. A. Lazaro, B. Romain, P. Josep, "Direct 10 Gb/s Modulation of a Single-Section RSOA in PONs with High Optical Budget," *IEEE Photon. Technol. Lett*., Vol. 22, No. 6, pp. 392-394, (2010).

[49] W.R. Lee, M.Y. Park, S.H. Cho, J.H. Lee, C.Y. Kim, G. Jeong, B.W. Kim, "Bidirectional WDM-PON based on gain-saturated reflective semiconductor optical amplifiers," *IEEE Photon. Technol. Lett.,* Vol. 17, pp. 2460-2462, (2005).

[50] R. Lang, "Injection locking properties of a semiconductor laser," *IEEE J. Quantum Electron*., Vol. 18, No. 6, pp. 976–983, (1982).

[51] T.H. Wood, E.C. Carr, B.L. Kasper, R.A. Linke, C.A. Burrus, K.L. Walker, "Bidirectional fibre-optical transmission using a multiple-quantum-well (MQW) modulator/detector," *IEEE Electron. Lett.,* Vol. 22, pp. 528, (1986).

[52] L. Noel, D. Wake, D.G. Moodie, D.D. Marcenac, L.D. Westbrook, D. Nesset, "Novel techniques for high-capacity 60-GHz fiber-radio transmission systems", *IEEE Trans. Microw. Theory Technol.*, Vol. 45, pp. 1416 (1997).

[53] W. S. Tsai, H. L. Ma, H. H. Lu, Y. P. Lin, H. Y. Chen, and S. C. Yan, "Bidirectional direct modulation CATV and phase remodulation radio-over-fiber transport systems," *Opt. Express* Vol. 18, No. 25, pp. 26077–26083 (2010).

[54] C. H. Chang, P. C. Peng, H. H. Lu, C. L. Shih, and H. W. Chen, "Simplified radio-over-fiber transport systems with a low-cost multiband light source," *Opt. Lett*. Vol. 35, No. 23, pp. 4021–4023 (2010).

[55] C. H. Chang, H. H. Lu, H. S. Su, C. L. Shih, and K. J. Chen, "A broadband ASE light source-based full-duplex FTTX/ROF transport system," *Opt. Express* Vol. 17, No. 24, 22246–22253 (2009).

[56] A. Polley, P. J. Decker, J. H. Kim, and S. E. Ralph, "Plastic optical fiber links: a statistical study," *IEEE Optical Fiber Communication Conference*, San Diego, CA, (2009).

[57] A. Polley, P. J. Decker, and S. E. Ralph, "10 Gb/s, 850 nm VCSEL based large core POF links," *Lasers and Electro-Optics (CLEO)*, San Jose, California, (2008).

[58] H. Yang, S. C. Lee, E. Tangdiongga, F. Breyer, S. Randel, and A. M. J. Koonen, "40-Gb/s transmission over 100m graded-index plastic optical fiber based on discrete multitone modulation," *IEEE Optical Fiber Communication Conference*, San Diego, CA, (2009).

[59] J. Yu, D. Qian, M. Huang, Z. Jia, G. K. Chang, and T. Wang, "16Gbit/s radio OFDM signals over graded-index plastic optical fiber," *Optical Communication, (ECOC)*, Brussels, (2008).

[60] M. Asai, R. Hirose, A. Kondo, and Y. Koike, ""High-bandwidth graded-index plastic optical fiber by the dopant diffusion coextrusion process," *IEEE J. Lightw. Technol*., Vol. 25, No. 10, pp. 3062–3067, (2007).

[61] T. Katayama, T. Ooi, and H. Kawaguchi, "4-bit all-optical buffer memory with shift register function using polarization bistable VCSELs," *IEEE Optical Fiber Communication Conference*, San Diego, CA, (2009).

[62] H. Kawaguchi, "Bistable laser diodes and their applications: State of the art," *IEEE J. Sel. Topics Quantum Electron.*, Vol. 3, No. 5, pp. 1254–1270, (1997).

[63] M. Takenaka and Y. Nakano, "Multimode interference bistable laser diode," *IEEE Photon. Technol. Lett.*, Vol. 15, No. 8, pp. 1035–1037, (2003).

[64] M. T. Hill, H. J. S. Dorren, T. de Vries, X. J. M. Leijtens, J. H. den Besten, B. Smalbrugge, Y. S. Oei, H. Binsma, G. D. Khoe, and M. K. Smit, "A fast low-power optical memory based on coupled micro-ring lasers," *Nature*, Vol. 432, pp. 206–209, (2004).

[65] K. Inoue and M. Yoshino, "Bistability and waveform reshaping in a DFB-LD with side-mode light injection," *IEEE Photon. Technol. Lett*., Vol. 7, No. 2, pp. 164–166, (1995).

[66] H. Kawaguchi, K. Inoue, T. Matsuoka, and K. Otsuka, "Bistable output characteristics in semiconductor laser injection locking," *IEEE J. Quantum Electron*., Vol. 21, No. 9, pp. 1314–1317, (1985).

[67] T. Kakitsuka, S. Matsuo, K. Hamamoto, T. Segawa, H. Suzuki, and R. Takahashi, "Injection-Locked Flip-Flop Operation of a DBR Laser," *IEEE Photon. Technol. Lett*, Vol. 23, No. 17, (2011).

[68] B. K. Mathason and P. J. Delfyett, "Pulsed injection locking dynamics of passively modelocked external-cavity semiconductor laser systems for all-optical clock recovery," *J. Lightw. Technol*., Vol. 18, No. 8, pp. 1111-1120, (2000).

[69] S. Yamashita and D. Matsumoto, "Waveform reshaping based on injection locking of a distributed-feedback semiconductor laser," *IEEE Photon. Technol. Lett*., Vol. 12, No. 10, pp. 1388-1390, (2000).

[70] A. Kuramoto and S. Yamashita, "All-optical regeneration using a side-mode injectionlocked semiconductor laser," *IEEE J. Sel. Topics Quantum Electron*., Vol. 9, No. 5, pp. 1283-1287, (2003).

[71] S. Yamashita and J. Suzuki, "All-optical 2R regeneration using a two-mode injection-locked Fabry-Perot laser diode," *IEEE Photon. Technol. Lett*., Vol. 16, No. 4, pp. 1176-1178, (2004).

[72] Y. Onishi, F. Koyama, N. Nishiyama, C. Caneau, and C. E. Zah, "Dynamic behavior of 1.55-ìm vertical-cavity surface-emitting laser with external light injection," *Lasers and Electro-Optics (CLEO)*, Vol. 1, (2004).

[73] H. Kawaguchi, Y. Yamayoshi, and K. Tamura, "All-optical format conversion using an ultrafast polarization bistable vertical-cavity surface-emitting laser," *Lasers and Electro-Optics (CLEO)*, pp. 379-380, (2000).

[74] K. Hasebe, Y. Onishi, and F. Koyama, "Novel polarization controller based on injectionlocked vertical-cavity surface-emitting laser," *Lasers and Electro-Optics (CLEO)*, pp. 164-165, (2005).

[75] "MICS band plan," FCC, Washington, DC, FCC Rules and Regulations, Part 95, (2003).

[76] M. Chae, W. Liu, Z. Yang, T. Chen, J. Kim, M. Sivaprakasam, and M. Yuce, "A 128-channel 6 mW wireless neural recording IC with on-the fly spike sorting and UWB transmitter," *Solid-State Circuits Conf. Tech. Dig.*, pp. 146–603, (2008).

[77] J. N. Y. Aziz, K. Abdelhalim, R. Shulyzki, B. L. Bardakjian, M. Derchansky, D. Serletis, and P. L. Carlen, "256-channel neural recording and delta compression microsystem with 3-D electrodes," *IEEE J. Solid-State Circuits*, Vol. 44, No. 3, pp. 995–1005, (2009).

[78] S. Diao, Y. Zheng,, Y. Gao, S.J. Cheng, X. Yuan, M. Je, and C.H. Heng, "A 50-Mb/s CMOS QPSK/O-QPSK Transmitter Employing Injection Locking for Direct Modulation," *IEEE Trans. on Microwave Theory and Techniques*, Vol. 60., No. 1, pp. 120-130, (2012).

[79] S.M. Lee, K. M. Choi, S.G. Mun, J.H. Moon and C.H. Lee, "Dense WDM-PON based on wavelength locked Fabry-Perot lasers," *IEEE Optical Fiber Communication Conference*, Vol. 3, (2005).

[80] M. Zirngibl, C. R. Doerr, and L. W. Stulz, "Study of spectral slicing for local access applications," *IEEE Photon. Technol. Lett*., Vol. 8, No. 5, pp. 721-723, (1996).

[81] D. K. Jung, S. K. Shin, C. -H. Lee, and Y. C. Chung, "Wavelength-division-multiplexed passive optical network based on spectrum-slicing techniques," *IEEE Photon. Technol. Lett*., Vol. 10, No. 9, pp. 1334-1336, (1996).

[82] R. D. Feldman, E. E. Harstead, S. Jiang, T. H. Wood, M. Zirngibl, "An evaluation of architectures incorporating wavelength division multiplexing for broad-band fiber access," *IEEE J. Lightw. Technol.*, Vol. 16, No. 9, pp. 1546-1559, (1998).

[83] S. L. Wroodward, P. P. Iannone, K. C. Reichmann, and N. J. Frigo, "A spectrally sliced PON employing Fabry-Perot Lasers," *IEEE Photon.Technol. Lett.*, Vol. 10, No. 9, pp. 1337-1339, (1998).

[84] K. Petermann, "Laser diode modulation and noise", *Kluwer Academic Publishers*, London, (1988).

[85] S. Kobayashi, J. Yamada, S. Machida, and T. Kimura, "Single-mode operation of 500 Mbit/s modulated AlGaAs semiconductor laser by injection locking," *IEEE Electron. Lett.*, Vol. 14, No. 19, pp. 746-748, (1980).

[86] K. Iwashita and K. Nakagawa, "Suppression of mode partition noise by laser diode light injection," *IEEE J. Quantum Electron*., Vol. 18, No. 10, pp. 1669-1674, (1982).

[87] P.Healy, P. Townsend, C. Ford, L. Johnston, P. Townley, I. Lealman, L. Rivers, S. Perrin, R. Moore, "Spectral slicing WDM-PON using wavelength-seeded reflective SOAs", *IEEE Electron. Lett*, Vol. 37, No, 19, pp. 1181-1182, (2001).

[88] N.Buldawoo, S.Mottet, H.Dupont, D.Sigogne, D. Meichenin, "Transmission experiment using a laser amplifier-reflector for DWDM access network", *Optical Communication, ECOC '98*, Vol. 1, pp. 273-274, (1998).

[89] H. D. Kim, S. G. Kang, and C. H. Lee, "A low cost WDM source with an ASE injected Fabry-Perot semiconductor laser," *IEEE Photon.Technol. Lett*., Vol. 12, No. 8, pp. 1067-1069, (2000).

[90] Banibrata Bag, Akinchan Das, Hai-Hun Lu, A. S. Patra, "Injection-Locked DFB Laser Diode in Main and Multiple Side Modes", *International Journal of Soft Computing and Engineering (IJSCE)*, Vol. 1, No. NCRAMT2011, (2011).

[91] http://www.lightreading.com/

[92] A. Pikovsky, M. Rosenblum, and J. Kurths, "Synchronization: A Universal Concept in Nonlinear Science", *Cambridge University Press*, (2001).

[93] R. Adler, "A study of locking phenomena in oscillators," *Proc. IRE*, Vol. 34, pp. 351–357, (1946).

[94] Y. Yamamoto and T. Kimura, "Coherent optical fiber transmission systems," *IEEE J. Quantum Electron.*, Vol. 17, pp. 919–935, (1981).

[95] P. Gallion, H. Nakajima, G. Debarge, and C. Chabran, "Contribution of spontaneous emission to the linewidth of an injection-locked semiconductor laser," *IEEE Electron. Lett.*, Vol. 22, pp. 626–628, (1985).

[96] K. Iwashita and K. Nakagawa, "Suppression of mode partition noise by laser diode light injection," *IEEE J. Quantum Electron.*, Vol. 18, pp. 1669–1674, (1982).

[97] N. A. Olsson, H. Temkin, R. A. Logan, L. F. Johnson, G. J. Dolan, J. P. V. der 158 Ziel, and J. C. Campbell, "Chirp-free transmission over 82.5 km of single mode fibers at 2 Gbit/s with injection locked DFB semiconductor lasers," *J. Lightw. Technol.*, Vol. 3, No. 1, pp. 63–66, (1985).

[98] X. Meng, T. Chau, and M. C. Wu, "Experimental demonstration of modulation bandwidth enhancement in distributed feedback lasers with external light injection," *IEEE Electron. Lett.*, Vol. 34, No. 21, pp. 2031–2032, (1998).

[99] Chih-Hao Chang "High Speed Vertical Cavity Surface Emitting Lasers with Injection Locking", *A dissertation submitted in partial satisfaction of the requires for the degree of Doctor of Philosophy in Engineering – Electrical Engineering and Computer Science*, University of California, Berkeley, (2002).

[100] G. P. Agrawal and N. K. Dutta, "Semiconductor Lasers", *Van Nostrand Reinhold*, (1993).

[101] M. Krstić, J. Crnjanski, M. Mašanović, L. Johansson, L. Coldren, D. Gvozdić, "Multivalued Stability Map of an Injection-Locked Semiconductor Laser," *IEEE J. Sel. Topics Quantum Electron.*, DOI 10.1109/JSTQE.2013.2241026

[102] C. H. Henry, N. A. Olsson, and N. K. Dutta, "Locking range and stability of injection locked 1.54 μm InGaAsP semiconductor lasers," *IEEE J. Quantum Electron.*, Vol. 21, No. 8, pp. 1152–1156, (1985).

[103] A. Murakami, K. Kawashima, K. Atsuki, "Cavity resonance shift and bandwidth enhancement in semiconductor lasers with strong light injection" *IEEE J. Quantum Electron.*, Vol. 39, pp. 1196-1204, (2003).

[104] E. Lau, H. K. Sung, M. C. Wu, "Frequency Response Enhancement of Optical Injection-Locked Lasers," *IEEE J. Quantum Electron.*, Vol. 44, pp. 90-99, (2008).

[105] Y. Hong and K. A. Shore, "Locking characteristics of a side-mode injected semiconductor laser," *IEEE Journal of Quantum Electronics*, Vol. 35, No. 11, pp. 1713–1717, (1999).

[106] L. A. Coldren, S. W. Corzine, and M. L. Mašanović, "Diode Lasers and Photonic Integrated Circuits", *New York: Wiley Series in Microwave and Optical Engineering*, (2012).

[107] Marko M. Krstić, Jasna V. Crnjanski, and Dejan M. Gvozdić, "Injection Power and Detuning-Dependent Bistability in Fabry–Perot Laser Diodes", *IEEE J. Sel. Topics Quantum Electron.*, Vol. 18, No. 2, pp. 826-833, (2012).

[108] C. G. Van de Walle, "Band lineups and deformation potentials in the model-solid theory," *Phys. Rev. B*, Vol. 39, pp. 1871–1883, (1989).

[109] I. Vurgaftman, J. R. Meyer, and L. R. Ram-Mohan, "Band parameters for III–V compound semiconductors and their alloys," *J. Appl. Phys.*, Vol. 89, pp. 5815–5875, (2001).

[110] A. T. Meney, B. Gonul, and E. P. O'Reilly, "Evaluation of various approximations used in the envelope-function method," *Phys. Rev. B*, Vol. 50, pp. 10893–10904, (1994).

[111] A G R Zlitni, M M Krstić and D M Gvozdić, "Modulation response and bandwidth of injection-locked Fabry–Perot laser diodes", *Physica Scripta*, Vol. T149. (2012).

BIOGRAPHY

ABDULGADER G.R. ZLITNI was born on 29.04.1969. in Tripoli, Libya. He completed the elementary school in "Jamea Amora School" Tripoli, and high school in "Ased Altogoor School" Tripoli. He finished his studies at Technical Faculty of Civil Aviation and Meteorology, Libya, where he graduated in August 1991 at the Department of Communication Engineering.

On 29.09.2003., he defended Master's thesis, titled "Positioning analysis of laser illuminated object," at the Faculty of Electrical engineering, University of Belgrade, Department of Physical Electronics.

- **1992 - 1994**, he was a member of the group which developed and improved the telemetry unit of long-range missiles in the Research Center and Development, Tripoli, Libya.
- **1995 - 2001**, he was a member of the group for anti-tank missiles transceiver units design.
- **2001 - 2003**, he spent pursuing Master's degree in Belgrade, Serbia, in the field of laser guidance.
- **2003 - 2005**, he was one of four engineers who have been selected to work on the Serbian-Libyan project to develop the transceiver system for anti-tank missile "FAGOT". The new design changed the old method in which a correction signal was sent to the missile with a copper wire link between the launcher and the missile. In the new design the signal is sent by the laser communication system in the range up to 3km.
- **2005 - 2007,** the Libyan-Serbian project had stopped, and he started to complete the rest of the work on his own. He tested the laser guidance system in the laboratory and in the field.

  He also designed several new laser driver circuits with different divergences and powers to cover the trajectory of the missile from the begging to the end of distance (3km). The

design used very small-sized components suitable to be put it in small places in the missile. In addition to this, he worked on the printed circuit board (BCB) for that design.

The most important activities:

- Member in a research group dealing with the modification of the guidance system of the anti-tank FAGOT missile (from wire to laser system).
- Design and implementation of the diode laser driver units.
- Design and implementation of DC to DC converter units used for pumping high power laser diode (wavelength = 904nm).
- Design and implementation of a high power laser transmitter (single diode array).
- Design and implementation of a high power laser transmitter (array of eight diodes).
- Design and implementation of laser receivers (wavelength = 904nm).
- Measurements of the radiation pattern of the laser transmitters.
- Measurements of the effective beam divergence for the laser transmitters mentioned above in order to cover the guidance distance with the sufficient laser power.
- Contribution in the field tests measurements on the laser transmitter and receiver units related to the modified FAGOT anti tank missile.
- Contribution in the stationary field test on the sustainer motor of the Fagot missile and its smoke effects on the receiver unit.
- Contribution in the field tests measurements of the laser guidance subsystems for the modified FAGOT missile.
- Contribution in the field tests on the old and the modified antitank FAGOT complex.
- The analysis of the different field test results.
- Theoretical study on the calculation of the minimum laser power required in semi-active guidance scheme.
- Design and implementation of low power IR transmitters used in the laboratory.

Publications:

International School and Conference on Photonics IOP**.** Physica Scrripta 014033. 2012.

Received 2 September 2011, accepted for publication 5 October 2011 Published 27 April 2012.

Authors: *A.G.R.Zlitni, M.M. Krstić and D.M. Gvozdić*.

Title: Modulation response and bandwidth of injection-locked Fabry-Perot laser diodes.

Issue: T149

Volume: 2012.

Article ID: pstop419030.

doi: 10.1088/0031-8949.